AGARD-AG-204

AGARD-AG-204

AGARD

ADVISORY GROUP FOR AEROSPACE RESEARCH & DEVELOPMENT

7 RUE ANCELLE 92200 NEUILLY SUR SEINE FRANCE

AGARDograph No. 204

on

Vortex Wakes of Conventional Aircraft

by

C.duP.Donaldson and A.J.Bilanin

NORTH ATLANTIC TREATY ORGANIZATION

DISTRIBUTION AND AVAILABILITY
ON BACK COVER

NORTH ATLANTIC TREATY ORGANIZATION

ADVISORY GROUP FOR AEROSPACE RESEARCH AND DEVELOPMENT

(ORGANISATION DU TRAITE DE L'ATLANTIQUE NORD)

AGARDograph No.204

VORTEX WAKES OF CONVENTIONAL AIRCRAFT

by

Coleman duP. Donaldson and Alan J. Bilanin

Aeronautical Research Associates of Princeton, Inc.,
50 Washington Road, Princeton, New Jersey 08540, USA

Edited by

R.H. Korkegi

Aerospace Research Laboratories,
Wright-Patterson Air Force Base,
Ohio 45433, USA

This work was prepared at the request of the Fluid Dynamics Panel of AGARD.

THE MISSION OF AGARD

The mission of AGARD is to bring together the leading personalities of the NATO nations in the fields of science and technology relating to aerospace for the following purposes:

- Exchanging of scientific and technical information;
- Continuously stimulating advances in the aerospace sciences relevant to strengthening the common defence posture;
- Improving the co-operation among member nations in aerospace research and development;
- Providing scientific and technical advice and assistance to the North Atlantic Military Committee in the field of aerospace research and development;
- Rendering scientific and technical assistance, as requested, to other NATO bodies and to member nations in connection with research and development problems in the aerospace field;
- Providing assistance to member nations for the purpose of increasing their scientific and technical potential;
- Recommending effective ways for the member nations to use their research and development capabilities for the common benefit of the NATO community.

The highest authority within AGARD is the National Delegates Board consisting of officially appointed senior representatives from each member nation. The mission of AGARD is carried out through the Panels which are composed of experts appointed by the National Delegates, the Consultant and Exchange Program and the Aerospace Applications Studies Program. The results of AGARD work are reported to the member nations and the NATO Authorities through the AGARD series of publications of which this is one.

Participation in AGARD activities is by invitation only and is normally limited to citizens of the NATO nations.

Published May 1975

533.6.048.3:629.735.3

Printed by Technical Editing and Reproduction Ltd
Harford House, 7–9 Charlotte St, London. W1P 1HD

VORTEX WAKES OF CONVENTIONAL AIRCRAFT

by

Coleman duP. Donaldson and Alan J. Bilanin

Aeronautical Research Associates of Princeton, Inc.
50 Washington Road, Princeton, New Jersey 08540

SUMMARY

A review is made of the present state of our knowledge of the vortex wakes of conventional aircraft. Included are discussions of wake rollup, geometry, instability, and turbulent aging. In the light of these discussions, a brief review is made of the persistence of vortices in the atmosphere and design techniques which might be used to minimize wake hazard are considered.

LIST OF SYMBOLS

a	dimensionless constant in turbulent model equations
$a_1 - a_3$	constants, see Eq (4.24)
A	wing aspect ratio, and acceleration function (see Fig. 1.14)
b	wing span, and dimensionless constant in turbulent model equations
$b_1 - b_5$	constants, see Eq (4.24)
b'	trailing vortex separation
B	see Eq (2.13)
c	wing chord, breakdown velocity, and concentration
$\bar{c}$	mean wing chord
c_d	wing sectional drag coefficient
c_{d_i}	wing sectional induced drag coefficient
c_{d_p}	wing sectional profile drag coefficient
c_g	group velocity
C_ℓ	rolling moment coefficient
C_L	lift coefficient
C_μ	momentum coefficient
d	distance between tip and flap vortex, see Eq (6.4)
D	dispersion of vorticity, see Eq (1.16)
D_{ind}	induced drag
E	kinetic energy per unit length of wake, see Eq (1.5)
F_{q^2}	see Eq (4.50)
h	altitude or height
$\hat{i}, \hat{j}, \hat{k}$	unit vectors (x, y, z)
J	see Eq (2.10)
$J_m(x)$	Bessel function of the first kind of order m
k	wave number
ℓ	sectional wing loading on the fluid
m	integer azimuthal mode number
N	Brunt-Väisälä frequency
N_s	swirl parameter, see Eq (4.38)
p	pressure
p_c	dimensionless constant in turbulent model equations
q	$\sqrt{\overline{u'^2} + \overline{v'^2} + \overline{w'^2}}$, dynamic pressure
r, θ, z	circular cylindrical coordinates with velocity components u, v, w, respectively
r_c	viscous core radius
$\vec{r}$	position vector
R	vortex tube radius
R_1, R_2	upstream and downstream vortex tube radius, respectively

s	wing semispan
S	swirl parameter, see Figure 3.5
t	time
T	modified kinetic energy per unit length of wake
T_L	time to link, see Eq (5.11)
u, v, w	velocity components in the r,θ,z directions, respectively
U, V, W	velocity components in the x,y,z directions, respectively
U_∞	free stream or flight speed
v_c	dimensionless constant in turbulent model equations
v_ε	characteristic atmospheric turbulent velocity, see Eq (5.8)
v_Γ	characteristic vortex velocity, see Eq (5.8)
W^*	vortex descent rate
x, y, z	cartesian coordinates with velocity components U,V,W, respectively
y^*	see Figure 1.11
$\bar{y}$	spanwise location of the centroid of trailed vorticity
$\bar{y}_{12}$	see Eq (1.36)
$\bar{y}_v$	spanwise location of developing vortex, see Figure 1.17
$\bar{z}$	location of the centroid of trailed vorticity in the z direction
α	constant
$\alpha_{\lvert m\rvert,n}$	n^{th} zero of $J_{\lvert m\rvert}$
β	dimensionless constant in turbulent model equations
γ	trailed vortex sheet strength and Euler's constant
Γ	circulation
Γ_o	wing root circulation
Γ'	circulation in the rolled-up vortex
Γ_y	see Eq (1.8)
Γ_z	see Eq (1.9)
Γ_r	see Eq (1.10)
δ_f	flap deflection angle
ε	deformation rate and turbulent dissipation
ζ	trailed axial vorticity
η	see Eq (5.10)
λ	wave length
Λ	turbulent scale parameter (integral scale)
ν	kinematic viscosity
π_{ij}	viscous stress tensor
ρ	fluid density
σ	see Eq (5.1)
χ	see Eq (5.48)
ω	circular frequency
Ω	angular rate of rotation

TABLE OF CONTENTS

INTRODUCTION

It is generally acknowledged today that the near wake of a large modern jet airliner poses a significant hazard to any smaller aircraft that follows it into or out of an air terminal. Thus, for the past few years, a significant effort has been underway, both in the United States and Europe, aimed at gaining a sufficient understanding of wakes to permit quantitative evaluation of the nature and persistence of the wake hazard problem. What has emerged from these studies is the realization that the wake of a modern flap-equipped aircraft operating in the vicinity of an airport is far more complex than the simple two-trailing-vortex model that has been used so extensively in the past to describe the flow behind a conventional airplane. It has become clear that if one wishes to describe accurately the rolling moments or other aerodynamic forces that might be experienced as one aircraft encounters the wake of another, one must know in quite some detail just how the lift is distributed along the wing of the generating aircraft. Only when this information is in hand can one compute a first approximation to the general features of the wake in question. Indeed, for a complete description of a wake, we shall see in what follows that one must have the spanwise distributions of both lift and drag on the wing and, at times, on tail surfaces of the generating aircraft. In addition, under certain circumstances, the propulsion system of the aircraft must be specified. Only when this complete information is in hand can one proceed with the process of evaluating wake hazard.

The first step in this process is the computation of how the vorticity trailed by the wing and tail organizes itself into two or more centers of vorticity behind and to each side of the airplane. This initial organization or roll-up of the trailed vorticity behind an airplane is a relatively rapid process and is generally complete within the space of several spans. For most intents and purposes, since the roll-up is rapid, the part played by viscosity in this initial organization is small and the roll-up process may, to first order, be computed as an inviscid process.

Given a valid description of the roll-up process, there are several more aspects of the life of an aircraft wake that must be understood before an analysis of vortex hazard can be made that is suitable for operational studies.

The second aspect of wake behavior that must be understood is the interaction and stability of the discrete centers of vorticity that are formed in the roll-up process. If more than one pair of vortices is trailed by the wing, the centers of vorticity on one side of the airplane interact strongly with each other and with their opposites on the other side of the airplane. It is essential that one know whether the vortices on each side will rotate about each other, as has generally been assumed in past studies, or will move apart. Further, it is essential to know the stability of the rolled-up centers of vorticity when they are subjected to disturbances. There are two major types of instability which have been studied in some detail in recent years. One instability to be considered is that in which sinuous disturbances of the vortex lines grow in amplitude until opposed vortices can connect up to form a series of vortex rings. Another instability which may occur is vortex breakdown. This phenomenon is associated with the strong coupling that exists between the tangential and axial velocity components of the vortex. When conditions on the tangential and axial velocity profiles are such that breakdown is possible, a disturbance applied to a vortex line can cause the flow in the vortex to change rather abruptly from a state of tightly centered angular momentum to a state where the angular momentum of the vortex is more widely dispersed. It is clear that the long-term behavior of an aircraft wake must be dependent on the interactions and instabilities described above.

The third aspect of wake behavior that must be understood will be referred to in this monograph as "aging." We will use this term to describe diffusion effects on the centers of vorticity that form behind a wing that are due to viscous phenomena — both those resulting from molecular transport and those resulting from small-scale turbulent transport associated with the rate of deformation of the fluid elements in the wake.

The fourth and final aspect of wake behavior that must be understood before an operational assessment of vortex hazard can be made is the interaction of the wake with the atmosphere in which it is embedded. In considering this problem, attention must be paid to the effects of atmospheric shear, turbulence, and lapse rate or stability.

It might be well, for the sake of emphasis, to display below the four major problems that must be understood before an analysis of vortex hazard may be carried out. They are

1. Roll-up
2. Interaction and Instability
3. Aging
4. Atmospheric Effects

In what follows, we will attempt to discuss each of these problems in some detail. The treatment of each of these areas will not be complete, however, for two reasons. First, this monograph is only intended to serve as an introduction to the problem of computing the behavior of aircraft wakes. Second, the very large amount of research being conducted in these areas at the present time adds some new piece of information to the puzzle almost on a day-to-day basis. Thus, whenever one decides to stop writing, one will find that something has been left out. The authors hope that, in spite of the rapid advances that are being made in our understanding of vortex wakes at the moment, this monograph will prove useful to the engineer seeking an introduction to the rather fascinating subject of aircraft wakes.

1. THE ROLL-UP OF TRAILED VORTICITY

It is well known that a vortex sheet is trailed from a finite aspect ratio wing as a consequence of the nonuniform spanwise lift on the wing. The roll-up of this sheet into discrete vortices as a result of a convective motion was recognized as early as 1907 by

Lanchester (see Fig. 1.1). Since then, there have been numerous studies to describe this complicated phenomenon. In this section, we will review some of the models from which it has been proposed that the inviscid structure of each discrete wake vortex might be deduced.

1.1 Point Vortex Computations of the Roll-Up Phenomenon

We begin our discussion of aircraft vortex wakes quite appropriately at the trailing edge of a lifting wing and attempt to estimate at what distance downstream the wake may be considered essentially rolled up. In Figure 1.2 we have sketched the near wake of an elliptically loaded wing of span b and wing root circulation Γ_o. The downwash velocities in the wake are $\mathcal{O}(\Gamma_o/b)$, the downwash velocity at the wing being exactly $\Gamma_o/2b$ from lifting line theory. An estimate of the downstream distance at which roll-up is complete is obtained by noting that roll-up requires a redistribution of trailed vorticity over the length scale $\mathcal{O}(b)$. The time required for this redistribution must then be $\mathcal{O}(b^2/\Gamma_o)$ or, in terms of downstream distance, $\mathcal{O}(U_\infty b^2/\Gamma_o)$. The nondimensional distance which characterizes the roll-up phenomenon is then $x/b \sim \mathcal{O}(A/C_L)$ where A and C_L are the wing aspect ratio and lift coefficient, respectively. For an aspect ratio 7 wing at a cruise C_L of 0.4, the downstream distance is of the order of 20 wing spans. As will become apparent, more accurate estimates of the distance downstream at which roll-up is complete must be obtained by detailed calculation.

Details of the roll-up phenomenon, other than of a qualitative nature obtained from flow visualization studies, have been difficult to obtain. Clearly, the three-dimensionality of the flow field has hindered both theoretical and experimental investigations. However, with the advent of high lift wings, where wake geometry becomes a factor in determining the downwash at the wing, and with the realization that wake vortices from large aircraft can pose a hazard to other aircraft, the study of the roll-up problem has received new impetus. The calculation of the downstream development of a vortex wake from a flat sheet is a formidable task, and estimates are made from approximate models. With recent advances in numerical computation procedures and as computers become larger, the numerical solution of the entire vortex wake is nearly possible. However, to date, a description of roll-up is obtained by considering the motion of an initially plane two-dimensional vortex sheet of strength

$$\gamma = -\frac{d\Gamma}{dy} = \int_{-\infty}^{\infty} \zeta \, dz \tag{1.1}$$

where ζ is the axial or trailed vorticity. The sheet initially lies in the x-y plane, between $-b/2 \leq y \leq b/2$. The procedure is to break the sheet up into discrete elements [Refs. 2-8] with $\bar{n}$ point vortices and then numerically calculate their subsequent positions. This "discretization" process is illustrated in Figure 1.3 where it is shown that some ambiguity arises as to whether one should choose vortices of equal strength or space them uniformly. Other discretization schemes are obviously also possible, and these procedures have received wide treatment in the literature. Of course, the correct scheme would be one which exactly predicts the unsteady velocity at each vortex. However, there is evidence that this may never be possible, since the similarity solution obtained by Kaden [9] shows that the arc length between two neighboring points on the initially plane sheet become spaced arbitrarily far apart as roll-up proceeds. The spiral structure of the vortex is sketched in Figure 1.4 where points s_1 and s_2 are shown prior to and after roll-up has proceeded for some time. The never-ending stretching of the sheet (not the vorticity) and hence ever-increasing separation between discrete vortices which model the sheet is a continuing source of frustation.

In Figure 1.5(a) we have shown a typical calculation using point vortices of equal strength. The problems with point vortex computations in their present form are clear.

It is interesting to note that the chaotic appearance of the sheet does not result from a numerical instability. Moore [6] has demonstrated this by simply reversing time once the sheet has displacements which appear physically unrealistic and integrating back to time zero. Here he regained, to a high order of accuracy, the initial conditions.

Apparently, discrete vortices cannot model the tip region correctly, and two fixes are being used to render the results of the calculation more physically appealing. The first is to discretize the sheet with vortices which are not singular at the center (Chorin and Bernard [5] and Bloom and Jen [7]). One such vortex is the Lamb vortex whose well-known swirl velocity distribution is given by

$$v = \frac{\Gamma}{2\pi r}\left[1 - \exp\left(-\frac{r^2}{r_c^2}\right)\right] \tag{1.2}$$

The radial distance r is measured from the center of each vortex and the parameter r_c, which has the dimensions of length, can be chosen to set the level of the maximum tangential velocity in the vortex. The results of using discrete vortices given by Eq (1.2) are shown in Figures 1.5(b) and (c) for the same initial conditions used in the calculations shown in Figure 1.5(a). The effect of nonzero r_c is to introduce an artificial viscosity into the computation and therefore slow down or dampen the roll-up. Unfortunately, as can be seen, the calculations are somewhat sensitive to the value of r_c used and, to our knowledge, no rigorous procedure exists to determine its value. The question of whether the roll-up phenomenon is being modeled accurately or whether the calculation merely looks correct remains.

The second technique is to dispense with any hope of modeling the spiral structure of the tip region [6]. One then deletes discrete vortices from the calculation as they become part of the spiral and become separated from their neighbor by more than some

prescribed arc length. As the vortices are removed from the calculation, they are added back by increasing the circulation of one tip vortex by the appropriate amount. The results of such a calculation are shown in Figure 1.6. Again the question of whether the roll-up phenomenon is being modeled accurately or whether the calculation merely looks correct is yet to be resolved.

Although discrete vortex calculations have shortcomings, they have proven to be extremely useful in providing insight into the initial deformation of the vortex sheet from which subsequent development may be inferred. As an illustration, we again cite the calculations in Ref. 7 and show in Figure 1.7 the roll-up of a sheet into what appears to be two pairs of discrete vortices. The roll-up of two or more pairs of discrete vortices occurs quite frequently and will be discussed in Section 1.2.

1.2 The Methods of Prandtl and Betz

When the exact details of the actual roll-up are not required, two models have been developed to describe the inviscid structure of the vortex wake. The first model was due to Prandtl [10] and is based on the conservation of mechanical energy. By dotting the momentum equation with U_i, it follows that

$$\frac{\rho}{2}\frac{D}{Dt}(U_iU_i) = U_i\frac{\partial}{\partial x_j}\pi_{ij} \tag{1.3}$$

where π_{ij} is the stress tensor. If Eq (1.3) is integrated over a large volume of fluid (the bulk of the fluid being at rest) containing the airplane and the complete wake, the result is

$$\iiint_V\left[\frac{D}{Dt}\left(\frac{U^2}{2}\right) + \pi_{ij}\frac{\partial U_i}{\partial x_j}\right]d\tau = U_\infty\iint_S \pi_{1j}n_j\,d\sigma \tag{1.4}$$

where use has been made of Gauss' divergence theorem. The integral over S is carried out on the surface of the aircraft whose velocity is $U_1 = U_\infty$. When the fluid is incompressible, $\pi_{ij}\cdot\partial U_i/\partial x_j$ is only the viscous dissipation and may be neglected for high Reynolds number. The bulk of the work done on the fluid by the aircraft therefore goes into the turbulent and mean kinetic energy of the fluid. Prandtl assumed that the induced drag of the aircraft might be equated to the kinetic energy of the fluid motion in the Trefetz plane, thereby neglecting the kinetic energy of the axial velocity and turbulent fluctuations. He then calculated the kinetic energy per unit length of wake to be

$$E = \frac{\rho}{2\pi}\Gamma_o^2\left(\ln\frac{b'}{R} + \frac{1}{4}\right) \tag{1.5}$$

where it was assumed that the vortex tubes had a uniform distribution of vorticity in circles of radius R. The pair separation is b' and is fixed by the wing lift distribution. By equating Eq (1.5) to the induced drag of an elliptically loaded wing, namely,

$$D_{ind} = \frac{\pi}{8}\rho\Gamma_o^2 \tag{1.6}$$

the vortex tube radius R is determined to be approximately 8% of the wing span.

Unfortunately, the choice of the swirl velocity distribution is somewhat arbitrary, being only constrained by circulation at large radius from the vortex center and the integral constraint on kinetic energy. One might expect that the details of the span load distribution should in some way determine the swirl velocity distribution.

The second model, which overcomes the arbitrariness inherent in the Prandtl calculation, was developed by Betz [11]. Since this model and recent extensions have explained many of the observed details of vortex structure, we find it appropriate to give a somewhat more complete development than might ordinarily have been anticipated.

The Betz model was developed from the integral invariants of an incompressible, two-dimensional bounded vorticity distribution. The global integral invariants are obtained by considering the time rates of change of the following moments of the vorticity distribution:

$$\Gamma = \int \zeta\,dA \tag{1.7}$$

$$\Gamma_y = \int y\zeta\,dA \tag{1.8}$$

$$\Gamma_z = \int z\zeta\,dA \tag{1.9}$$

$$\Gamma_r = \int (y^2 + z^2)\zeta\,dA \tag{1.10}$$

where ζ is the vorticity and is defined by

$$\zeta = \frac{\partial W}{\partial y} - \frac{\partial V}{\partial z} \tag{1.11}$$

Using the continuity equation,

$$\frac{\partial V}{\partial y} + \frac{\partial W}{\partial z} = 0 \tag{1.12}$$

and the vorticity equation

$$\frac{\partial \zeta}{\partial t} + V \frac{\partial \zeta}{\partial y} + W \frac{\partial \zeta}{\partial z} = \nu\left(\frac{\partial^2 \zeta}{\partial y^2} + \frac{\partial^2 \zeta}{\partial z^2}\right) \tag{1.13}$$

it is not difficult to show that the time derivatives of Eqs (1.7) through (1.10) are zero. It has been customary to define the centroid of vorticity when $\Gamma \neq 0$ as

$$\bar{y} = \frac{\Gamma_y}{\Gamma} \tag{1.14}$$

$$\bar{z} = \frac{\Gamma_z}{\Gamma} \tag{1.15}$$

The polar moment of the vorticity distribution Γ_r divided by Γ defines a length squared, or

$$D = \left[\frac{\Gamma_r}{\Gamma}\right]^{1/2} \tag{1.16}$$

which represents the dispersion of the vorticity about the centroids $\bar{y}$, $\bar{z}$ and is also an invariant of the motion. Howard [12] has elegantly shown that no other invariants of this flow exist.

Behind an aircraft, the flow field in a plane normal to the flight direction is shown in Figure 1.8. In 1932, Betz investigated the moments of the vorticity distribution over the half plane, $y \geq 0$, using systems of point vortices in an inviscid fluid. Our colleague John E. Yates, generalized the Betz result in a viscous fluid for distributed vorticity. He showed that the time rate of change of Eqs (1.7) through (1.10) was

$$\frac{d\Gamma}{dt} = -\nu \int_{-\infty}^{\infty} \left.\frac{\partial \zeta}{\partial y}\right|_{y=0} dz \tag{1.17}$$

$$\frac{d\Gamma_y}{dt} = 0 \tag{1.18}$$

$$\frac{d\Gamma_z}{dt} = -\int_{-\infty}^{\infty}\left[\left.\frac{W^2}{2}\right|_{y=0} + \nu z \left.\frac{\partial \zeta}{\partial y}\right|_{y=0}\right] dz \tag{1.19}$$

$$\frac{d\Gamma_r}{dt} = -\int_{-\infty}^{\infty} (z - \bar{z}) \left.\frac{W^2}{2}\right|_{y=0} dz + 2\nu\Gamma \tag{1.20}$$

where the integrals which define Γ, Γ_y , Γ_z , and Γ_r are carried out over the area defined by $y \geq 0$.

Since the wake centerline is a streamline, the time rate of change of the circulation can only result from the diffusion of vorticity across the centerline as shown by Eq (1.17). The constancy of Γ_y is related to the invariance of the vertical inpulse of the fluid motion.

When viscous effects are ignored, the rate of descent of the centroid of the wake is given by

$$\frac{d\bar{z}}{dt} = \frac{1}{\Gamma}\frac{d\Gamma_z}{dt} = -\frac{1}{\Gamma}\int_{-\infty}^{\infty} \left.\frac{W^2}{2}\right|_{y=0} dz \tag{1.21}$$

For a trailing pair of irrotational vortices of strength Γ separated by spacing b' , it is not difficult to show the well-known result

$$\frac{d\bar{z}}{dt} = -\frac{\Gamma}{2\pi b'} \tag{1.22}$$

and the descent rate is constant. This is not necessarily the case when the wake is made up of two or more vortex pairs.

The polar moment or the dispersion length D is a measure of the spread of the vorticity. As can be seen from Eq (1.20), the time rate of change is related to the symmetry of the function $W(0,z,t)^2$ about $\bar{z}$ and increases due to viscous diffusion. In the absence of viscosity and when the vorticity is symmetric about $z = \bar{z}$, which is the case when the vorticity distribution is a sheet or that of a rolled-up trailing vortex, $d\Gamma_r/dt = 0$. Betz reasoned that Γ_r should not in fact change significantly during roll-up and then made the assumption that not only should Γ_r be constant when defined over the half plane but should be approximately correct locally as well. In this manner he replaced the difficult computation of the precise details of the inviscid roll-up of the vortex sheet with a local axisymmetric distribution of vorticity, so constituted and so located that "proper" consideration is given to the conservation of vorticity and moments of vorticity behind each half of the wing.

If the second moment of the vorticity is to hold locally as well as globally, Betz reasoned

$$-\int_y^s \frac{d\Gamma(\eta)}{d\eta}\,[\eta - \bar{y}(y)]^2\,dy = \int_0^r \zeta^2\,\frac{d\Gamma'(\zeta)}{d\zeta}\,d\zeta \tag{1.23}$$

$\bar{y}(y)$ is defined by

$$\bar{y}(y) = -\frac{1}{\Gamma(y)}\int_y^s \frac{d\Gamma(\eta)}{d\eta}\,\eta\,d\eta \tag{1.24}$$

and is the centroid of the vorticity trailed between the wing station y and the wing tip at $y = s$. Equation (1.23) is approximate and, as will be shown, can be manipulated to allow physical interpretations of the underlying assumptions.

When Eq (1.23) is combined with a statement of Kelvin's theorem

$$\Gamma(y) = -\int_y^s \frac{d\Gamma(\eta)}{d\eta}\,d\eta = \int_0^r \frac{d\Gamma'(\zeta)}{d\zeta}\,d\zeta = \Gamma'(r) \tag{1.25}$$

Donaldson, et al. [13], Rossow [14], and Jordan [15] have independently shown the surprisingly simple result that the relationship between r and y is

$$r = \bar{y}(y) - y \tag{1.26}$$

This result, taken with Eq (1.25), states that the value of the circulation at wing station y is the value of the circulation at radial distance r in an axisymmetric vortex. Referring to Figure 1.9, the radial distance r is equal to the distance from y to the centroid $\bar{y}$ of all the trailed vorticity outboard of y. When all the vorticity can be considered rolled up, the vortex center is located at $y = \bar{y}(0)$ in order to preserve the vertical impulse of the flow. Since, at this point, r also equals $\bar{y}(0)$, the circular regions containing vorticity just touch along the aircraft centerline.

The Betz model has now been checked against measurements made behind model and full-scale aircraft. In Figure 1.10 the computed swirl velocity distribution is compared with measurements made by Versteynen and Dunham [16] behind a C5A aircraft. As can be seen, the Betz model predicts distributions which are in far better agreement than the Prandtl model. Further comparisons will be given after we have discussed recent extensions of the Betz method.

The approximations which underlie the Betz method are identified by the manipulation of the roll-up relations. Equation (1.23) is multiplied by $-\rho U_\infty/2$ and integrated by parts to yield

$$\frac{\rho U_\infty}{2}\left\{\Gamma(y)[y - \bar{y}(y)]^2 - \Gamma'(r)r^2\right\} + \int_y^s \ell(\eta)[\eta - \bar{y}(y)]d\eta = 2\pi\rho U_\infty \int_0^r v(\xi)\xi^2 d\xi \tag{1.27}$$

where $\ell(y) = -\rho U_\infty \Gamma(y)$ is the sectional wing loading exerted on the fluid. The first term in Eq (1.27) vanishes when (1.25) and (1.26) are substituted. The remaining terms prescribe the distribution of angular momentum in the vortex. The model distributes the angular momentum such that the torque exerted by the wing (calculated about $\bar{y}(y)$) between wing station y and the tip equals the axial flux of angular momentum through a circle of radius r. To extend the Betz model to include the effect of nonuniform axial velocity, Eq (1.27) was modified to read

$$\int_y^s \ell(\eta)[\eta - \bar{y}(y)]\,d\eta = 2\pi\rho \int_0^r U(\xi)v(\xi)\xi^2 d\xi \tag{1.28}$$

Introduction of the unknown $U(r)$ into the problem requires that an additional relationship be provided. The axial momentum equation provides this relationship and in this manner couples wing drag to vortex structure.

The discussion of the Betz method to this point has considered wing load distributions whose trailed vortex sheets proceed to roll up from the tip with $r = \bar{y}(y) - y$ a monotonic function of y in the interval $0 \le y \le s$. This may not always be the case when the aircraft is in an unclean configuration (during landing and takeoff when flaps, etc. are deployed). That r may not be a single-valued function of y is easily shown by a geometric argument. First we calculate the rate of change of r as y is varied. Differentiating Eq (1.26) with respect to y yields

$$\frac{dr}{dy} = \frac{d\bar{y}}{dy} - 1 \tag{1.29}$$

From the definition of $\bar{y}$, we may obtain an expression for $d\bar{y}/dy$; substituting this into (1.29) yields

$$\frac{dr}{dy} = -\frac{(\bar{y} - y)}{\Gamma}\frac{d\Gamma}{dy} - 1 \tag{1.30}$$

Now, to have a conventional roll-up as y decreases from the tip, r increases. Therefore, a conventional roll-up is possible if

$$-\frac{\bar{y} - y}{\Gamma}\frac{d\Gamma}{dy} < 1 \tag{1.31}$$

In Figure 1.11 a load distribution typical of a flapped wing is shown. If the tangent to the load distribution at point P is drawn, it is easy to see that this line intersects the $\Gamma = 0$ axis at $y = y^*$. The distance $|y^* - y|$ is given by

$$|y^* - y| = \left|\frac{\Gamma}{d\Gamma/dy}\right| \tag{1.32}$$

The location of the centroid of the vorticity outboard of point P is $\bar{y}(y)$. Comparing the ratio of $|\bar{y} - y|$ and $|y^* - y|$ and in light of Eq (1.32), it is clear that

$$\left|\frac{\bar{y} - y}{\Gamma}\frac{d\Gamma}{dy}\right| = \left|\frac{\bar{y} - y}{y^* - y}\right| \tag{1.33}$$

A conventional roll-up has $y^* > \bar{y}$. Also $\bar{y} > y$ and $d\Gamma/dy < 0$ so that

$$-\frac{\bar{y} - y}{\Gamma}\frac{d\Gamma}{dy} = \frac{\bar{y} - y}{y^* - y} < 1 \tag{1.34}$$

Therefore, the condition for a single roll-up is seen to be that $y^*(y)$ always remains outboard of $\bar{y}(y)$ as y decreases from the tip.

From this discussion, we see that for the load distribution shown any attempt to apply the roll-up relations much inboard of point P will result in multivalued behavior of the function $r(y)$. For this case, this behavior may be avoided if we consider the roll-up of not one but two vortices. In Figure 1.12, we have sketched the wake which will result from the flapped load distribution shown in Figure 1.10. If the Betz method is to be modified to compute the structure of "interior" vortices, it is clear from this sketch that two questions must first be resolved; namely,

1. Where does roll-up originate or what portion of the sheet forms the center of an "interior" vortex?
2. Where does the vortex sheet trailed from the wing divide itself into tip and "interior" vortices?

The answer to the first question is to take the origin of roll-up to be the station at which the sheet strength $-|d\Gamma/dy|$ is maximum. This would seem logical — maximum sheet strength corresponding to a maximum in vorticity which becomes the center of the vortex. The answer to the second question, however, is not straightforward. As an engineering approximation, the locations at which the minimum of the absolute value of sheet strength occurs were taken to be the locations at which the vortex sheet divides itself. These assumptions are shown in Figure 1.13 where the load distribution shown is one which will produce three vortices. Roll-up proceeds from the maximums of sheet strength at wing stations y_{mC}, y_{mB}, and $b/2$, and the sheet divides itself at the local minimums of $|d\Gamma/dy|$. The vorticity shed between points B and C rolls up into a fuselage vortex, between points A and B into a flap vortex, and outboard of A into a tip vortex.

This rule of thumb for dividing the lift distribution has recently been checked by Yates [17] who has calculated the initial inplane accelerations of a two-dimensional vortex sheet. His results are summarized in Figure 1.14 where it is shown that the centers of roll-up are in exact agreement. The locations at which the sheet divides are predicted within the accuracy generally associated with the computation of wing load distributions.

To proceed to extend the method of Betz to include "interior" roll-ups, we first assume that each vortex in a multiple vortex wake develops without significantly interfering with the roll-up of the other vortices. The accuracy of such an assumption unfortunately is difficult to check but is surely most correct during the early stages of roll-up and is one which has been used by Betz.

If we now apply the Betz assumptions to an "interior" vortex (for example, the flap vortex in Figure 1.15), we may write

$$\int_{y_1}^{y_2} \ell(\eta)(\eta - \bar{y}_{12})d\eta = \int_0^r \rho\xi v(\xi)U(\xi)2\pi\xi\, d\xi \tag{1.35}$$

where

$$\bar{y}_{12} = \frac{1}{\Gamma(y_2) - \Gamma(y_1)}\int_{y_1}^{y_2} \eta\frac{d\Gamma}{d\eta}\, d\eta \tag{1.36}$$

$\bar{y}_{12}$ is the centroid of the trailed vorticity between wing stations y_1 and y_2 which are, for the present, the arbitrary points inboard and outboard of y_{mB}, respectively. Equation (1.35) states that the torque exerted by the wing on the fluid between wing stations y_1 and y_2 (computed about $\bar{y}_{12}$) equals the axial flux of angular momentum through a circle of radius r.

A consequence of Kelvin's theorem is that

$$\Gamma(r) = \Gamma(y_1) - \Gamma(y_2) \tag{1.37}$$

However, unlike the roll-up of a tip vortex where $y_2 = b/2$, a relationship between y_1 and y_2 is needed. This relationship is taken to be

$$(y_2 - \bar{y}_{12})^2 = (y_1 - \bar{y}_{12})^2 \tag{1.38}$$

and is one which specifies how the vorticity enters the "interior" vortex from each side of the sheet. Differentiating Eq (1.35) and using (1.38), one obtains the simple result that

$$U_\infty d(y_1 - \bar{y}_{12})^2 = U(r)\, dr^2 \tag{1.39}$$

Setting $y_1 = y$ and $y_2 = b/2$ yields

$$U_\infty d(y - \bar{y}(y))^2 = U(r)\, dr^2 \tag{1.40}$$

and the connection with the Betz result, Eq (1.26), is clear.

Before coupling the wing drag distribution to the axial velocity in the vortex, it is possible to determine the swirl velocity $v(0)$ at the center of the vortex. Assuming $U(0)$ is finite, Eq (1.39) may be integrated for small r to yield

$$r = \left[\frac{U_\infty}{U(0)}\right]^{1/2} (\bar{y}_{12} - y_1) \tag{1.41}$$

as $r \to 0$. The tangential velocity for the "interior" vortex is

$$v(r) = \frac{\Gamma'(r)}{2\pi r} = \frac{\Gamma(y_1) - \Gamma(y_2)}{2\pi r} \tag{1.42}$$

As $r \to 0$,

$$v(0) = \frac{1}{2} \left.\frac{d\Gamma}{dy}\right|_{y=y_m} \left.\left(\frac{dy_1}{dr} - \frac{dy_2}{dr}\right)\right|_{y_1=y_2=y_m} \tag{1.43}$$

Calculating dy_1/dr and dy_2/dr from Eq (1.39) and substituting these values into (1.43) yields

$$v(0) = -\frac{1}{\pi}\left[\frac{U(0)}{U_\infty}\right]^{1/2} \left.\frac{d\Gamma}{dy}\right|_{y=y_m} \tag{1.44}$$

It may be shown that this relationship holds for a tip vortex if $d\Gamma/dy$ is evaluated at $y = b/2$. This result is significant and shows how the exact behavior of the load at the position where roll-up initiates has a profound effect on the inviscid swirl velocity at the center of the vortex. The effect of axial velocity on the centerline swirl velocity is somewhat weaker, going as the axial velocity ratio to the 1/2-power. For both interior and tip vortices, deficits in axial velocity $(U(0)/U_\infty < 1)$ result in a reduction of the inviscid centerline swirl velocity.

We now turn our attention to coupling the axial velocity in the vortex to the wing drag distribution. Making an axial momentum balance across a "cylindrical" control volume of radius r containing the portion of the wing between stations y_1 and y_2 yields

$$\int_{y_1}^{y_2} c_d(\eta)c(\eta)q\, d\eta = -2\pi \int_0^r [p + \rho U(\xi)(U(\xi) - U_\infty)]\xi\, d\xi \tag{1.45}$$

where the axial velocity of the fluid entering the "cylindrical" control surface is approximated by U_∞. The section drag coefficient and the wing chord are c_d and c, respectively. When the U^2 term is linearized and $y_2 = b/2$, Eq (1.45) is that given by Brown [18]. Equation (1.45) is approximate and is written in the same spirit as the statement regarding the axial flux of angular momentum, Eq (1.35). That is, it assumes that the wing drag distributes itself in the rolled-up vortex in the same manner as the trailed axial vorticity. As discussed by Brown, the assumption is a natural one since the axial vortex lines and the viscous wake are one and the same. The wing profile drag is therefore included in Eq (1.45) correctly. However, the effect of induced drag is only approximated in that the force on the control volume outside of the vortex tubes is neglected. That is to say that the effect of drag is only manifested in the fluid containing vorticity in the far wake.

Differentiating Eq (1.45) and substituting (1.39) yields

$$c_d(y_1)c(y_1) - c_d(y_2)c(y_2)\frac{dy_2}{dy_1} = \pi U_\infty \left[\frac{p}{U} + \rho(U - U_\infty)\right] \frac{d(y_1 - \bar{y}_{12})^2}{dy_1} \tag{1.46}$$

The appropriate axial momentum equation for a tip roll-up is obtained by setting $dy_2/dy_1 = 0$. The nonuniform pressure in the vortex is primarily a result of the swirl and may therefore be calculated from

$$p = -\frac{\rho}{4\pi^2}\int_r^\infty \frac{\Gamma'^2}{\xi^3}\,d\xi \tag{1.47}$$

Equations (1.39), (1.46), and (1.47) taken with the boundary conditions

$$\left.\begin{aligned} p\big|_{y_1=y_A} &= -\frac{\rho}{2}\,v^2\big|_{y_1=y_A} \\ r\big|_{y_1=y_m} &= 0 \end{aligned}\right\} \tag{1.48}$$

form the coupled system of nonlinear equations to be solved. These equations determine the inviscid axial and swirl velocities in either an "interior" or tip vortex given the lift and drag distribution over the appropriate portion of the wing from which the vortex develops.

When one considers all the assumptions which have been used to develop the Betz method and extensions, it is perhaps wise to restate that the above relations which have been derived to calculate roll-up are only an approximate model of the actual phenomenon. This is not to say that they cannot describe the vortex wake of an aircraft. As will be shown, measured wake velocity distributions are, in many cases, adequately predicted by these methods so that, undoubtedly, the Betz model contains much of the physics of the roll-up phenomenon.

Nonlinearity and the nature of the boundary conditions dictate that, in general, the roll-up equations must be solved numerically. It is therefore appropriate to find an analytic solution which illustrates the effect of wing drag on vortex structure. For simplicity, we assume the wing load distribution and axial velocity in the vortex to be

$$\Gamma = \Gamma_0(1 - y/s) \tag{1.49}$$

$$U = U_\infty[a_1 + a_2(r/R)^2] \tag{1.50}$$

respectively. The constants a_1 and a_2 are chosen so that $U > 0$ since negative axial velocities would imply an axial flux of angular momentum from downstream and violate the assumptions implicit in Eq (1.35).

The details of the computation may be found in Ref. 18 and the results are summarized in Figure 1.16. Clearly, wing drag results in axial velocity defects and enlarged regions containing trailed vorticity. It is important to remember that since the lift distribution is unchanged, the total axial flux of angular momentum from the region containing axial vorticity is not changed. Therefore, the intensity of the vortex, as measured by the flux of angular momentum, is unchanged by drag. The deintensification which does in fact occur is brought about by redistributing the angular momentum outward so that small encountering aircraft could interact with less of the vortex. As drag is likely to result in higher turbulence levels in the vortex, it is likely that the outward redistribution of angular momentum, as calculated here, is further aided by turbulent processes.

Before comparing the Betz model and its extensions to experimental results, we present one last piece of information which has been gleaned from the Betz result. It has been possible to estimate the time required to roll up a two-dimensional sheet of vorticity. The model that has been used is shown in Figure 1.17. The time rate of change of circulation in the rolled-up vortex is given by

$$\frac{d\Gamma'}{dt} = \left[v - \frac{d\bar{y}_v}{dt}\right]\gamma\left(\bar{y}_{v,t}\right) \tag{1.51}$$

where v is the horizontal velocity at station A induced by the vorticity and γ is the vortex sheet strength at station A. The term $d\bar{y}_v/dt$ accounts for the inward motion of the vortex as roll-up proceeds. Estimates of v, $d\bar{y}_v/dt$, and $\gamma(\bar{y}_{v,t})$ are given in Ref. 19 along with details of the computation. The results for elliptic, parabolic, and linear wing loadings are shown in Figure 1.18. For an elliptic load distribution, nearly 90% of the circulation is rolled up when $x/b \approx \pi A/2C_L$. Recall that our original order of magnitude arguments were $x/b \sim \mathcal{O}(A/C_L)$.

In Figure 1.19 a comparison is shown with the discrete vortex calculations made by Moore [6]. The discrepancy is believed to be explained in part by the fact that Moore has chosen the station past which the sheet is to be considered rolled up at a location 90° in the counterclockwise sense from station A in Figure 1.17. His results are, therefore, biased to be lower.

1.3 Comparison with Experimental Measurements

Undoubtedly motivated by the wake hazard problem, many measurements of the velocity distributions in trailing vortices are appearing in the literature. Unfortunately, since the Betz method did not receive widespread attention until recently and due to the difficulty of making these measurements, wing load distributions for the most part were not determined. For simply loaded wings (load distributions which trail a one-pair wake) at high Reynolds number, lifting surface theory has proved adequate for most purposes.

One of the earliest checks of the Betz model was made by Donaldson [20]. Shown in Figure 1.20 is the swirl velocity in the wake of an Army O-1 aircraft as measured by McCormick [21]. By assuming the load distribution on the wing to be elliptic, the swirl velocity has been computed with the Betz model. As can be seen, the agreement is quite satisfactory.

If we now compare the vorticity distributions calculated from Betz and the more familiar Prandtl models, it is possible to explain an experimental observation that appears to have created some misunderstandings in the past. That is, that the circulation in the wake as calculated by integrating the measured vorticity distribution appears not to add up to Γ_o . The vorticity distributions for the velocities shown in Figure 1.20 are shown in Figure 1.21. It is seen that the Betz model has a rather large spike of vorticity near $r = 0$ and, outward of $r/b = 0.05$, a long tail. It is an unfortunate fact for the experimentalist that only 54% of the circulation is found in $r/b < 0.05$. In all probability, it is for this reason that several investigators [22, 23] have failed to account for the total bound circulation on the wing. The more the load distribution departs from uniform loading, the more the Betz model predicts the vorticity will be widely distributed.

Measurement of the swirling velocities in the vortices of full-scale aircraft has been undertaken by the Federal Aviation Administration at their National Aviation Facilities Experimental Center, Atlantic City, New Jersey. Here a tower is instrumented with hot film anemometry, sensitive to velocities in a plane perpendicular to the flight direction. The aircraft follows a flight path perpendicular to the prevailing wing, and the resulting wake is convected downward and with the wind across the tower. Details of the tests may be found in Ref. 24; some of the results are presented here. Measured and computed swirl velocity distributions are shown in Figures 1.22 and 1.23 for the DC-7 aircraft in landing and takeoff configurations, respectively. Results for the C-141 aircraft in holding, landing, and takeoff configurations are shown in Figures 1.24 through 1.26, respectively. Wing lift distributions were supplied by the aircraft manufacturers. The probe orientation is such that half of the vortex is attacking (tangential velocities directed towards) the probe (solid curve) and half the vortex is in the wake of the probe (dashed curve); therefore the solid curves are deemed more accurate. As can be seen, the agreement is satisfactory.

More recently, an investigation has been made in the wake behind a flapped wing [25]. Here the load distribution on the wing was determined from both pressure taps on the wing and lifting surface theory. One configuration tested had a 1/3 semispan inboard flap deflected 30°. The load distribution for this case is shown in Figure 1.27. As can be seen, the load distribution from lifting surface theory is substantially different from that determined from surface pressure measurements. In Figures 1.28 through 1.31 the horizontal V and vertical W velocities are shown for the tip and flap vortex measured 10 chords downstream. Traverses were made across the vortices at constant elevation z . Considering that the measurements could only be made at modest downstream distances due to the unsteadiness of the vortex positions (vortex meander), the agreement is again quite reasonable. Additional swirl velocity measurements and comparisons with the Betz model may be found in Refs. 25 through 27.

The effect of distributed drag is difficult to check experimentally against the extended Betz model. This difficulty is three-fold. First, the most significant change in the structure of the vortices as a result of drag occurs at the vortex center. This is a consequence of the fact that as roll-up proceeds, the vortex sheet is spread over an ever-increasing area. It is therefore primarily the drag at the wing station where roll-up initiates that will be centered in the downstream vortex. It is of great importance, then, to have accurate knowledge of the wing lift and drag distributions at the wing stations where roll-up initiates. Second, even if it were possible to accurately determine these distributions, it is doubtful that an inviscid model will be adequate to predict detailed structure in a region highly dominated by viscous transport. This is clearly suggested by the observation that the small r structure of the swirling velocity distribution is always proportional to r and quite naturally defines what has come to be called the viscous core region of the vortex. Last, it is pointed out that velocity measurements near the center of a vortex are extremely difficult to make with any degree of confidence due to the problem of vortex meander [27, 28, 29].

Experience suggests that at cruise the effect of distributed wing drag is not significant. However, when an aircraft is in landing or takeoff configuration, the effect of wing drag can be significant, particularly on the structure of "interior" or flap vortices. The computed wing lift and drag distributions of a large jetliner in a landing configuration are shown in Figure 1.32. The computed swirl velocity distribution as computed with the extended Betz method with axial velocity equal to U_∞ is shown in Figure 1.33. The effect of distributed wing drag on the structure of the flap vortices (vortex 2 and 4) and on the tip vortex is shown in Figures 1.34 through 1.36, respectively. As can be seen, drag has little effect on the tip vortex since, on conventional wings, the drag drops to zero smoothly at the tip. It is not known at this time how significant a role wing drag may play in the ultimate turbulent decay of the wake, but the inviscid wake models considered here strongly suggest that any attempt to deintensify a wake solely through increased wing drag will result in a substantial penalty in terms of power needed.

To summarize this section, we have discussed models which are being used to predict the inviscid structure of the discrete vortices which comprise the aircraft wake. We have shown that the method of Betz gives a good description of the vortex structure at distances behind the aircraft where turbulent mechanisms have not had time to act. While the role of wing lift and drag distributions on vortex structure is reasonably well understood, the effect of jet exhaust has yet to be explored in detail. Within the Betz framework, it is now possible to access wake deintensification devices, such as spoilers, slats, and

flaps in terms of the modifications they make to the lift and drag distributions on the wing. Inherent in the Betz method is the fact that any device which affects only the wing drag distribution and leaves the lift distribution unchanged does not change the axial flux of angular momentum in the rolled-up vortex tube.

2. AIRCRAFT WAKE GEOMETRY

To complete the description of the inviscid wake, there remains the determination of the positions of the discrete vortices in the wake or the determination of what we shall call wake geometry. When the wing is simply loaded (i.e., cruise configuration), one vortex pair is trailed and the wake geometry is easily described. The vortices of strength Γ are separated by $2\bar{y}(0)$ and descend downward with velocity $\Gamma/4\pi\bar{y}(0)$. However, when the aircraft is operating in a landing or takeoff configuration, wake geometry can become quite complicated. Here, flaps, slats, and spoilers may be deployed such that the wing lift distribution may depart significantly from the cruise distribution. As we have shown, under such circumstances, the resulting wake contains multiple vortex pairs. In an attempt to gain qualitative information regarding wake geometry, a simple lumped vorticity model is used to estimate discrete vortex positions.

2.1 Lumped Vorticity and the Approximations Involved

In Section 1 a criterion was given which determines the number and strength of the vortices which will ultimately inviscidly roll up behind the aircraft. The idea here will therefore be to model each discrete vortex by one irrotational, two-dimensional point vortex insofar as one is only interested in obtaining information regarding the position of the vortices. It is prudent to discuss what approximations are implied by this model.

The assumption of two-dimensionality is easily justified, provided streamwise gradients are small. Under this condition, we may determine the equivalence between time and downstream distance through $x = U_\infty t$. Streamwise gradients are necessarily $\mathcal{O}(W/U_\infty)$ where W is a characteristic downwash velocity in the wake and is $\mathcal{O}(\Gamma/b)$. Therefore, streamwise gradients are $\mathcal{O}(C_L/A)$ and are safely neglected under most circumstances. A qualification is added here with regard to the phenomena of sinusoidal instability and vortex breakdown where axial gradients play a subtle role. These phenomena will be discussed separately in the next section, and the approximation of two-dimensionality appears appropriate when one is only interested in determining vortex positions.

Treating the vorticity as though it were concentrated at a point is a somewhat more subtle concept whose justification lies in the fact that the motion of a vortex tube with straight vortex lines does not depend critically on the cross-section of the tube. To see this, we compute the velocity of the centroid of a tube of vorticity

$$\frac{d\vec{r}_c}{dt} = \frac{\int \vec{r}\, \partial\zeta/\partial t \, dA}{\int \zeta \, dA} \tag{2.1}$$

where $\vec{r} = y\hat{j} + z\hat{k}$ and the integrals are taken over the vorticity distribution in question. Substituting the vorticity and continuity equation into Eq (2.1), it is not difficult to show that

$$\frac{d\vec{r}_c}{dt} = \frac{\int \vec{U}\zeta \, dA}{\int \zeta \, dA} \tag{2.2}$$

where $\vec{U}$ is the fluid velocity. $\vec{U}$ may be thought to be the sum of two contributions: $\vec{U}_o$ and $\vec{U}_s$. The velocity $\vec{U}_o$ is that field due to the presence of other distant and discrete concentrations of vorticity, while $\vec{U}_s$ is the velocity field which is induced from the vorticity concentration in question. $\vec{U}_s$ is computed from the well-known Biot-Savart law

$$\vec{U}_s = -\frac{1}{2\pi}\int \frac{\vec{r} \times \zeta(y',z')dA(y',z')}{r^2} \tag{2.3}$$

where $\vec{r} = (y - y')\hat{j} + (z - z')\hat{k}$. It is not difficult to show that

$$\int U_s \zeta \, dA = 0 \tag{2.4}$$

and, therefore,

$$\frac{d\vec{r}_c}{dt} = \frac{\int \vec{U}_o \zeta \, dA}{\Gamma} \tag{2.5}$$

The velocity of the centroid of vorticity is proportional to the irrotational velocities from other discrete distributions of vorticity averaged with the vorticity over the area.

The velocity field of an irrotational point vortex of strength Γ at position (y_1, z_1) is

$$V = -\frac{\Gamma}{2\pi}\left[\frac{(z - z_1)}{(y - y_1)^2 + (z - z_1)^2}\right] \tag{2.6}$$

$$W = \frac{\Gamma}{2\pi}\left[\frac{(y - y_1)}{(y - y_1)^2 + (z - z_1)^2}\right] \tag{2.7}$$

Therefore, the motion of the j^{th} vortex (equivalently the centroid of the j^{th} vortex) in a system of n point vortices is given by

$$\frac{dy_j}{dt} = -\frac{1}{2\pi}\sum_{i(\neq j)}^{n}\frac{\Gamma_i(z_j - z_i)}{r_{ij}^2} \tag{2.8}$$

$$\frac{dz_j}{dt} = \frac{1}{2\pi}\sum_{i(\neq j)}^{n}\frac{\Gamma_i(y_j - y_i)}{r_{ij}^2} \tag{2.9}$$

where $r_{ij}^2 = (y_i - y_j)^2 + (z_i - z_j)^2$. The exclusion in the summation is a consequence of the fact that a vortex induces no motion on its own centroid (Eq. (2.5)).

2.2 The Wake Geometry of Multiple Pair Wakes

The equations governing the motion of the vortex centroids simplify somewhat since aircraft vortices occur in pairs and are located symmetrically about the aircraft centerline. Figure 2.1 illustrates the general geometry. However, even with this simplification, vortex trajectories must often be obtained by numerical calculation.

We have discussed four invariants of a two-dimensional, incompressible, rotational fluid motion: circulation, centroid, dispersion, and kinetic energy. The constancy of circulation computed about each vortex is assured by Kelvin's theorem, while the horizontal centroid of the half-plane distribution of vorticity is proportional to the vertical impulse of the fluid. That is,

$$J = \sum_{1}^{n}\Gamma_i y_i \tag{2.10}$$

is a constant. The dispersion length D in the half plane is not, strictly, an invariant and does not provide as much useful information as does the kinetic energy which is a strict invariant.

It is appropriate now to point out that the kinetic energy of the system of vortex pairs is, in fact, infinite. This is easily seen since the kinetic energy of the fluid in a circle of radius ε centered about one vortex is proportional to

$$\int_0^{\varepsilon}\frac{dr}{r} \tag{2.11}$$

The logarithmic singularity results from concentrating the vorticity at a point in the flow field. To eliminate this singularity, it is convenient to subtract out the kinetic energy in a small circle of radius ε about each vortex. It is then not difficult to show that the kinetic energy is

$$T = -\rho\pi\left[\sum_{j}^{n}\sum_{\substack{i\\(i\neq j)}}^{n}\Gamma_j\Gamma_i \log r_{ij} + \sum_{j}^{n}\frac{\Gamma_j^2}{(2\pi)^2}\log\varepsilon\right] \tag{2.12}$$

The first term is that portion of the kinetic energy associated with the relative positions of the vortices and is proportional to the Kirchhoff-Routh path function [30]. If Eqs (2.8) and (2.9) are combined so as to eliminate time, it is not surprising to find that T is an integral of the resulting equation.

If we concern outselves for the moment with two vortex-pair wakes, it becomes apparent that Eqs (2.10) and (2.12) provide sufficient information to determine all possible relative trajectories. Equation (2.12) can be written in the form

$$B = \frac{e^2 + (y_1 + y_3)^2}{e^2 + (y_1 - y_3)^2}(y_3)^{\Gamma_3/\Gamma_1}(y_1)^{\Gamma_1/\Gamma_3} \tag{2.13}$$

where e is one-half the vertical separation between the pairs. Also y_1 or y_3 may be eliminated from Eq (2.13) by substituting (2.10). The constant B may be evaluated with $e = 0$; that is, when the vortices are in the plane of the wing.

The obvious question is, "For what values of J (Eq (2.10)) and B are trajectories which have $e \to \infty$ possible?" This investigation yields what might be called a "wake classification chart" as shown in Figure 2.2 and suggests that two-pair wakes may be classified such that they fall into one of four categories:

1. The pairs are of the same sign and remain together.
2. The pairs are of the same sign and separate.
3. The pairs are of opposite sign and remain together.
4. The pairs are of opposite sign and separate.

Wakes which fall into Category 1 are most typical of conventional aircraft with one set of flaps deployed, while wakes in Category 2 may result on aircraft with an inboard blown flap. Figures 2.3 through 2.6 show trajectories computed for the four cases denoted by Roman numerals I, II, III, and IV on Figure 2.2. As can be seen, the predicted geometry of the resulting wakes from the various wake categories differs significantly.

When wing lift distributions are such that more than two vortex pairs are trailed, the only recourse appears to be numerical integration of the trajectory equations. Figures 2.7 through 2.9 show the computed wake geometry for a large jetliner in the landing configuration (the wing lift distribution is shown in Figure 1.32). As can be seen from Figures 2.8 and 2.9, some care must be exercised when interpreting these results. Whether the breaking away of the rather weak fuselage and inboard flap vortices will ever be observed in practice is highly speculative, and it is likely that rather weak concentrations of vorticity do not remain distinct but become dispersed about stronger vortices. There is mounting evidence that this dispersion does in fact occur and may even occur between vortices of equal strength. The turbulent merging of vortices is a phenomenon important to the rate of turbulent decay of the wake and will be discussed in Section 4 when we consider the aging of vortices.

3. SINUSOIDAL INSTABILITY AND VORTEX BREAKDOWN

Sinusoidal instability and vortex breakdown are phenomena which result in wake deintensification, the former by causing the trailing pair to pinch off and take ring-like forms (see, for instance, MacCready [31]) and the latter by outwardly redistributing the angular momentum in the trailing vortex. While the phenomenon of sinusoidal instability for single vortex pairs is well understood, to date there is no generally accepted explanation of vortex breakdown. In this section, we will briefly review the mechanisms which result in sinusoidal instability and give an explanation of vortex breakdown based on the phenomenon of wave trapping.

3.1 Sinusoidal Instability

Sinusoidal or the Crow instability (as it is now called after Crow [32] who first investigated the phenomenon) is a convective instability which arises by balancing the self-induced rotation of a sinusoidally deformed vortex with the velocity induced at this vortex by the deformed and descending opposed vortex. The divergence of the trailing pair occurs in planes tipped from the horizontal, as shown in Figure 3.1. The theory for sinusoidal instability is now quite well understood. Widnall, Bliss, and Zalay [33] have examined the problem in detail and were able to determine the way in which amplification rates of the instability depend on details of the vortex tube structure. One result of this analysis was to indicate that the presence of axial velocity reduces this instability of the vortex wake. Moore [34] has numerically followed the sinusoidal instability to completion.

The physical mechanisms responsible for sinusoidal instability can be understood by first examining the motion of a line vortex whose centerline is given an in-plane sinusoidal perturbation. The deformed vortex is shown in Figure 3.2. The lines outlining the vortex tube may be thought of as the boundaries in which much of the axial vorticity is found. In cross section A, the effect of stretching vortex lines as a result of bending is illustrated. Vortex filaments located at $y' > 0$ are lengthened and result in positive perturbations of axial vorticity, while those filaments located at $y' < 0$ are shortened, resulting in negative perturbations. The perturbation flow field in the cross-flow plane is dipole-like. However, this induced flow field implies that fluid in the vortex tube would leave the rotational region. The vortex therefore rotates in a counterclockwise sense with angular velocity sufficient to close the streamlines about the rotational tube (when viewed by an observer sitting on the vortex). To lowest order, the sinusoidally perturbed vortex preserves its shape. The motion is referred to as the self-induced motion of a bent filament. Kelvin [35] first described the motion as the retrograde mode in his study of wave motion on line vortices.

Sinusoidal instability results when the cross-flow about the deformed vortex has a velocity component U_T, which balances the self-induced rotation, and a radial component which results in a planar divergence. When the trailing pair is undeformed, the velocity field induced about a vortex from the opposing vortex is a stagnation point flow field (cross-section B) where a uniform upward velocity has been added to cancel the descent of the pair. When the vortex is perturbed, the induced cross-flow from the distant vortex is, locally, to first approximation, a constant perturbation velocity. The direction and magnitude of this velocity is a function of the position of the perturbed vortex. If one component of this velocity cancels the self-induced rotation of the deformed vortex and the other component carries the vortex away from its unperturbed position, Crow instability occurs. The divergence occurs in planes tipped at angle θ where $0 < \theta < \pi/2$, maximum amplification occurring with $\theta \simeq \pi/4$. The instability is exponential in time, and amplification rates are given in Figure 3.3. Since the component of velocity which results in the divergence is induced by the distant vortex and is $\mathcal{O}(\Gamma/2\pi b')$, the time scale of the instability is $\mathcal{O}(2\pi b'^2/\Gamma)$ where b' is the undisturbed trailer separation. An asymmetric form of instability is also predicted by theory; however, it has not been observed on aircraft trailing vortices.

3.2 Vortex Breakdown

Vortex breakdown or vortex bursting may be described as the abrupt structural change of the tube of a vortex which is precipitated on a smooth flow (one with small axial gradients) seemingly for no reason. Peckham and Atkinson [36] first observed the phenomenon over leading edge vortices on a gothic wing. Vortex breakdown on aircraft trailing vortices was first observed by Smith and Beesmer [37] who were involved in studies to

suppress condensation trails from B-47 aircraft. The importance of the phenomenon as related to the eventual decay of aircraft vortices is two-fold. Breakdown outwardly redistributes the angular momentum of the vortex and also often results in a very turbulent flow. Redistribution of the angular momentum is not likely to be important in terms of the rolling moment induced on an encountering aircraft unless the flow field is changed on a length scale commensurate with the encountering aircraft's wing span. The introduction of turbulence is important in that turbulent decay is the dominant mechanism of dissipation in the absence of sinusoidal instability.

3.2.1 *Wave Trapping*

The phenomenon of vortex breakdown has, since 1957, been the subject of many investigations. An excellent review of the subject through 1972 can be found in Ref. 38. Recently, however, the concept of wave trapping (see Landahl [39]) has supplied the physical mechanisms from which a wave mechanical explanation of breakdown can be given. As we shall see, this mechanism is one which can explain the significant features of the phenomenon. It will be our purpose here to discuss this mechanism. A more complete treatment may be found in Refs. 40 and 41.

Fundamental to the phenomenon of vortex breakdown is the property of vortices to support highly dispersive inertial waves. This property was recognized as early as 1880 by Kelvin [35] who investigated the wave motion on a vortex tube of uniform axial vorticity. The general problem of infinitesimal amplitude wave motion on a vortex with arbitrary swirl and axial velocity distributions has been formulated by Chandrasekhar [42]. Unfortunately, the resulting eigenvalue problem is one which, in general, requires numerical solution.

Several swirl velocity distributions, however, lend themselves to analysis and contain the essential characteristic of a real vortex, namely, a central region containing a large concentration of vorticity. One such vortex in polar coordinates (r,θ,z) with velocity components (u,v,w) is

$$v = \Omega r \qquad r < R \tag{3.1}$$

$$v = \Omega \frac{R^2}{r} \qquad r > R \tag{3.2}$$

The radial dimension R characterizes the region containing the axial vorticity. It is associated with the vortex tube radius and is not to be confused with the viscous core radius. The axial velocity is taken to be w_o, a constant. The wave motion on this vortex has received the attention of several investigators [35, 40, 43, 44, 45].

The inviscid incompressible equations of motion are perturbed in cylindrical coordinates and perturbations are assumed of the form

$$f(r) \exp i(kz + m\theta + \omega t) \tag{3.3}$$

k is the axial wave number, m the integer azimuthal mode number, and ω the circular frequency. The resulting eigenvalue problem has nontrivial solutions provided that the dispersion relation

$$\omega = \omega(k,m,R,\Omega,w_o) \tag{3.4}$$

is satisfied. This dispersion relation determines ω as a function of k.

In the long wave limit $(kR \to 0)$, it can be shown that

$m = 0$

$$\frac{\omega}{\Omega} = -\frac{kw_o}{\Omega} + \frac{2kR}{\alpha_{o,n}}\left[1 + \frac{(kR)^2 \ln|kR|}{2\alpha_{o,n}^2}\right] + \ldots \tag{3.5}$$

$m = \pm 1$

$$\frac{\omega}{\Omega} = -\frac{kw_o}{\Omega} + \frac{m}{2}(kR)^2\left[+\frac{1}{4} + \ln 2 - \gamma - \ln|kR|\right] + \ldots \tag{3.6}$$

$$\frac{\omega}{\Omega} = -\frac{kw_o}{\Omega} - m + \frac{2kR}{\alpha_{1,n}}\left[1 + \frac{4}{\alpha_{1,n}^2} - \frac{(kR)^2}{2\alpha_{1,n}^2}\right] + \ldots \tag{3.7}$$

$m = \pm 2$

$$\frac{\omega}{\Omega} = -\frac{kw_o}{\Omega} + \frac{|m|}{m}(1 - |m|) + \frac{(kR)^2}{3m} + \ldots \tag{3.8}$$

$$\frac{\omega}{\Omega} = -\frac{kw_o}{\Omega} - m + \frac{2kR}{\alpha_{2,n}}\left[1 + \frac{4}{\alpha_{2,n}^2} - \frac{(kR)^2}{2\alpha_{2,n}^2}\right] + \ldots \tag{3.9}$$

$m = \pm 3$

...

Here $\alpha_{|m|,n}$ is obtained from $J_{|m|}(\alpha_{|m|,n}) = 0$ where the roots $\alpha = 0$ are to be excluded, and $\gamma = 0.577$ is Euler's constant. As can be seen for each k and azimuthal mode number m, there still exists an infinite number of inertial wave modes. Presumably, however, it is only the modes which are given by $n = 1$ or 2 which may be observed since modes with larger n have perturbation velocities which are highly oscillatory radially. Therefore, they may be expected to be damped in a viscous fluid.

Since inertial waves on vortices are highly dispersive, it is crucial to distinguish between phase velocity (ω/k) and group velocity ($\partial\omega/\partial k$). The former is the velocity of wave crests or any point of constant phase ($kz + m\theta + \omega t$) along the wave, and the latter is the velocity at which a wave packet carries energy. It is therefore the group velocity which is particularly significant for dispersive systems, since it is this velocity which determines the rate and direction at which energy or information is transmitted.

The group velocities for the modes given by Eqs (3.5) through (3.9) are

$m = 0$

$$c_g = \frac{2R\Omega}{\alpha_{0,n}} - w_o + \frac{3\Omega k^2 R^3}{\alpha^3_{0,n}} \ell n(|kR|) + \ldots \tag{3.10}$$

$m = \pm 1$

$$c_g = - w_o + \Omega m k R^2 (- \ell n(|kR|/2) - \tfrac{1}{4} - \gamma) + \ldots \tag{3.11}$$

$$c_g = \frac{2R\Omega}{\alpha_{1,n}} - w_o - \frac{6\Omega k^2 R^3}{\alpha^3_{1,n}} + \ldots \tag{3.12}$$

$m = \pm 2$

$$c_g = - w_o + \frac{2kR^2}{3m} + \ldots \tag{3.13}$$

$$c_g = \frac{2R\Omega}{\alpha_{2,n}} - w_o - \frac{6\Omega k^2 R^3}{\alpha^3_{2,n}} + \ldots \tag{3.14}$$

If we now examine the long wave limit ($kR \to 0$), it is apparent that the modes given by Eqs (3.11) and (3.13) represent waves which are merely convected downstream with the mean flow w_o (negative group velocity corresponds to downstream propagation). However, the modes given by Eqs (3.10), (3.12), and (3.14) may have upstream propagation provided w_o is not too great. For instance, since $\alpha_{0,1} = \pm 2.405$, upstream propagation of the (0,1) mode is possible provided $w_o/R\Omega < 0.83$. For the (1,1) mode, $w_o/R\Omega < 0.53$ to have upstream propagation. These axial-to-swirl-velocity ratios above which upstream propagation of a particular mode is not possible define critical conditions or states. It is reasonable to presume that a trailing vortex or a vortex in a diverging tube may have many locations where critical conditions occur. Assuming that the swirl velocity is diminished downstream, upstream of the critical condition (say, for the (m,n) mode), the flow is supercritical and downstream subcritical.

The terms sub- and supercritical have been used before when discussing vortex breakdown, particularly by Benjamin [46]. However, the definition used here is different than that used previously, and it is important to make this distinction here. Note that the critical state with the largest axial-to-swirl-velocity ratio is, for an axisymmetric wave, the (0,1) mode. From Eq (3.5) it is seen that in the long wave limit it is at this critical state that axisymmetric waves of indefinite length can first stand ($\omega/k = 0$) and the wave is steady in time. Benjamin has used the condition of standing, steady, axisymmetric waves of indefinite length as a definition of the critical state. The definition of critical state as used in this monograph is based on zero group velocity. When considering axisymmetric waves, the distinction mathematically is trivial since long, axisymmetric waves are nondispersive, and when $w_o/R\Omega = 0.83$, $\partial\omega/\partial k = \omega = 0$. Physically, however, the distinction is crucial. Examining Eqs (3.7), (3.9), (3.12) and (3.14), when $w_o/R\Omega = 2/\alpha_{|m|,n}$ with $|m| \geq 1$, the group velocity of an asymmetric wave mode (m,n) of indefinite length is zero but the wave is unsteady. The wave packet is stationary (it cannot advance along the vortex ($c_g = 0$)) but is unsteady.

In a strict sense, a supercritical flow is one in which there can be no upstream transport of information through wave motion or, equivalently, the group velocity of infinitesimal waves is directed downstream. Subcritical vortices necessarily have upstream propagation of information. However, the critical state and the terms subcritical and supercritical vortices are unique to the wave mode considered, and therefore are meaningless without specifying the wave type. A vortex is supercritical with respect to the (m,n) mode provided there exists no k for which the group velocity is directed upstream. Clearly, such a distinction need not be made in the theory of water wave propagation where only one wave mode is possible.

Naturally occurring or forced axial variations along a vortex may therefore establish critical states or, more appropriately, since the group velocity is zero, signal barriers along a vortex. That these signal barriers are in some way associated with breakdown has

been suggested by several investigators. The first of these was Squire [47] who believed that if infinitesimal axisymmetric waves could stand, disturbances originating downstream would propagate upstream and cause breakdown. Since axisymmetric standing waves of indefinite length first stand when the swirl is gradually increased from zero, he suggested that the limiting condition for such waves was the onset condition for vortex breakdown.

Jones [48], in an attempt to clarify Squires' hypothesis, suggests that since swirl-to-axial-velocity ratio varies along the axis in a real vortex, the point where long-standing axisymmetric waves first become possible may be a barrier to disturbances traveling upstream or downstream. He then suggests that disturbances might be expected to accumulate at the barrier and ultimately lead to a step of such size that the flow breaks down. More recently, a similar conjecture has been made by Moore and Saffman [43]. They hypothesize that when axial velocities are approximately equal to swirl velocities inertial waves may become "trapped" and cause breakdown.

Shortly thereafter, Landahl [39] advanced a general theory to demonstrate when a nonhomogeneous continuum system, capable of supporting waves of scale much smaller than the background inhomogeneity may not remain smooth. Landahl applies this theory to explain the localized breakdown of laminar shear flow and also suggests that the hydraulic jump, vortex breakdown, and other phenomena may be investigated along these lines. His theory supplies the physical mechanisms from which a trapped finite amplitude wave theory of vortex breakdown may be put on a firmer basis than has previously been possible.

The concept of wave trapping at a critical state is now needed. Curiously, this phenomenon has been understood for some time, having been used by Kantrowitz [49] to explain the formation and stability of normal shock waves in channel flows. Essentially the trapping process involves the accumulation of disturbances at some location in the flow (at a critical state) through space-time focusing and a nonlinear rectification of these disturbances. In compressible flows the critical state is Mach number equal to one. Wave trapping is a process by which disturbances become stationary or get stuck on a spatial inhomogeneity. The accumulation of infinitesimal disturbances by the trapping process can change an initially smooth inhomogeneous flow into an alternate stationary flow which is a trapped finite amplitude wave, if the trapping process is stable or self-limiting and the downstream conditions support the wave. By stationary, we do not imply steady, but only that the trapped wave cannot advance upstream of a certain location in the flow field. By self-limiting, we imply that mechanisms may exist which will limit the amplitude of the trapped wave, and therefore additional interaction of the wave with small disturbances will not result in a change of wave amplitude. One such amplitude-limiting mechanism is wave breaking, a violently turbulent phenomena, which will be discussed in Section 3.2.2.

Since wave trapping will result in a finite amplitude wave, ultimately a nonlinear analysis will be needed to analyze the complete phenomenon. To date, investigations of nonlinear wave propagation on vortices are just beginning; however, the results, particularly for axisymmetric waves, are most encouraging. As pointed out by Landahl [39], a qualitative description of the trapping process which results in vortex breakdown may be obtained from studying infinitesimal wave propagation on a slowly varying vortex. As will now be shown, a trapped wave model of vortex breakdown can explain many of the experimentally observed features of the phenomenon.

At this point, we restrict our comments to vortex breakdowns in tubes which are more readily observed in the laboratory than breakdowns on trailing vortices. Sarpkaya [50] has performed a series of experiments in a diverging vortex tube over a wide range of conditions, and his results are particularly relevant to the previous development. Sarpkaya's experimental apparatus is shown in Figure 3.4. The swirl-to-axial-velocity ratio in the diverging tube was controlled by adjustable inlet vanes and is measured by the parameter S which is directly related to the angle of attack of the vanes. The swirl-to-axial-velocity ratio is, however, not constant along the diverging tube and is roughly proportional to the tube radius. This is reasoned from the fact that the swirl and axial velocity are proportional to the reciprocal of the tube radius and reciprocal of the tube radius squared, respectively. A flow which is axial velocity-dominated upstream becomes less so as the tube diverges downstream.

The effect of tube walls on wave propagation can be shown to alter the values of the critical swirl-to-axial-velocity ratio but does not change the order in which the critical states are reached. Therefore, the dispersion relation for a single isolated vortex in an unbounded flow can be used to obtain qualitative information regarding the sequence of breakdowns to be expected in a diverging tube. If we now recall our discussion of the dispersion relation (Eqs (3.5)-(3.9)), it is the axisymmetric wave which has a critical condition for the smallest value of the swirl parameter. The next mode to become critical at a larger value of the swirl parameter is the spiral mode, Eq 3.7. In Figure 3.5 we show breakdown position in Sarpkaya's vortex tube as a function of Reynolds number and swirl parameter. Axisymmetric breakdowns are shown to occur at low values of the swirl parameter and in the upstream portion of the diverging tube, while spiral breakdowns occur at larger values of the swirl parameter and in the downstream portion of the tube. As noted by Sarpkaya, at fixed flow rate and vane setting, the axisymmetric breakdown was stationary and nearly steady. However, while the spiral breakdown was stationary, it was never steady. This feature can be observed in Figure 3.6 where an axisymmetric breakdown is shown followed by a spiral type.

Sarpkaya also made observations of the effect on axisymmetric breakdown position and structure when the inlet vanes were rapidly changed to a new setting. With a rapid increase in swirl, by increasing the vane angle, the breakdown first moved a short distance downstream and then rapidly upstream, overshooting its final new upstream equilibrium position. A decrease in inlet vane angle caused the above-noted motion to occur in reverse.

The change in vane setting alters the position at which the critical state is reached in the tube and is consistent with a trapped wave interpretation of breakdown.

Observation of the effect of small changes in the downstream flow conditions illustrates the concept of downstream support for the wave. By constricting the exit hole, the axisymmetric breakdown moved upstream into the supercritical flow. This construction might be thought to be analogous to increasing the size of a barrier in the subcritical portion of an open channel flow, so that the hydraulic jump becomes stronger and moves further upstream into the supercritical flow. Sarpkaya noted that as the axisymmetric breakdown advanced upstream when the exit was constricted, the flow upstream of the bubble (visualized with ink) remained practically unchanged. Unfortunately, Sarpkaya does not report on the effect of downstream changes on the asymmetric modes. It would be interesting to input an unsteady asymmetric flow disturbance in the tube exit (possibly by rotating an object at the proper rate) and observe the resulting forms of breakdown.

Up to now, the theoretical development has been largely qualitative and it is appropriate at this time to discuss some of the computations which have been made. Only the axisymmetric mode has been treated with any detail since complexity of the computations, even in this case, is enormous. Randall and Leibovitch [40] have developed a nonlinear partial differential equation to describe the amplitude of an axisymmetric wave advancing into a critical flow in a diverging tube. The equation is that of Korteweg and deVries with an additional term that is proportional to wave amplitude. Some coefficients in this equation are nonconstant and vary as a result of flow divergence. The computation proceeds as an initial value problem. Wave amplitude is prescribed on a flow whose mean swirl and axial velocity attempts to model Sarpkaya's test conditions. The wave form is followed until the wave oscillates about an equilibrium position in the tube. The equilibrium position and resulting wave form are in reasonable agreement with observation. The streamline pattern in the neighborhood of the breakdown region is shown in Figure 3.7 and may be compared to Sarpkaya's photographic results (see Fig. 3.8).

Several criticisms of Randall and Leibovitch's calculations can be raised, the first being that their model equation is not valid for the large amplitude waves which are computed. This we feel is a valid criticism. However, as stated by Randall and Leibovitch, the important effects of nonlinearity, dispersion, and tube geometry are all contained in the model. Another criticism is that the kdV equation governs only wave propagation in one direction — in this case, upstream propagation. Reflection of waves downstream is not possible and this, perhaps, is the reason the equilibrium breakdown position and hence amplitude is a strong function of the circulation Reynolds number Γ/ν. Bilanin [41], using a simple model, has shown that reflection of a nonlinear wave of indefinite length advancing into the critical state is small; therefore, the kdV model equation is appropriate. However, the wavelength of the equilibrium wave form shown in Figure 3.7 is not long when compared to the tube radius. Quite possibly a balancing of the amplifying effects of the tube geometry against reflection will deëmphasize the role of viscosity in the model equation.

The amplitude and hence violence of a breakdown is an important question as far as vortex wake dissipation rate is concerned. Possibly, breakdowns observed in tubes are milder than those which might be observed on trailing vortices, and we will investigate the intensity of a breakdown in the next section.

To summarize, we have attempted to argue here that vortex breakdown is a trapped nonlinear wave whose upstream propagation is blocked by upstream supercritical flow. We have argued that the definition of critical state which separates a supercritical from a subcritical flow must include the wave mode being considered and should be based on a group velocity rather than phase velocity. This distinction is not necessary in the case of water waves in a finite depth channel where only one mode is possible and the waves are nondispersive in the long wave limit. Finally, for the breakdown to occur and convert the steady flow to one with a stationary but not necessarily steady trapped wave, the downstream conditions must support the wave, much like downstream resistance is needed in a channel to support a hydraulic jump.

The trapped wave mechanism of breakdown is quite appealing, but the difficult computations necessary to verify the trapping phenomenon for asymmetric waves are lacking. Hopefully, these computations will not be a long time in coming. Leibovitch has derived nonlinear equations governing wave amplitude but, to our knowledge, no solutions have appeared.

3.2.2 *Vortex Deintensification as a Result of Breakdown*

The very practical problem of assessing whether the breakdown phenomenon is likely to play any significant role in the decay of aircraft trailing vortices is unfortunately very difficult. Estimating the intensity of a strong breakdown will have to await a better understanding of nonlinear wave propagation, wave breaking, and the related problem of turbulent momentum transport. However, through the use of a simple model, it is possible to gain some qualitative information regarding the breakdown phenomenon and also point out the difficult problems which remain.

The procedure to be used here will be to specify flow conditions upstream of a breakdown and, by conserving the appropriate flow quantities across the breakdown, deduce conditions downstream. This approach is not new, having been used by Landahl and Widnall [51], Mager [52], and Lakshmikantha [53]. The model to be reviewed here is an extension to that developed in Ref. 51 to describe an axisymmetric breakdown.

The development up to now has argued that breakdown is a trapped finite amplitude wave. Observations of breakdown on trailing vortices have shown that they may be violently turbulent (see Tombach [54]). Any analytic model will therefore have to be nonlinear.

In Figure 3.9 the breakdown model to be discussed here is shown. Upstream at Station 1, the swirl and axial velocities are taken to be

$$\left.\begin{aligned} v &= \frac{\Gamma r}{2\pi R^2} \\ w &= c + w_1 \end{aligned}\right\} \qquad r \leq R \tag{3.15}$$

$$\left.\begin{aligned} v &= \frac{\Gamma}{2\pi r} \\ w &= c \end{aligned}\right\} \qquad r \geq R \tag{3.16}$$

The velocity c is the axial velocity required to hold the breakdown stationary. The fluid passing through the area $\pi(R_1^2 - R^2)$ is irrotational and is entrained into the breakdown control volume. The vortex tube radius R characterizes the radial extent of vorticity and w_1 is a characteristic axial velocity in the vortex. Downstream we allow some flexibility in the swirl velocity distribution and take

$$\left.\begin{aligned} v &= \frac{\Gamma}{2\pi R_2}\left(\frac{r}{R_2}\right)^{\alpha} \\ w &= c + w_2 \end{aligned}\right\} \qquad r \leq R_2 \tag{3.17}$$

The parameter α is positive and the vortex tube radius downstream of the breakdown R_2 is to be determined.

By conserving mass and the axial flux of angular momentum, it may be shown that the mass of irrotational fluid flowing into the control volume divided by the mass flowing in through the area πR^2 is $(1 - \alpha)/2(1 + \alpha)$. The value of α must then be taken to be less than 1 to keep this ratio positive. Since the entrainment of irrotational fluid is irreversible, c is therefore positive so that irrotational fluid can only enter the mixing volume. Conservation of mass and axial flux of angular momentum also yields that

$$\left(\frac{R_1}{R}\right)^2 = 1 + \frac{1}{2}\left(\frac{U_1}{c} + 1\right)\frac{(1 - \alpha)}{(1 + \alpha)} \tag{3.18}$$

The characteristic axial velocity excess or defect w_1 in a vortex is presumably small as was shown in Section 1 (although engines or drag devices may invalidate this assumption). Therefore, with the numerical value of w_1/c small, the maximum irrotational fluid is entrained with $\alpha = 0$. In this case, the entrained fluid is one-half the mass flux from the control volume. However, with $\alpha < 1$, the vorticity becomes singular at $r = 0$ and intuitively one would suspect that the breakdown phenomenon would spread the vorticity more uniformly downstream of the breakdown region. Part of the problem is the rather restrictive functional form used to represent the downstream swirl velocity. However, the conservation of the axial flux of angular momentum places a very strong constraint on the amount of irrotational fluid which may be entrained into the breakdown. This, in our opinion, suggests that the breakdown phenomenon may not result in as large deintensifications as some investigators have suggested.

To obtain some estimate as to the downstream tube radius R_2 requires information regarding the characteristic axial velocity excess or defect w_2. Intuitively one might feel that the turbulent momentum transport would attempt to smooth out the axial profile. Therefore, as a first approximation, we take $w_2 = 0$ (no defect). However, that this is correct is far from obvious since immediately behind the breakdown the flow is subcritical and is influenced by conditions still further downstream.

With the rather strong assumption that $w_2 = 0$, the significant result is obtained that the maximum increase in vortex tube radius R is only about 22%. This result tends to confirm earlier conjecture regarding the vortex deintensification which can result as an immediate consequence of breakdown. We should again point out that the real deintensification that may be associated with vortex breakdown is strongly dependent on the turbulence generated by the breakdown process.

We have yet to show that the simple breakdown computed above is possible since axial momentum and energy conservation must still be considered. Balancing the axial momentum is straightforward, and it can be shown that the breakdown must satisfy

$$\left[\frac{(w_1 + c)2\pi R}{\Gamma}\right]^2 = \frac{\ell n\,(R_2/R) + \dfrac{\alpha - 1}{4(1 + \alpha)}}{1 - \left[\dfrac{(\alpha + 3)}{2(\alpha + 1)}\dfrac{R}{R_2}\right]^2 + \dfrac{1}{R_1^2/R^2 - 1}\left[\dfrac{1 - \alpha}{2(1 + \alpha)}\right]^2} \tag{3.19}$$

With $\alpha = 1$, the result given in Ref. 51 is obtained.

The final constraint is to accept solutions which result in a loss in the flux of mechanical energy or

$$\Delta E = E_2 - E_1 < 0 \tag{3.20}$$

It is also interesting to calculate the change of energy in the vortex tube which is given by

$$\Delta E_T = E_2 - E(R) \qquad (3.21)$$

The permissible breakdowns described by this model with $w_1 = 0$ are shown in Figure 3.10. For a given α, the breakdown which results in the minimum axial velocity gradients downstream is along the $\Delta E = 0$ curve. Solutions below this line, which have not been plotted, represent breakdowns which result in a gain of mechanical energy in the process and are therefore impossible. It is interesting that breakdowns can occur in which the turbulent mixing process results in a loss of mechanical energy, but the downstream vortex tube is energized.

From examination of Figure 3.10, the difficulty of estimating breakdown strength should be apparent. One piece of missing information is the axial velocity directly after the breakdown or, equivalently, the new tube radius. However, fixing R_2 still leaves the swirl velocity distribution to be determined. A knowledge of these downstream conditions requires that we understand the turbulent mechanisms involved in the jump and how the downstream flow must adjust to support the wave. The relationship between the flow conditions after the breakdown and those found far downstream are interdependent. This downstream influence is supported by experiment. The proper downstream boundary conditions are still a matter that is under contention, having been investigated by both Bossel [55] and Mager [53]. As might now be apparent, we feel that the computation of a violent breakdown on aircraft trailing vortices will be extremely difficult, requiring a computational model which includes nonlinear wave breaking and the associated turbulent momentum transport, as well as the influence of downstream boundary conditions.

3.3 Coupling of Instabilities

As we mentioned earlier, the phenomenon of Crow instability breaks the trailing vortex pair into crude vortex rings which are more unstable than the initial wake configuration and hence tend to increase the rate at which the wake of an aircraft is dispersed. An obvious question is: Can this naturally occurring breakup of trailing vortices be forced by suitably oscillating control surfaces so that this instability is accelerated? Two experimental investigations have sought to answer this question.

Chevalier [56] has conducted a series of flight tests in which the angle of attack of a light aircraft (a Beaver DHC-2) was periodically oscillated so as to sinusoidally perturb the vertical positions of the trailing vortices. The angle of attack change was ±2° and resulted from sinusoidally oscillating the elevator of the aircraft at frequencies of 1/8, 1/4, and 1/2 Hz. These frequencies gave vertical perturbations whose wavelengths were 22.5, 11.7, and 5.7 aircraft spans, respectively. Chevalier found that the most rapid acceleration of the instability occurred at the 1/4 Hz oscillation frequency or at a perturbation wavelength of 11.7 aircraft spans. The periodic oscillations in angle of attack and hence lift permit only qualitative comparison with the analyses of Crow [32] and Widnall, et al. [33] since these analyses do not account for circulation variation along the trailer. The perturbation wavelength of 11.7 aircraft spans is slightly larger than would be predicted by theory (see Fig. 3.3). Chevalier reported that time to breakup was one to two minutes under calm atmospheric conditions and steady flight. This time was approximately halved when angle of attack variations of ±2% were imposed. These results are of considerable interest theoretically. However, a ±2% oscillation in angle of attack at a frequency of 1/4 Hz resulted in vertical accelerations of magnitude .15g which are not acceptable for commercial jetliners.

Vortex breakdown was observed to occur along the trailing vortices under steady flight and calm atmospheric conditions. A surprising result of Chevalier's tests was that vortex breakdown, made visible by smoke, occurred regularly along the trailing vortices undergoing sinusoidal instability, as shown in Figure 3.11. The quantitative deintensification of the wake as a result of breakdown was not known, but it was reported by the pilot of the chase aircraft in these experiments that the wake was reduced to a mild random atmospheric turbulence.

Crow [57] suggested an alternative means of exciting sinusoidal instability through differential oscillation of two pairs of flaps. By suitably sizing flaps and flap amplitudes, lift could be held constant while the centroid of trailed vorticity was shifted periodically inboard and outboard. This idea was tested by Bilanin and Widnall [58] in a ship model towing tank. The model wing is shown in Figure 3.12. Frequencies of oscillation were chosen such that perturbations to trailer separation were at wavelengths corresponding to theoretical values at which amplification rates were maximum. Flap deflection angles were larger than might be implemented on a full-scale aircraft (±2%) so as to afford viewing large vortex excursions before interference from the towing tank floor became significant.

The tests were successful in that it was shown that the Crow instability could be excited by this method. An analysis was undertaken to include the effect of trailer circulation variation on amplitude of the instability, and agreement with experiment was reasonable. Unfortunately the towing tank size precluded observation of the linking of the vortices.

Vortex breakdown was observed to occur on the trailing vortices undergoing sinusoidal instability although the breakdown appeared mild in comparison with that observed on trailing vortices from full-scale aircraft. Vortex tube enlargement or bulging occurred at points along the vortices where trailer horizontal separation was a maximum. An analysis which computed the pressure induced along the trailing vortex as a result of sinusoidal instability predicted the observed behavior of the vortices. However, again the effect of circulation variation along the trailing vortex was neglected. No measurements were taken to determine what deintensification resulted as a consequence of the breakdowns observed.

The experimental programs described above show that the Crow instability may be forced by suitable oscillation of control surfaces. The technique of sloshing the load distribution so that lift remains constant but vortex centroids are periodically shifted inboard and outboard can be considered as a possible means of increasing the rate at which aircraft wakes might be dispersed, especially when aircraft are in clean configurations. It is not clear at the present time that this technique can or should be implemented when an aircraft is in its takeoff or landing configuration.

4. AGING OF VORTICES

An evaluation of the effects of viscous action on the complete wake of a real airplane, even in a quiescent, neutrally stable atmosphere, is an enormously difficult problem. Even for the highly idealized case of a wing shedding two steady vortices in the absence of any engine heat or any tail lift, so that no gravitational forces and only a single pair of vortices is involved, the problem is complicated. This is due to the fact that there are really two problems involved. These two problems may be appreciated by reference to Figure 4.1 where the streamlines produced by a pair of vortex tubes of opposite sign are shown as they would appear to an observer at rest relative to the two vortices.

The first of the two problems that we may identify is an essentially local one confined to the immediate vicinity of the vortex tubes. The problem is that of the diffusion of vorticity away from the centers of vorticity concentration that were formed in the roll-up process. Since the flow in the immediate vicinity of the vortex tubes is almost axially symmetric, this problem can be studied in some detail by considering what might be the fate of a single axially symmetric tube of vorticity. This is a problem which, as we shall see, does not lend itself readily to the use of an eddy viscosity approach. This has been the source of some confusion in the past, but it appears that the new second-order closure approaches to turbulent shear flow (see, for example, Refs. 59 through 63) can contribute significantly to our understanding of this diffusion process.

The second aging problem is far more complicated. It is associated with the fact that, in an aircraft wake, there are at least two vortex tubes of opposite sign so that, in an ideal inviscid situation, a trapped mass of air inside the boundary (O, A, O', A', O) descends with the vortex pair. If one is to understand the general problem of vortex aging, it is essential that one understand the nature of viscous transport (both molecular and turbulent) on the boundary of the descending mass of air, as well as on the vertical line OO' dividing the regions of positive and negative vorticity. Both these aspects of the second problem are transport problems with nonsimple geometries.

The problems just discussed for a very simple vortex-pair wake are difficult enough. When one considers that the real wakes of transport aircraft have multiple centers of vorticity shed from each wing, the problem of aging becomes even more difficult. For this case, it is necessary to consider the straining effect of vortices of like sign upon each other as the wake ages, for it is this effect that can break two or more individual centers of concentrated vorticity down into a single center of widely distributed vorticity. This redistribution of vorticity by an aging process can be most important in determining the degree of hazard encountered by any aircraft interacting with the near wake of a generating aircraft.

These more complicated aging problems can also be attacked by second-order closure methods. Digital computer codes which can attack these problems have become available only very recently, so that very few computational results are available. Nevertheless, we will include a discussion of this very important aging problem, together with some very preliminary computational results.

There have been a number of empirical approaches taken in the past in an attempt to describe the vortex aging process (see, for example, Refs. 64 and 65). Most of these have been developed to cope with the aging of a single vortex and are not really applicable to the general problem posed by the wake of a real airplane in its takeoff or landing configuration. They will, therefore, not be reviewed here.

Although we recognize that it is but a minor part of the overall aging process, we will begin our study of vortex aging with a discussion of the decay of an isolated vortex according to a second-order closure modeling of turbulent transport.

4.1 Decay of an Isolated Vortex

In what follows, we shall use an invariant second-order closure model to discuss the decay of an isolated vortex. The senior author of this monograph and his colleagues have, for some time now, been engaged in the development and application of such a method to a large variety of high Reynolds number turbulent shear flows (for example, Refs. 66 through 69). An application of this method to the decay of an isolated vortex was first presented by Donaldson and Sullivan [70]. A further discussion of the nature of turbulence in axisymmetric vortices was given by Donaldson [71]. The development given below will closely follow that given in the papers referenced above. It will be noted, however, that a slightly different model will be used in the calculations given here. This new model is one which has evolved as our research on invariant turbulence models has progressed. Although, as a result of our recent studies, the model has been changed and improved so that it does a far better job of predicting the measured characteristics of all the turbulent flows to which it has been applied, the basic features of vortex transport predicted by the original modeling have not been altered.

Let us assume a time-independent vortex motion in a medium of constant density. The equations which govern the motion in this vortex, if the velocity and pressure are written as sums of mean and fluctuating parts

$$u_i = \bar{u}_i + u'_i \tag{4.1}$$

$$p = \bar{p} + p' \tag{4.2}$$

are, in tensor notation [72]

$$\bar{u}^{\ell}{}_{,\ell} = 0 \tag{4.3}$$

$$\bar{u}^{\ell}\bar{u}_{i,\ell} + \left(\overline{u'^{\ell}u'_i}\right)_{,\ell} = -\frac{1}{\rho}\bar{p}_{,i} + \nu g^{\ell m}\bar{u}_{i,\ell m} \tag{4.4}$$

$$\begin{aligned}\bar{u}^{\ell}\left(\overline{u'_i u'_j}\right)_{,\ell} + \overline{u'_j u'^{\ell}}\,\bar{u}_{i,\ell} + \overline{u'_i u'^{\ell}}\,\bar{u}_{j,\ell} + \left(\overline{u'^{\ell}u'_i u'_j}\right)_{,\ell} \\ = \frac{1}{\rho}\left[-\left(\overline{u'_j p'}\right)_{,i} - \left(\overline{u'_i p'}\right)_{,j} + \overline{p'u'_{i,j}} + \overline{p'u'_{j,i}}\right] \\ + \nu g^{\ell m}\left[\left(\overline{u'_i u'_j}\right)_{,\ell m} - \overline{u'_{i,m}u'_{j,\ell}} - \overline{u'_{i,\ell}u'_{j,m}}\right]\end{aligned} \tag{4.5}$$

In order to close this system of equations, Eqs (4.3) through (4.5), it is necessary to adopt certain models for certain terms which occur in (4.5). The principal criteria used in closing these models are invariance under coordinate and Galilean transformations, dimensional consistency, and simplicity. The following rather general modeling has been studied extensively and will be used in this discussion of vortex motion.

$$\overline{u'_i u'_j u'_k} = -v_c \Lambda q\left[\left(\overline{u'_i u'_j}\right)_{,k} + \left(\overline{u'_j u'_k}\right)_{,i} + \left(\overline{u'_k u'_i}\right)_{,j}\right] \tag{4.6}$$

$$\overline{u'_i p'} = -p_c \rho \Lambda q\left(\overline{u'^{\ell}u'_i}\right)_{,\ell} \tag{4.7}$$

$$\overline{p'u'_{i,j}} + \overline{p'u'_{j,i}} = -\rho\frac{q}{\Lambda}\left(\overline{u'_i u'_j} - \frac{1}{3}g_{ij}q^2\right) \tag{4.8}$$

$$g^{\ell m}\,\overline{u'_{i,\ell}u'_{j,m}} = a\frac{\overline{u'_i u'_j}}{\Lambda^2} + b\frac{q}{\nu\Lambda}\left(\beta\,\overline{u'_i u'_j} + \frac{1-\beta}{3}g_{ij}q^2\right) \tag{4.9}$$

where

$$q^2 = \overline{u'^{m}u'_m} \tag{4.10}$$

In these models, Λ is a variable length, locally representative of the integral scale of the turbulence, and v_c, p_c, a, b, and β are dimensionless constants for which tentative values have been determined by comparison of experimental results with solutions of the above equations obtained by digital computation for a variety of shear flows.

For simple turbulent flows such as axisymmetric free jets, two-dimensional shear layers, simple wakes, and turbulent boundary layers, it is possible to relate the scale length Λ to the local scale of the mean motion defined in some way. This is possible because, for such flows, the integral scale of the turbulence can, in general, be quite simply related to the scale of the mean motion. For more complicated flows, it is necessary to have a dynamic equation for the length scale Λ. A number of such equations have been proposed in connection with second-order closure schemes (see, for example, Refs. 61, 62, 69). It appears that there are almost as many scale equations as there are research groups investigating second-order closure techniques. In studies carried out at A.R.A.P. [69], we have found that the scale equation given below

$$\frac{\partial\Lambda}{\partial t} + \bar{u}^{j}\Lambda_{,j} = -0.35\frac{\Lambda}{q^2}\overline{u'^{i}u'^{j}}\,\bar{u}_{i,j} + \frac{0.6\nu}{\lambda^2}\Lambda + 0.3g^{ij}\left[q\Lambda\Lambda_{,i}\right]_{,j} - \frac{0.375}{q}g^{ij}(q\Lambda)_{,i}(q\Lambda)_{,j} \tag{4.11}$$

yields the best agreement with experimental data when used in conjunction with Eqs (4.5) through (4.10) and when agreement is sought with all known experiments on turbulent flows that are considered valid.

A complete second-order closure solution for a turbulent shear layer requires the simultaneous solution of Eqs (4.3) through (4.11). We have found, however, in our studies that most of the characteristic behavior of free turbulent shear layers can be discovered by uncoupling Eq (4.11) from the rest of the equations and assuming that Λ is proportional to a typical length scale of the turbulent flow generated by Eqs (4.3) through (4.10). The computational results that will be discussed below have been obtained under this restrictive assumption. Only very recently have numerical results been obtained for

vortex flows with the scale equation coupled to the rest. These results were not obtained in time to be analyzed and included in this monograph. Thus, while the results in what follows are characteristic of vortex flows computed by second-order closure techniques, the results should not be considered correct as to the specific numerical values that are presented.

In our earlier studies of turbulent vortex motion, the values of the model parameters used were $v_c = 0.1$, $p_c = 0.1$, $a = 2.5$, $b = 0.125$, and $\beta = 1$. This early model, while giving adequate results, was found to have too simple a dissipation model, for it did not distinguish between the rate of dissipation of the turbulent energy correlations and the shearing correlations. This early model has been replaced by $v_c = 0.1$, $p_c = 0.1$, $a = 3.25$, $b = 0.125$, and $\beta = 0$. This gives results in close agreement with the previous model but causes the dissipation of the turbulent energy correlations to be isotropic and far more rapid than that for the shearing correlations.

To study an isolated vortex, we introduce cylindrical coordinates (r,θ,z) and denote the physical components of the velocity by (u,v,w). Using the modeling scheme given above, equations suitable for the study of axisymmetric line vortices have been obtained by Sullivan [73]. They are

$$\bar{u}_r + \frac{\bar{u}}{r} + \bar{w}_z = 0 \tag{4.12}$$

$$\frac{1}{\rho}\bar{p}_r = \frac{\bar{v}^2}{r} \tag{4.13}$$

$$\bar{w}\bar{v}_z = -\frac{\bar{u}}{r}(r\bar{v})_r - \frac{1}{r^2}(r^2\overline{u'v'})_r + \nu\left[\frac{1}{r}(r\bar{v}_r)_r - \frac{\bar{v}}{r^2}\right] \tag{4.14}$$

$$\bar{w}\bar{w}_z = -\bar{u}\bar{w}_r - \frac{1}{\rho}\bar{p}_z - \frac{1}{r}(r\overline{u'w'})_r + \nu\frac{1}{r}(r\bar{w}_r)_r \tag{4.15}$$

$$\begin{aligned}\bar{w}(\overline{u'u'})_z = &-\bar{u}(\overline{u'u'})_r + 4\overline{u'v'}\frac{\bar{v}}{r} + (3v_c + 2p_c)\left(\Lambda q(\overline{u'u'})_r\right)_r \\ &+ \frac{v_c\Lambda q}{r}(3\overline{u'u'} - 2\overline{v'v'})_r + \frac{2p_c}{r}\left(\Lambda q(\overline{u'u'} - \overline{v'v'})\right)_r \\ &- 2(2v_c + p_c)\frac{\Lambda q}{r^2}(\overline{u'u'} - \overline{v'v'}) - \frac{q}{\Lambda}\left[\overline{u'u'}(1 + 2b\beta) - \frac{q^2}{3}\left(1 + 2b(\beta - 1)\right)\right] \\ &+ \nu\left[\frac{1}{r}\left(r(\overline{u'u'})_r\right)_r - \frac{2}{r^2}(\overline{u'u'} - \overline{v'v'}) - \frac{2a}{\Lambda^2}\overline{u'u'}\right]\end{aligned} \tag{4.16}$$

$$\begin{aligned}\bar{w}(\overline{v'v'})_z = &-\bar{u}(\overline{v'v'})_r - 2\overline{u'v'}\frac{1}{r}(r\bar{v})_r + v_c\left(\Lambda q(\overline{v'v'})_r\right)_r \\ &+ \frac{\Lambda q}{r}\left(3v_c(\overline{v'v'})_r + 2p_c(\overline{u'u'})_r\right) + \frac{2v_c}{r}\left(\Lambda q(\overline{u'u'} - \overline{v'v'})\right)_r \\ &+ 2(2v_c + p_c)\frac{\Lambda q}{r^2}(\overline{u'u'} - \overline{v'v'}) - \frac{q}{\Lambda}\left[\overline{v'v'}(1 + 2b\beta) - \frac{q^2}{3}\left(1 + 2b(\beta - 1)\right)\right] \\ &+ \nu\left[\frac{1}{r}\left(r(\overline{v'v'})_r\right)_r + \frac{2}{r^2}(\overline{u'u'} - \overline{v'v'}) - \frac{2a}{\Lambda^2}\overline{v'v'}\right]\end{aligned} \tag{4.17}$$

$$\begin{aligned}\bar{w}(\overline{w'w'})_z = &-\bar{u}(\overline{w'w'})_r - 2\overline{u'w'}\bar{w}_r + v_c\left(\Lambda q(\overline{w'w'})_r\right)_r + \frac{v_c\Lambda q}{r}(\overline{w'w'})_r \\ &- \frac{q}{\Lambda}\left[\overline{w'w'}(1 + 2b\beta) - \frac{q^2}{3}\left(1 + 2b(\beta - 1)\right)\right] + \nu\left[\frac{1}{r}\left(r(\overline{w'w'})_r\right)_r - \frac{2a}{\Lambda^2}\overline{w'w'}\right]\end{aligned} \tag{4.18}$$

$$\begin{aligned}\bar{w}(\overline{u'v'})_z = &-\bar{u}(\overline{u'v'})_r - \overline{u'u'}\frac{1}{r}(r\bar{v})_r + 2\overline{v'v'}\frac{\bar{v}}{r} + (2v_c + p_c)\left(\Lambda q(\overline{u'v'})_r\right)_r \\ &- 2(v_c - p_c)\frac{1}{r}(\Lambda q\overline{u'v'})_r + (4v_c - p_c)\frac{\Lambda q}{r}(\overline{u'v'})_r - 4(2v_c + p_c)\frac{\Lambda q}{r^2}\overline{u'v'} \\ &- \frac{q}{\Lambda}\overline{u'v'}(1 + 2b\beta) + \nu\left[\frac{1}{r}\left(r(\overline{u'v'})_r\right)_r - \frac{4}{r^2}\overline{u'v'} - \frac{2a}{\Lambda^2}\overline{u'v'}\right]\end{aligned} \tag{4.19}$$

$$\begin{aligned}\bar{w}(\overline{u'w'})_z = &-\bar{u}(\overline{u'w'})_r + 2\overline{v'w'}\frac{\bar{v}}{r} - \overline{u'u'}\bar{w}_r + (2v_c + p_c)\left(\Lambda q(\overline{u'w'})_r\right)_r \\ &+ \frac{p_c}{r}(\Lambda q\overline{u'w'})_r + \frac{2v_c\Lambda q}{r}(\overline{u'w'})_r - (2v_c + p_c)\frac{\Lambda q}{r^2}\overline{u'w'} - \frac{q}{\Lambda}\overline{u'w'}(1 + 2b\beta) \\ &+ \nu\left[\frac{1}{r}\left(r(\overline{u'w'})_r\right)_r - \frac{1}{r^2}\overline{u'w'} - \frac{2a}{\Lambda^2}\overline{u'w'}\right]\end{aligned} \tag{4.20}$$

$$\bar{w}(\overline{v'w'})_z = -\bar{u}(\overline{v'w'})_r - \overline{u'w'}\frac{1}{r}(r\bar{v})_r - \overline{u'v'}\,\bar{w}_r + v_c\left(\Lambda q(\overline{v'w'})_r\right)_r$$
$$- \frac{v_c}{r}(\Lambda q\overline{v'w'})_r + \frac{2v_c\Lambda q}{r}(\overline{v'w'})_r - \frac{v_c\Lambda q}{r^2}\overline{v'w'} - \frac{q}{\Lambda}\overline{v'w'}(1 + 2b\beta)$$
$$+ \nu\left[\frac{1}{r}\left(r(\overline{v'w'})_r\right)_r - \frac{1}{r^2}\overline{v'w'} - \frac{2a}{\Lambda^2}\overline{v'w'}\right] \tag{4.21}$$

The equation for q is

$$q^2 = \overline{u'u'} + \overline{v'v'} + \overline{w'w'} \tag{4.22}$$

The boundary conditions to be applied to these equations are

(a) at $r \to \infty$

$$\begin{aligned} \bar{p} &\to p_\infty \\ r\bar{v} &\to \Gamma_\infty/2\pi \\ \bar{w} &\to w_\infty \\ \overline{u'u'} &= \overline{v'v'} = \overline{w'w'} = \overline{u'v'} = \overline{u'w'} = 0 \end{aligned} \tag{4.23}$$

(b) at $r \to 0$

$$\begin{aligned} \bar{v} &= \alpha r \\ \overline{u'u'} &= a_1 + b_1 r^2 \\ \overline{v'v'} &= a_1 + b_2 r^2 \\ \overline{w'w'} &= a_3 + b_3 r^2 \\ \overline{u'v'} &= b_4 r^2 \\ \overline{u'w'} &= b_5 r^2 \end{aligned} \tag{4.24}$$

where the a_n's and b_n's and α are functions of z to be determined. Γ_∞ is the circulation, w_∞ is an undisturbed axial velocity, and p_∞ is the ambient pressure at large r. It is not obvious that $\overline{u'u'} = \overline{v'v'}$ at $r = 0$ from a first look at the equations for these quantities (Eqs (4.16) and (4.17)); nevertheless, it is a fact that the two equations become identical for $r \to 0$.

Sullivan [73] has developed a program for the solution of the set of parabolic equations and boundary conditions given above, and we shall presently examine the nature of these solutions as the initial conditions of the problem are varied. Before going on to a discussion of these results, however, we will exhibit some of the general characteristics of turbulent transport in vortices by considering a very special solution of the equations under consideration.

4.1.1 *Superequilibrium Behavior of a Line Vortex*

It can be shown [71] that the basic features of classical eddy transport methods may be extracted from a second-order closure description of a turbulent shear flow by considering a limiting case of the set of equations consisting of Eqs (4.5) through (4.10). In order to extract the nature of eddy transport models from the model or rate equations for the second-order correlations, we must consider what is implied when we assume that a turbulent flow can exhibit an eddy viscosity.

First, it is apparent that, if the turbulent transport of a quantity depends only on the local gradient of that quantity and a scale associated with the mean flow at the location under consideration, the turbulent transport can have no "memory" of its past history along the streamline. This is tantamount to the assumption that at each point in the flow the turbulent transport correlations can track their local equilibrium value. These local equilibrium values can be obtained from the rate equations for the correlations by setting the left-hand sides of Eqs (4.5) equal to zero. Thus it is assumed that the rate of change of a transport correlation as it follows the mean motion is small compared to the production, dissipation, and diffusion terms which occur at the point in question.

Second, the notion of an eddy transport coefficient is one which does not allow the behavior of the turbulent transport on one streamline of the flow to directly affect the turbulent transport on another streamline. This notion is equivalent to the neglect of the diffusion terms in the equations for the second-order correlations, for it is these terms which link the generation of transport correlations on one streamline in the flow to those on another. Neglect of the diffusion terms in the modeling is accomplished by setting $v_c = p_c = 0$ in Eqs (4.6) and (4.7).

Finally, the use of an eddy transport model is a practice generally restricted to high Reynolds number flows. Therefore, we can take the high Reynolds number limit of the equations for the second-order correlations if we wish to derive a simple form of eddy transport model.

If we follow these rules, it should be possible to derive from the equations for the second-order correlation a simple theory of eddy transport. As discussed above, this theory represents the equilibrium, nondiffusive, high Reynolds number limit of a second-order closure model. For reasons of brevity, we have, for some time, referred to this limit as the "superequilibrium" limit.

For the purposes of discussing eddy transport in a vortex in this monograph, we will follow the prescription given above for a line vortex in which the axial velocity is constant and independent of r and z. The superequilibrium equations for such a vortex are found to be (noting that $\bar{w}$ = constant and $\bar{u} = \overline{u'w'} = 0$):

$$\bar{w}\frac{\partial\overline{u'u'}}{\partial z} = 0 = \frac{4\bar{v}}{r}\overline{u'v'} - \frac{q}{\Lambda}\left[\overline{u'u'}(1 + 2b\beta) - \frac{q^2}{3}\left(1 + 2b(\beta - 1)\right)\right] \tag{4.25}$$

$$\bar{w}\frac{\partial\overline{v'v'}}{\partial z} = 0 = -2\left(\frac{\partial\bar{v}}{\partial r} + \frac{\bar{v}}{r}\right)\overline{u'v'} - \frac{q}{\Lambda}\left[\overline{v'v'}(1 + 2b\beta) - \frac{q^2}{3}\left(1 + 2b(\beta - 1)\right)\right] \tag{4.26}$$

$$\bar{w}\frac{\partial\overline{w'w'}}{\partial z} = 0 = -\frac{q}{\Lambda}\left[\overline{w'w'}(1 + 2b\beta) - \frac{q^2}{3}\left(1 + 2b(\beta - 1)\right)\right] \tag{4.27}$$

$$\bar{w}\frac{\partial\overline{u'v'}}{\partial z} = 0 = -\left(\frac{\partial\bar{v}}{\partial r} + \frac{\bar{v}}{r}\right)\overline{u'u'} + \frac{2\bar{v}}{r}\overline{v'v'} - \frac{q}{\Lambda}(1 + 2b\beta)\overline{u'v'} \tag{4.28}$$

Now, in an eddy viscosity model, one attempts to relate the momentum transport correlation $\overline{u'v'}$ to the mean deformation rate of a fluid element. Pursuing this line of thought, we will introduce the following expressions for the second-order correlations into Eqs (4.25) through (4.28):

$$\overline{u'u'} = UU\Lambda^2\left(\frac{\partial\bar{v}}{\partial r} - \frac{\bar{v}}{r}\right)^2 \tag{4.29}$$

$$\overline{v'v'} = VV\Lambda^2\left(\frac{\partial\bar{v}}{\partial r} - \frac{\bar{v}}{r}\right)^2 \tag{4.30}$$

$$\overline{w'w'} = WW\Lambda^2\left(\frac{\partial\bar{v}}{\partial r} - \frac{\bar{v}}{r}\right)^2 \tag{4.31}$$

$$\overline{u'v'} = UV\Lambda^2\left|\frac{\partial\bar{v}}{\partial r} - \frac{\bar{v}}{r}\right|\left(\frac{\partial\bar{v}}{\partial r} - \frac{\bar{v}}{r}\right) \tag{4.32}$$

$$q = Q\Lambda\left|\frac{\partial\bar{v}}{\partial r} - \frac{\bar{v}}{r}\right| \tag{4.33}$$

From this substitution, one obtains the following equations:

$$Q(1 + 2b\beta)UU = \frac{Q^3}{3}\left(1 + 2b(\beta - 1)\right) + 4UVN_s \tag{4.34}$$

$$Q(1 + 2b\beta)VV = \frac{Q^3}{3}\left(1 + 2b(\beta - 1)\right) - 2UV - 4UVN_s \tag{4.35}$$

$$Q(1 + 2b\beta)WW = \frac{Q^3}{3}\left(1 + 2b(\beta - 1)\right) \tag{4.36}$$

$$Q(1 + 2b\beta)UV = -UU + 2(VV - UU)N_s \tag{4.37}$$

In these equations,

$$N_s = \frac{\bar{v}/r}{(\partial\bar{v}/\partial r) - (\bar{v}/r)} \tag{4.38}$$

The solution of Eqs (4.34) through (4.37) in terms of the parameters b, β, and N_s is

$$UU = \frac{Q^2}{1 + 2b\beta}\left[\frac{1 + 2b(\beta - 1)}{3} - 4bN_s\right] \tag{4.39}$$

$$VV = \frac{Q^2}{1 + 2b\beta}\left[\frac{1 + 4b + 2b\beta}{3} + 4bN_s\right] \tag{4.40}$$

$$WW = \frac{Q^2}{1 + 2b\beta}\,\frac{1 + 2b(\beta - 1)}{3} \tag{4.41}$$

$$UV = -bQ^3 \tag{4.42}$$

$$Q^2 = UU + VV + WW$$

$$= \frac{1}{b(1+2b\beta)^2}\left[\frac{1+2b(\beta-1)}{3} - 8bN_s - 16bN_s^2\right] \tag{4.43}$$

It is clear, since Q^2 is positive definite, that under the assumptions made here turbulence is impossible if

$$N_s < -\frac{1}{4}\left(1 + \sqrt{\frac{1+2b(\beta-1)}{3b}}\right) \tag{4.44}$$

or if

$$N_s > \frac{1}{4}\left(1 - \sqrt{1 + \frac{1+2b(\beta-1)}{3b}}\right) \tag{4.45}$$

Introducing the values of $b = 0.125$ and $\beta = 0$ from our current model of turbulent shear flow, these limits become $N_s < -0.683$ and $N_s > 0.183$.

Figure 4.2 shows the behavior of the quantities UU, VV, WW, UV, and Q^2 with variations of the stability parameter N_s for $b = 0.125$ and $\beta = 0$. The results are plotted in terms of the ratios of the quantities UU, VV, etc., to their values for $N_s = 0$, namely, $(UU)_o$, $(VV)_o$, etc. Thus, Figure 4.2 shows the ratios of $\overline{u'u'}$, $\overline{v'v'}$, $\overline{w'w'}$, $\overline{u'v'}$, and q^2 in a vortex to these quantities in a parallel shearing motion having the same mean deformation rate and scale.

It may be seen from Figure 4.2 that the turbulent energy and shear have the same value for $N_s = -1/2$ that they do for $N_s = 0$. Between $N_s = -1/2$ and $N_s = 0$, the turbulent energy and shear correlations are larger than they are in a parallel shearing motion. For $N_s < -0.683$ and $N_s > 0.183$, as mentioned previously, no locally sustained turbulent flow is possible. Thus, for $-0.683 < N_s < -0.5$, locally self-sustained turbulence is possible although the turbulence is damped by centrifugal effects. For $0 < N_s < 0.183$, turbulence is also possible but here, again, it is damped by the action of centrifugal forces.

Let us see what sort of flows each of these regions represents. First, we note that when $\partial\bar{v}/\partial r = 0$, $N_s = -1$. Thus, at the edge of the viscous core of a vortex (defined here as the radius where $\partial\bar{v}/\partial r = 0$), a turbulent vortex is stable. Near the center of a free vortex, the tangential velocity $\bar{v}$ is of the form $\bar{v} = mr - 2nr^2$ so that as $r \to 0$, $N_s \to -\infty$. Also, for a free vortex, $\bar{v} \to \Gamma/2\pi r$ as $r \to \infty$ and one then finds that as $r \to \infty$, $N_s \to -1/2$. Thus, for the classical vortex distribution

$$\bar{v} = \frac{\Gamma}{2\pi r}\left(1 - e^{-r^2/r_c^2}\right) \tag{4.46}$$

The flow in the outer regions of the vortex exhibits an eddy diffusivity similar to a parallel flow. As the core of the vortex is approached, the flow becomes more and more stable. It becomes completely stable somewhat outside the viscous core of the vortex. Indeed, the flow is stable at the point of maximum deformation $\partial\bar{v}/\partial r - \bar{v}/r$. This behavior of the stability parameter N_s for the classical vortex is shown in Figure 4.3.

We can understand the region of increased turbulence and shear between $N_s = -1/2$ and $N_s = 0$ if we note that the stability parameter may be written

$$N_s = \frac{\bar{v}/r}{\frac{1}{2\pi}\frac{\partial\Gamma}{\partial r} - \frac{2\bar{v}}{r}} \tag{4.47}$$

Thus the region $-1/2 < N_s < 0$ represents flows for which $d\Gamma/dr$ is negative. These are, of course, flows which exhibit the well-known Taylor instability [74].

The region $0 < N_s < 0.183$ is representative of flows occurring between two cylinders rotating in the same direction such that Γ at the outer cylinder is larger than Γ at the inner cylinder when the centrifugal forces due to the general level rotation cannot completely stabilize the flow.

Returning now to the case of a free vortex, it may be surmised from this analysis that the core regions of vortices are locally stable. Regions outside the core are unstable and can generate turbulence. If the core regions of vortices are to exhibit a turbulent shear, this, according to the model, must be caused by turbulence which has diffused into the core region from outer regions which are unstable or by turbulence which has been generated by a shear in the axial direction that is not considered in this analysis. This fact, namely, that the turbulent shear $-\rho\overline{u'v'}$ in a vortex is not directly related to the local deformation $\partial\bar{v}/\partial r - \bar{v}/r$, would lead one to believe that it would be impossible to establish any general rules for determining an eddy viscosity for a vortex. To calculate such flows reliably, it will probably be necessary to use the full power of second-order closure methods.

It might be noted, in this connection, that if one were to use an energy method on such flows, much of the physics of the problem would be lost. This may be seen by considering the sum of Eqs (4.34), (4.35), and (4.36) which is an equation for Q^2. Then, if UU is set equal to VV in Eq (4.37) to evaluate UV , we see that the parameter N_s disappears from the equations and we have lost the essential physics of the problem.

Some idea of the sensitivity of the conclusions discussed above to the choice of the dissipation model parameter β may be obtained from an inspection of Figure 4.4. This figure which is taken from Ref. 71 presents the same data that were shown in Figure 4.2; however, the model parameters in this case were $b = 0.125$ and $\beta = 1$. It is seen that the general features of vortex behavior are not dependent on the choice of dissipation model although the numerical values of the stability limits and magnitudes of the correlation ratios are somewhat affected.

Using the results obtained here, we can get an idea of the local turbulence-producing capabilities of a given vortex by calculating the distribution of $q^2 = \overline{u'u'} + \overline{v'v'} + \overline{w'w'}$ that might be produced in the vortex according to superequilibrium theory. This is best done by dividing the equation for q^2 by Λ^2 and the square of the maximum deformation rate in the vortex. Thus,

$$\frac{q^2}{\Lambda^2\left(\frac{\partial \bar{v}}{\partial r} - \frac{\bar{v}}{r}\right)^2_{max}} = Q^2 \frac{\left(\frac{\partial \bar{v}}{\partial r} - \frac{\bar{v}}{r}\right)^2}{\left(\frac{\partial v}{\partial r} - \frac{v}{r}\right)^2_{max}} = Q^2 \left(\frac{\varepsilon}{\varepsilon_{max}}\right)^2 \tag{4.48}$$

The behavior of this quantity for a classical vortex (Eq (4.46)) is shown in Figure 4.5. It will be noted that according to superequilibrium theory the production of turbulence is limited to a narrow region outside the core of the vortex. This behavior is due to the fact that the vortex is stable to disturbances within and just outside the viscous core and, while it becomes unstable as the point under consideration moves away from the core, the square of the deformation rate, on which the production of turbulence depends, falls off very rapidly – in fact, as the inverse fourth power of r/r_c.

Of course, in real vortices turbulence is diffused, as we shall see in what follows. Nevertheless, experiments do tend to show that the production of turbulence in a vortex which does not have appreciably axial velocities is confined to regions outside its viscous core.

With this very brief introduction to the character of shear generation in simple vortices, we will now proceed to a discussion of some solutions of the full set of equations for the viscous behavior of single vortices having both tangential and axial velocities.

4.1.2 *Simple Vortex with Axial Velocity*

In the previous section, we obtained a very simplified view of the regions of instability of a line vortex. This view has been obtained by considering a vortex in which there was no diffusion of turbulence and in which flows in the axial direction were not considered. In real aircraft vortices, both of these effects are important. We will, therefore, examine the behavior of a vortex when these two effects are considered. We do this by examining the results of numerical solutions of Eqs (4.12) through (4.21) subject to the boundary conditions set forth in Eqs (4.23) and (4.24). To carry out such solutions, we shall need initial conditions on a vortex at some station $z = 0$.

$$\begin{aligned} \bar{u}(r) &= \bar{u}(r,0) \\ \bar{v}_o(r) &= \bar{v}(r,0) \\ \bar{w}_o(r) &= \bar{w}(r,0) \\ (\overline{u_i'u_j'})_o(r) &= \overline{u_i'u_j'}(r,0) \end{aligned} \tag{4.49}$$

The computed solutions then yield the subsequent behavior of $\bar{u}$, $\bar{v}$, $\bar{w}$, and $\overline{u_i'u_j'}$ as functions of z and r.

Consider first the case of a laminar vortex. Let us assume that at $z = 0$ the vortex has the somewhat idealized swirl velocity profile shown in Figure 4.6. We will also assume that the axial velocity at $z = 0$ is uniform and equal to w_∞. The initial tangential velocity distribution chosen is that given by the Betz method for a wing with an elliptic span loading for which the radius of the Betz tube of vorticity was R, where R is $\pi/8$ times the span, b, of the wing. This velocity profile has been modified near its center by a straight line viscous core of extent $0.05R$. For this and subsequent computations, the Reynolds number based upon the dimension R, $\rho w_\infty R/\mu$, has been taken equal to 5×10^4; thus the calculations are representative of rather small-scale wind tunnel experiments.

In Figures 4.7 and 4.8 we show the behavior of the tangential and axial velocities resulting from the effect of molecular viscosity as one proceeds downstream from the initial position $z = 0$. Comparison of Figures 4.7 and 4.8 shows clearly that, when viscosity reduces the tangential velocities in a vortex, this effect is coupled to the axial velocities through the rise in static pressure that occurs near the center of the vortex. Note that for the case under consideration here the rate at which the change in pressure on the axis tends to decrease the centerline axial velocity exceeds the rate at which the transport of axial momentum towards the centerline by molecular motion tends to increase this velocity, at least as far as these computations were carried out, i.e., for $z/R < 40$.

Let us now investigate what would happen if a certain amount of turbulence was introduced into our vortex at $z = 0$. The problem to which we shall address ourselves is this: if a given amount of turbulent energy flux were to be inserted into a vortex at $z = 0$,

does it matter greatly where, within the vortex, this energy is placed? To answer this question, we shall insert a constant nondimensional flux of turbulent energy into the vortex just discussed at several locations and compute the response of the vortex. We define the nondimensional turbulent energy flux as

$$F_{q^2} = \frac{\int_0^\infty 2\pi r q^2 w \, dr}{\int_0^\infty 2\pi r w_\infty^3 \, dr} \tag{4.50}$$

The initial flux that we have chosen to introduce into the vortex at $z = 0$, where $w \equiv w_\infty$, is

$$F_{q_o^2} = \frac{\int_0^R 2\pi r q_o^2 w \, dr}{\pi R^2 w_\infty^3} = \frac{\int_0^R 2\pi r q_o^2 \, dr}{\pi R^2 w_\infty^2} = 4.93 \times 10^{-4} \tag{4.51}$$

This energy q^2 was spread in a $1 + \cos$ distribution centered about three nondimensional positions in the vortex, namely, $r/R = 0$, 0.2, and 0.8. The width of the distribution was allowed to extend $0.1R$ on either side of r, so that the total nondimensional width of the turbulent spot or annular ring of turbulence was $0.2R$. The idea behind studying the effect of turbulence in a vortex while holding the flux of turbulent kinetic energy in the vortex constant was motivated by the thought that a constant flux of turbulent kinetic energy is, in general, related to a constant input of power (constant drag) required to produce this flux of turbulent energy.

Since the areas over which the turbulent energy was introduced are quite different for the three cases ($r/R = 0$, 0.2, 0.8), it is clear that, even though the fluxes of energy are identical, the maximum level of turbulence will be very different in the three cases. For the cases studied here, these maxima are given:

r/R	$F_{q_o^2}$	$\sqrt{q^2_{max_o}}/w_\infty$
0	4.93×10^{-4}	0.816
.2	4.93×10^{-4}	0.220
.8	4.93×10^{-4}	0.111

To start the calculations at $z = 0$, it was assumed that all three components of the turbulent energy were equal, i.e., $\overline{u'^2} = \overline{v'^2} = \overline{w'^2}$ and that the shears $\overline{u'v'}$, $\overline{u'w'}$, and $\overline{v'w'}$ were equal to zero. As the calculation proceeds downstream from $z = 0$, all the correlations seek their appropriate level. As would be expected from the symmetry of the problem, $\overline{v'w'}$ remains identically zero.

One more piece of information is needed before we can proceed to discuss these computations, and that is the specification of the length scale Λ. For the calculations we shall discuss here, Λ was taken to be independent of r, i.e., a function of z only. Its value was related to the scale of the mean motion by setting Λ equal to 0.5 times the radius for which the mean tangential velocity was a maximum. More recent studies have indicated that this choice of the magnitude of Λ might be somewhat too small and that Λ should perhaps be taken, when the dynamic scale equation is not used, to be more like one-half the half-breadth of the local distribution of q^2. As pointed out above, such a choice affects the actual numbers which are computed but does not alter the general character of the results we shall present below.

Consider the case when the turbulent energy was introduced into the center of the vortex, i.e., $r/R = 0$. The behavior of the tangential velocities v/w_∞, the axial velocities w/w_∞, the r.m.s. turbulent energy q/w_∞, and the local radial turbulent shear correlations $\overline{u'v'}/w_\infty^2$ are shown in Figures 4.9 through 4.12, respectively. Although at the initial position of this vortex $z/R = 0$, no turbulent shear correlations were assumed to exist, i.e., $\overline{u'w'} \equiv 0$, the existence of a large level of turbulence at $z/R = 0$ very rapidly produced a turbulent shear which reduced the maximum tangential velocity in the vortex to one-half its original value by $z/R = 10$. (Note that for the laminar vortex, this reduction was only about 20%.) After $z/R = 10$, the rate of change of tangential velocity is seen to be rather slow. This is because the vortex cannot support the level of turbulence that was initially introduced into it (see Figure 4.11 and note the change in scale needed to describe the behavior of q/w_∞ between $z/R = 0$ and $z/R = 10$). An interesting behavior of the production of turbulent shear in a vortex can be observed by comparing Figure 4.12 with Figure 4.9. We see from this comparison that the maximum turbulent shear occurs well outside the position of the maximum tangential velocity; for example, for $z/R = 10$, $\overline{u'v'}_{max}$ occurs at $r/R = 0.255$ while v_{max} occurs at 0.095. We also note that the maximum in the turbulent kinetic energy is not in the center of the vortex. This is an indication that the center of the vortex forms a sort of sink for the turbulence that is produced. Some of this turbulence is produced outside the viscous core by tangential shear while some of it is produced near the center of this vortex by shear associated with the axial velocities shown in Figure 4.10. These axial velocities are a result of the axial pressure gradients set up when the initial tangential velocity was rapidly modified by shear. For this case it is interesting to note that from $z/R = 10$ to $z/R = 30$, there is virtually no change in centerline axial velocity (see Fig. 4.10).

This means, of course, that the effect of the slowly rising pressure on the centerline is just offset by the turbulent transport of axial momentum as a result of the shear in the axial direction. These two effects, as noted previously, are not in balance for the laminar vortex (refer again to Fig. 4.8).

We turn now to an examination of the introduction of roughly the same amount of turbulent energy into a region just outside the viscous core of the vortex. We introduce the turbulent energy centered about $r/R = 0.2$. The results of computations for such a case are shown in Figures 4.13 through 4.16. For this case, we again see that the maximum tangential velocity is about halved from $z/R = 0$ to $z/R = 10$ (see Fig. 4.13). It is also obvious that the vortex, as before, cannot support the level of turbulence introduced into it (see Fig. 4.15). Because a large amount of turbulence was introduced into the vortex at $r/R = 0.2$ while the vortex was initially most unstable at $r/R = 0.3$, a double hump appears in the shear correlation profile at $z/R = 10$ (see Fig. 4.16) before the turbulence distribution is attenuated to a shape which is more typical of axisymmetric vortices. Because of the noncentered introduction of turbulent energy and the resultant double hump character of the shear distribution at small z/R, the tangential velocity distribution acquires a rather noticeable bump at $r/R = 0.3$. Note, then, that the maxima of the shear correlations $\overline{u'v'}$ now occur even outside this bump, i.e., at r/R between 0.3 and 0.4. Since the maximum tangential velocity occurs in the neighborhood of $r/R = 0.1$, this means that the maximum shear for this case occurs at radii that are some three to four times the radii of v_{max}.

We should also note that the axial velocity defect caused by the initial adjustment of static pressure begins to be reduced for $z/R > 10$. That is, the transport of axial momentum towards the centerline of the vortex by axial shear is larger than the effect of centerline static pressure rise due to the decay of the tangential velocities in the vortex (see Fig. 4.14).

Consider now the case when the turbulence is introduced far outside the viscous core of the vortex. The results of computations for $r/R = 0.8$ are shown in Figures 4.17 through 4.19. A comparison of Figures 4.17 and 4.9 shows that the early behavior of the tangential velocities, when the turbulence is introduced so far out in the vortex, is, as might be expected, almost the same in the laminar and turbulent cases. The behavior of the axial velocities is also very similar to that of the laminar vortex (compare Figs. 4.18 and 4.10). Figure 4.19 is interesting. It shows that the vortex can not sustain the level of turbulence introduced into it at $r/R = 0.8$. This high level of local turbulence is partly dissipated and partially diffused by the turbulent motion itself away from its initial annular position. A portion of this initial turbulence eventually reaches the region of the viscous core of the vortex. Here the turbulent energy is amplified by an instability. What is the primary cause of this instability? We note that a lot of the turbulent energy is contained inside the viscous core where, according to our previous discussions, we have found the flow to be stable to tangential deformation rate. We also note that the level of turbulent energy is of the order of that which might be sustained by the axial shears associated with the axial velocity defect that has been produced by the laminar-like decay of the tangential velocities. Actually, it is impossible to completely separate the effects of tangential and axial strain rates in this case, but a significant part of the turbulent energy near the viscous core is produced by the axial velocity profile.

Some further insight into the behavior of vortices when the turbulence is introduced at various radial locations can be gleaned from Figures 4.20 through 4.25 where some typical characteristics of the Betz-like vortices we have been studying are compared. First of all, consider Figure 4.20. If we are to believe these results, we see that the introduction of high levels of turbulence into the core of a vortex will greatly affect the maximum tangential velocity initially. However, the long-range effect of this turbulence, if turbulence is all that is introduced, is not great. (Remember that the characteristic dimension R is about $\pi/8$ times the span of an aircraft generating a Betz-like vortex, so that $z/R = 30$ is approximately 12 spans behind a generating aircraft.) This is because the flux of turbulent energy cannot be sustained by the vortex, as is clear from Figure 4.21. That the actual turbulent energy levels that can be maintained by the vortex at any large downstream distances are pretty much the same, regardless of where the turbulence was inserted, is clear from Figure 4.22. Finally, we should observe that for large z/R the rate of decay of the tangential velocities in the vortices studied here causes a pressure rise on the centerline of the vortex that tends to maintain the axial velocity defect that was initially set up. This may be seen by observing the very low slopes of the $w(0)/w_\infty$ curves for large z/R in Figure 4.25.

4.1.3 *Discussion of Results Obtained for an Isolated Vortex*

In the previous discussion, we have used a second-order closure model of the flow in an axisymmetric vortex to infer some of the aging properties of single vortices. What have we learned? First of all, it is clear that compared to ordinary parallel shear flows an axisymmetric vortex, if it can be made turbulent, will support a level of turbulence and tangential shear that is far less for a given deformation rate and turbulence scale than the parallel flow. Second, it is clear that the level that can be supported depends on both the axial and tangential velocities that are present. The level of turbulent shear and turbulent kinetic energy will depend on the ratios of the rates of deformation in the tangential and axial directions as well as a swirl parameter

$$N_s = \frac{\bar{v}/r}{(\partial\bar{v}/\partial r) - (\bar{v}/r)} \tag{4.38}$$

This latter parameter N_s will depend directly, at a given point in a vortex, on the way in which the circulation varies as a function of r. This, of course, in turn depends

on the distribution of lift and drag on the wing for that portion of the wing that sheds the vortex. The distribution of turbulence level that is introduced into each vortex will also depend on the lift and drag distribution on the wing. Given all these factors, it would appear that each vortex shed by an aircraft will have rather different aging properties. Certainly this will be true in the near wake. We can also guess that we would not expect a flap vortex to have the same aging characteristics as a tip vortex, if indeed one could produce a single such vortex in isolation.

It is for the above-noted reasons that the authors have come to the conclusion that one must abandon the notion of an eddy viscosity that is valid for "vortices." They do not believe that, for the kind of aircraft in operation today, there is such a thing as "one typical vortex" for which one might define an eddy viscosity coefficient that would be useful. Each wake will, in general, be a thing unto itself, and methods which recognize this individuality of wakes should be used in their analysis.

Since, in this monograph, we are really interested in the vortex hazard problem, we should not just ask ourselves how the center of a given single vortex ages, but should concern ourselves with whether or not the aging process can be enhanced. We therefore inquire as to why the vortices we have just studied are so stable and long lived. The answer is that we have an axial symmetry that creates a stabilizing centrifugal force field. If we wish to get rid of vortices faster, we must get rid of as much axial symmetry as possible. Actually, behind real airplanes there is no global axial symmetry so that, ultimately, a pair of vortices of opposite sign can support a turbulent aging process. However, this can be greatly improved upon. If the wing is designed in such a way that, instead of a single vortex being shed from each side, two or more equal-strength vortices of the same sign are shed in such a way that the moment of the shed vorticity is preserved, then the scale on which axial symmetries may play a significant role in damping turbulent exchange is greatly reduced and the vortex aging process will be enhanced.

Since most airplanes in and around airports fly with some degree of flap extension, it is clear that, before a discussion of vortex aging is complete, something must be said about the aging of pairs and multiple pairs of vortices.

4.2 Aging of a Pair of Vortices

It is really beyond the scope of this monograph to enter into a discussion of the detailed methods used to solve the coupled set of equations given by Eqs (4.3) through (4.10) for nonsimple geometries. Suffice it to say that our colleagues, Drs. W. Stephen Lewellen and Milton Teske, have developed, under the sponsorship of the United States Navy, a digital computer code which allows one to obtain such solutions [68]. Here we are interested in the results of some preliminary computations using this new technology.

Let us consider the two-dimensional behavior of a pair of classical vortices of the kind given by Eq (4.46); they are of opposite sign and are spaced a distance b' apart. They are initially located at $y = \pm b'/2$ and $z = 0$ and extend from $x = -\infty$ to $x = \infty$ (airplane coordinates). Let there be a constant velocity in the x direction throughout the y-z plane so that we are really considering a time-dependent solution of Eqs (4.3) through (4.10) but may relate the behavior of the vortices with time to a spacial variation through the relation

$$x = U_\infty t \tag{4.52}$$

Into each vortex whose distribution of vorticity is given, at $t = x = 0$, by

$$\frac{\pi b'^2 \zeta}{100\Gamma} = e^{-100r^2/b'^2} \tag{4.53}$$

a Gaussian spot of turbulence given by

$$\frac{q^2}{q_o^2} = e^{-100r^2/b'^2} \tag{4.54}$$

at $t = x = 0$ is introduced. In these equations, the radius r is measured from the center of each vortex. We choose as an initial condition on the maximum turbulent kinetic energy $q_o^2 = 0.01$ and distribute the energy equally between $\overline{u'^2}$, $\overline{v'^2}$, and $\overline{w'^2}$. All initial shear correlations are taken equal to zero. The distributions of ζ and q^2/q_o^2 are shown in Figure 4.26

Since many experiments on vortices have been carried out using smoke to trace the behavior of the vortices shed by aircraft wings, we have also introduced into the pair of vortices a passive scalar, the concentration of which is measured by the variable c. This passive scalar might be considered to be the mean value of the concentration of smoke or some other passive tracer used to study the behavior of the vortex. The initial distribution of this passive scalar was taken to be

$$\frac{c}{c_o} = e^{-200r^2/b'^2} \tag{4.55}$$

with $c_o = 1.0$. This distribution is also shown in Figure 4.26.

One can make the results of the calculations described above nondimensional with respect to x by dividing x by $b'A/C_L$, where A is the aspect ratio of a rectangularly loaded wing of span b which is supposed to have produced a pair of vortices.

In Figures 4.27 and 4.28, we show some results of a calculation for the initial conditions just described. Figure 4.28 shows contours of constant turbulent kinetic energy on

the basis of q^2/q^2_{max} on one side of the centerline of the generating aircraft. Note that the vortex is descending as it should. Note also that the small nonaxial symmetry of the problem, when a pair of vortices is involved, causes a maximum in the production of turbulent energy that is initially largest on the top and bottom of the vortex. It is also evident that the turbulence level is less near the center of the vortex than it is outside the viscous core. Note by referring to Figure 4.29 that while the axial symmetry of the turbulent kinetic energy field has been strongly affected by the presence of the second vortex, the general appearance of the isopleths of the passive tracer we have introduced does not indicate the lack of symmetry very strongly, at least as far as these computations were taken.

If one were to compare the extend of the cloud of turbulent kinetic energy shown at $x/b' = 1.52\ A/C_L$ in Figure 4.28 with the extent of the streamlines that typically isolate a pair of descending vortices from the surrounding medium in which they descend (see Fig. 4.1), it is clear that as a pair of vortices age, turbulence can reach the isolating and dividing streamlines. When this occurs, the aging process will take on new dimensions as vorticity can be lost to the surrounding medium as well as transported across the dividing streamline (line O-O' in Fig. 4.1). The phenomena of loss of vorticity to the surrounding medium will not be large for tightly centered distributions of vorticity. However, as we shall see in what follows, when more than one vortex is shed from each side of an airplane, these centers of vorticity may interact to cause the vorticity to be widely distributed as a result of the aging process.

4.3 Aging of Multiple Vortices

Let us now perform the same type of calculation for two pair of equal and opposite vortices shed behind a single wing. We will assume a lift distribution on the wing such that our initial conditions at $t = x = 0$ are a pair of equal and opposite vortices located at $z = 0$ and $y = \pm 0.6\ b/2$ and a pair of equal and opposite vortices located at $z = 0$ and $y = \pm b/2$. These vortices were assumed to be classical Lamb vortices and each vortex had a Gaussian distribution of turbulent kinetic energy and tracer material injected into it at $t = x = 0$. The initial distributions of ζ, q^2, and c for each vortex are shown in Figure 4.29.

In Figures 4.30 and 4.31, we show the results of computations for these initial conditions. The lines of constant q^2/q^2_{max} are shown in Figure 4.30. Note the very sharp increase in q^2_{max} between $x/b' = 0.48\ A/C_L$ and $x/b' = 1.52\ A/C_L$. What is this increase in turbulence due to? If we look at Figure 4.31 we see that the two vortices which have been descending and rotating about each other from $x/b' = 0$ to $x/b' = 0.48\ A/C_L$ have, between $x/b' = 0.48\ A/C_L$ and $x/b' = 1.57\ A/C_L$, broken down into one somewhat distorted vortex. This vortex becomes somewhat more symmetrical between $x/b' = 1.57\ A/C_L$ and $x/b' = 2.70\ A/C_L$ with an accompanying drop in q^2_{max}. Note, however, that the vorticity, which is related to the tracer patterns, is now far more widely dispersed than it originally was. Note also that the kinetic energy produced by the merging of two vortices into one is now widely distributed and can easily cause a transport of vorticity across the dividing center streamline $y = 0$ or into a surrounding medium.

As may be seen from Figures 4.30 and 4.31, there are still some numerical difficulties with these programs which begin to give spurious spots of tracer material or smoke and turbulent kinetic energy well outside the remaining vortex at large x/b. In spite of these numerical difficulties, which are being straightened out at the present time, it is felt that the general results of these computations are correct and that the problem of evaluating aircraft wake hazard cannot be solved without an understanding of the straining effect of vortex upon vortex. That the near wake hazard to trailing aircraft was dependent on this phenomena was first pointed out by Dunham [75] who sketched the nature of this merging from dye trace experiments in the wake of a model 747. Figure 4.32, which is taken from Dunham's paper, illustrates this combining of vortices as observed experimentally.

We shall have occasion in the next section, when we discuss the effect of the atmosphere on the behavior of vortices, to return to a discussion of the fact that, at reasonable distances behind real airplanes in the flapped condition, the vorticity and turbulent kinetic energy may be fairly widely distributed in what is usually taken to be the descending oval of vorticity behind an airplane.

5. PERSISTENCE OF VORTICES IN THE ATMOSPHERE

A great deal of material concerning the nature of vortices has been presented in the previous sections. This material can only serve as an introduction to the behavior of real aircraft vortices, for vortices are generated by flight in a real, not an ideal, atmospheric environment. An atmospheric environment is not the constant density, quiescent medium that we have talked about so far, but, for all practical purposes, is one that is never at rest. A study of wakes in the atmosphere requires an investigation of three basic problems:

1. Atmospheric shear
2. Atmospheric turbulence
3. Atmospheric stratification

It is well known that one can have strong atmospheric shears within the planetary boundary layer in the presence of almost no turbulence at all. Over smooth terrain, when there is strong solar heating and radiative cooling, mean velocity profiles such as those shown in Figure 5.1 may be encountered at various times of day [76]. The turbulence levels for the conditions shown in Figure 5.1 are indicated by the values of q^2 in Figure 5.2. It is seen that very large values of both positive and negative shear can be

associated with the so-called low level jet that forms in the early hours of the morning. Both positive and negative shears are found at altitudes that are pertinent to aircraft operations in the vicinity of air terminals.

In the real atmosphere, there can also be times when the wind shear is small but the turbulence level is appreciable. This is also true of wind tunnels and towing tanks and, as we shall see, it does not take much turbulence to affect the long-time behavior of a vortex wake. Since one can have shear without turbulence and turbulence without shear, there is some logic to discussing these two effects separately in what follows.

The final effect we shall deal with is that of atmospheric stratification. Here again we find it useful to discuss the effect of stratification in an ideal medium without the effect of turbulent transport or shear. It is a fact, however, that such ideal conditions are almost never encountered in real flight operations.

Recently, Lissaman, et al. [77] presented a very fine discussion of existing knowledge of atmospheric effects on aircraft wakes. Much of what we will present here has been discussed in this publication. There are, however, a few new results and observations that should be considered in this monograph. This fact, coupled with the authors' desire to make this monograph reasonably self-sufficient, prompts the writers to review again our very meager knowledge of the effects of atmospheric shear, turbulence, and stratification on the nature of aircraft wakes.

5.1 The Effects of Shear

The effect of atmospheric shear must make itself evident on the development of the wake of an airplane from the very start of the roll-up process. If the airplane is flying in a crosswind, the atmospheric vorticity $\zeta_a = -\partial V_a/\partial z$ must introduce some asymmetry into the wake as it rolls up. The importance of this effect must be proportional to the amount of atmospheric vorticity rolled up into each vortex compared to the strength of each vortex Γ_o that would be rolled up in the absence of shear. Now the area of either half of the descending oval of air produced in the absence of shear (see Fig. 4.1) is $1.81\ \pi s_o'^2$, where s_o' is half the initial spacing between the vortices after roll-up is complete. Taking this as approximately $2\pi s_o'^2$, the effect of the atmospheric vorticity on the roll-up process should then be measured by

$$\frac{2\pi s_o'^2 \zeta_a}{\Gamma_o} = \sigma \tag{5.1}$$

To our knowledge, no studies have been made of the effect of shear on the details of the roll-up process. One would expect some asymmetry as σ is negative for the upwind vortex and positive for the downwin vortex when $\zeta_a > 0$, and vice versa when $\zeta_a < 0$.

If the flow is two-dimensional, the atmospheric shear is constant and the wake is out of ground effect, an exact solution for the streamlines about an irrotational vortex pair may be found. The solution depends on the shear parameter σ and the details may be found in Ref. 77. The streamlines for several values of σ that might be of interest in flight operations are shown in Figure 5.3 together with the result for $\sigma = 0$ for comparison. For this ideal solution, the two vortices descend, in the presence of shear, at their classical rate $W^* = \Gamma_o/4\pi s_o'$ and there is no tendency for the vortex pair to tip as has often been reported (see, for example, Refs. 54, 78, 79).

The effect of introducing a ground plane into the ideal solution considered in Figure 5.3 has been studied by Brashears, et al. [80]. They have found that unless more complicated phenomena associated with the formation and decay of the vortices are considered, there is no tendency for the vortices to tip.

There are a number of mechanisms which might be responsible for the tilting of vortices. All of these possible mechanisms have been discussed at one time or another but, as yet, no definitive treatment of the observed tipping has been presented. The mechanisms that have been put forward so far are

1. Asymmetry in the initial roll-up
2. Nonconstancy of the atmospheric shear [79]
3. Effect of the pressure field of the descending vortex pair on the low momentum air near the ground plane [78]
4. Asymmetric effect of transport phenomena on the deformed vortex that results from shear [77]

In the authors' opinion, none of these mechanisms may be ruled out at the present time. It does not seem likely that any simple rule can be laid down. At times the upwind vortex will appear to rise relative to the downwind vortex, while at other times, the opposite will occur. Indeed, the sign of the relative motion might change at various levels in the atmosphere on any given day. The authors do not believe that the tilting problem will be resolved quantitatively until the initial roll-up in the presence of shear has been properly treated and a general method for treating the aging process (possibly, but not necessarily, the method proposed in Section 4) has been brought to a state where it can be shown to give demonstrably reliable results.

5.2 Effects of Atmospheric Turbulence

The effect of atmospheric turbulence per se on wakes has been studied experimentally by Tombach [54]. He proposed to relate the behavior of wakes to the cube root of the turbulent dissipation, $\varepsilon(\mathrm{cm^2 sec^{-3}})$, in the atmosphere. The dissipation ε is not a direct measure of turbulent intensity. It can, however, be related to the turbulent

kinetic energy in the atmosphere through the following approximate formula:

$$\varepsilon = \frac{1}{8}\frac{q^3}{\Lambda} \tag{5.2}$$

where Λ is approximately one-half the longitudinal integral scale of the atmospheric turbulence and $q = \sqrt{\overline{u'^2} + \overline{v'^2} + \overline{w'^2}}$. For a neutral atmospheric boundary layer in approximate equilibrium, the scale parameter Λ has been estimated by

$$\Lambda = 0.65\ h \qquad \text{for} \quad 0 < h < 169 \text{ meters} \tag{5.3}$$

and

$$\Lambda = 110 \text{ meters} \quad \text{for} \quad h \geq 169 \text{ meters} \tag{5.4}$$

where h is the altitude above the ground in meters.

Since, from Eq (5.2), we have

$$q = (8\varepsilon\Lambda)^{1/3} \tag{5.5}$$

we can see that for altitudes in excess of 169 meters (roughly 600 feet) the turbulent intensity q can be considered proportional to $\varepsilon^{1/3}$. The actual value is

$$\begin{aligned} q &\cong (880\varepsilon)^{1/3} \\ &\cong 9.58\ \varepsilon^{1/3} \text{ meters/sec} \end{aligned} \tag{5.6}$$

when ε is measured in $m^2 sec^{-3}$, or

$$\begin{aligned} q &\cong (88000\varepsilon)^{1/3} \\ &\cong 44.5\ \varepsilon^{1/3} \text{ cm/sec} \end{aligned} \tag{5.7}$$

when ε is measured in cm^2/sec^{-3}. We must again point out that this very approximate result applies only for neutral atmospheres and for $h > 169$ meters.

Equations (5.6) and (5.7) must be used with great care since the integral scale and the scale parameter Λ are strongly affected by atmospheric stability. Nevertheless, it would seem that there can be some justification for using $\varepsilon^{1/3}$ as a measure of atmospheric turbulent energy when atmospheric stratification is not strong.

As can be seen from Figure 5.4 taken from Ref. 54, Tombach shows a strong effect of atmospheric turbulence upon both the linking and bursting instabilities discussed in Section 3. These measurements were made on a 910 kg airplane whose wing span was 11.0 meters. The airplane was flown at 56 m/sec and at 27 m/sec so that the two circulations of 16 and 30 m/sec^2 shown on the figure were attained.

5.2.1 *The Effect of Atmospheric Turbulence on Inviscid Instabilities*

Crow [77], [81] has studied the effect of turbulence on the linking instability which he first investigated and which was discussed in Section 3. In his study, it was assumed that the initial spacing of the vortices shed by an airplane in its clean condition is much less than the integral scale of the atmospheric turbulence. This assumption is certainly true for all but the largest aircraft, since the integral scale of the turbulence in the planetary boundary layer ($0 < h < 1000$ m) above an altitude of 169 m is of the order of 220 m and is probably larger than this outside the planetary boundary layer. Since atmospheric turbulence exhibits a Kolmogorov inertial subrange, a typical atmospheric turbulence velocity associated with a scale of the order of the vortex separation is

$$v_\varepsilon = (2\varepsilon s_o')^{1/3} \tag{5.8}$$

A typical velocity associated with the vortex motion itself is

$$v_\Gamma = \frac{\Gamma_o}{4\pi s_o'} \tag{5.9}$$

Thus, the relative effect of atmospheric turbulence on the linking instability should be measured by the ratio

$$\eta = \frac{(2\varepsilon s_o')^{1/3}}{\Gamma_o/4\pi s_o'} \tag{5.10}$$

From dimensional considerations, Crow [81] demonstrates that the wake lifespan or time to linking must be of the form

$$T_\ell = \frac{8\pi s_o'^2}{\Gamma_o}\,\tau\,(\eta,\ R/s_o') \tag{5.11}$$

where R is the radius of an effective tube of constant vorticity. Crow has evaluated the form of the function τ under the assumption that $R/s_o' = 0.2$, so that τ is a function of η only. For wake lifetime calculations, he treats the resulting $\tau(\eta)$ as a "universal lifespan function." For small values of η , i.e., for weak turbulence, Crow finds the relation between τ and η to be

$$\eta = 0.87\tau^{1/4}e^{-0.83\tau} \quad , \ \eta \leq 0.3 \tag{5.12}$$

while for strong turbulence

$$\tau = 0.41\eta \qquad , \eta \gtrsim 0.3 \tag{5.13}$$

The form of this universal lifespan function is shown in Figure 5.5 taken from Ref. 81. The experimental points shown are those obtained by Tombach [54].

It appears, at the present time, from numerous experiments that have been carried out that the wakes of aircraft flown in a clean condition in relatively calm atmospheres exhibit the linking instability postulated and studied by Crow. When an aircraft is flown in its landing or takeoff condition with flaps extended so that at least two vortices are shed on each side of the airplane, it is not clear that the linking instability is always responsible for the attenuation of the vortex system. In this case, after a reasonable distance behind the aircraft, the idea of a vortex tube R small compared to s_o' cannot be supported, as has been shown in Section 4. Moreover, when for some reason vortex bursting occurs, it is questionable whether R can remain small compared to s_o' for any time appreciable compared with the linking time T_ℓ .

Indeed, Tombach, in the process of recording the data presented in Ref. 54, obtained a motion picture of one vortex pair for which conditions were right for vortex bursting to occur on one of the vortices. Shortly thereafter, the unburst vortex ceased its normal descent, and no linking or other instability occurred to disturb it for as long as the vortex was recorded on film (some 194 sec). Lissaman, et al. [77] discuss this observation in some detail and conjecture that it is the result of atmospheric shear (vorticity) under conditions of stability such that atmospheric turbulence effects were negligible. It is clear that when turbulence is produced by breakdown in a vortex whose vorticity is opposite to that of the atmospheric shear, this vortex could be rapidly dissipated while the other vortex remained relatively unaffected.

While Crow has studied the effect of atmospheric turbulence on the linking instability, the authors know of no equivalent study of the effect of turbulence on vortex breakdown. It is apparent from experiment, however, as might be expected, that the linking instability can excite the bursting instability (see Ref. 56) and, as we have already discussed, bursting can have an effect on the linking instability. We have now reached the point when it would appear to be necessary to give some quantitative assessment of the effect of atmospheric turbulence on the aging process.

5.2.2 *The Effect of Atmospheric Turbulence on the Aging of Vortex Pairs*

Sooner or later, when one tries to explain the experimental results that are obtained by measuring the behavior of vortex pairs, one must consider the effect of turbulent or molecular transport. This is particularly true when one seeks to explain the rates of descent of vortices in either neutrally stable or stratified atmospheres. The inviscid theoretical result that a pair of vortices descends for all time in a neutral atmosphere at the rate

$$\frac{dh}{dt} = W^* = -\frac{\Gamma_o}{4\pi s_o'} \tag{5.14}$$

is just not observed to be so [82], [83], [84]. Maxworthy [85] in studying the behavior of vortex rings finds that when the vorticity was relatively well distributed over the ring, there was definitely an exchange of vorticity between the ring and the surrounding medium. As we have seen in Section 4, when an airplane sheds two vortices of like sign and magnitude from each side of the fuselage, it may not be long before the vorticity is rather widely dispersed inside each side of a descending oval that will look something like the ideal oval shown in Figure 4.1

Let us assume that an airplane in the flapped condition has produced a wake in a turbulent atmosphere. We will assume that the vorticity when we first observe the wake, say, at time $t = 0$, is fairly well distributed over each side of the descending oval. The oval at this time $t = 0$ is at altitude $h = h_o$.

If we consider that the case of high Reynolds number based on s_o' and the velocity $W^* = -\Gamma_o/4\pi s_o'$, then the equation that governs the transport of mean vorticity $\bar{\zeta}$ by turbulent action is

$$\frac{d\bar{\zeta}}{dt} = -\frac{\partial}{\partial x_j}\overline{u_j'\zeta'} \tag{5.15}$$

Now integrate Eq (5.15) over the region defined by the streamline OAO' in Figure 4.1. Thus

$$\int \frac{d\bar{\zeta}}{dt}\, dA = -\int \frac{\partial}{\partial x_j}\overline{u_j'\zeta'}\, dA \tag{5.16}$$

or

$$\frac{d\Gamma}{dt} = -\oint \overline{u_n'\zeta'}\, ds \tag{5.17}$$

where we have turned the area integral on the right-hand side of Eq (5.16) into a line integral taken around the perimeter of the region OAO'. In this line integral u_n' is the fluctuation of velocity normal to the surface. The perimeter of this surface is roughly $2\pi s'$. Thus

$$\frac{d\Gamma}{dt} = -2\pi s' \left\langle \overline{u_n'\zeta'} \right\rangle \tag{5.18}$$

where $\langle\ \rangle$ denotes an average value of $\overline{u_n'\zeta'}$ around the perimeter defined by OAO' in Figure 4.1. The value of $\overline{u'\zeta'}$ in a shearing flow is given by a number of the order of (see Ref. 86)

$$\overline{u_n'\zeta'} = -0.26\ \Lambda q \nabla\bar{\zeta} \tag{5.19}$$

where, again, $q = \sqrt{\overline{u'^2} + \overline{v'^2} + \overline{w'^2}}$. This result comes from equilibrium second-order closure theory (see Section 4). In this expression Λ is a measure of the integral scale of the turbulence and is usually about one-half the half-breadth of the turbulent cloud in question.

Now let us assume

$$\nabla\bar{\zeta} \cong -\frac{\bar{\zeta}}{s'} \tag{5.20}$$

and

$$\bar{\zeta} \cong \frac{\Gamma}{s'^2} \tag{5.21}$$

so that

$$\nabla\bar{\zeta} \cong -\frac{\Gamma}{s'^3} \tag{5.22}$$

If, from experience, we take Λ of the order of

$$\Lambda \cong \frac{s'}{4} \tag{5.23}$$

we obtain, substituting into Eq (5.18)

$$\frac{d\Gamma}{dt} = -0.41\ \frac{q\Gamma}{s'} \tag{5.24}$$

We can now proceed by two routes on the basis that experimental evidence does not clearly indicate whether s' increases or remains the same in atmospheric decay. There are two limits:

1. The vorticity that is exchanged across the line from O to O' in Figure 4.1 is annihilated, and that which crosses the perimeter OAO' gets so close together in the wake that it also is annihilated or its moment is zero. In this case we may assume

$$\Gamma s' = \Gamma_o s_o' \tag{5.25}$$

or

$$\frac{1}{s'} = \frac{\Gamma}{\Gamma_o s_o'} \tag{5.26}$$

where s_o' and Γ_o are the initial half-separation and circulation, respectively.

2. There is no change in the separation and $s' \equiv s_o'$.

If we put the first proposition into Eq (5.24), we get

$$\frac{d\Gamma}{dt} = -0.41\ \frac{q\Gamma^2}{s_o'\Gamma_o} \tag{5.27}$$

If we put the second proposition into Eq (5.24), we get

$$\frac{d\Gamma}{dt} = -0.41\ \frac{q\Gamma}{s_o'} \tag{5.28}$$

Integration of Eq (5.27) yields (assuming q = constant)

$$\frac{\Gamma}{\Gamma_o} = \frac{1}{1 + 0.41(qt/s_o')} \tag{5.29}$$

Integration of Eq (5.28) yields

$$\frac{\Gamma}{\Gamma_o} = e^{-0.41(qt/s_o')} \tag{5.30}$$

We can now compute the descent of the main vortices from

$$\frac{dh}{dt} = -\frac{\Gamma}{4\pi s'} \tag{5.31}$$

For the first proposition, Eq (5.31) becomes

$$\frac{dh}{dt} = -\frac{\Gamma^2}{4\pi\Gamma_o s_o'} = -\frac{\Gamma_o}{4\pi s_o'}\left(\frac{1}{1 + 0.41\ \frac{qt}{s_o'}}\right)^2 \tag{5.32}$$

For the second proposition, Eq (5.31) becomes

$$\frac{dh}{dt} = -\frac{\Gamma}{4\pi s'_o} = -\frac{\Gamma_o}{4\pi s'_o} e^{-0.41(qt/s'_o)} \tag{5.33}$$

Integration of Eq (5.32) for the condition $h = h_o$ at $t = 0$ gives

$$h_o - h = 0.19 \frac{\Gamma_o}{q}\left(1 - \frac{1}{1 + 0.41 \frac{qt}{s'_o}}\right) \tag{5.34}$$

Equation (5.34) yields for the maximum possible altitude drop

$$(h_o - h)_{max} = 0.19 \frac{\Gamma_o}{q} \tag{5.35}$$

Integration of Eq (5.33) yields

$$h_o - h = 0.19 \frac{\Gamma_o}{q}\left(1 - e^{-0.41(qt/s'_o)}\right) \tag{5.36}$$

Note the maximum possible altitude drop is the same in both cases, namely,

$$(h_o - h)_{max} = 0.19 \frac{\Gamma_o}{q} \tag{5.35}$$

Not only are both the altitude drops the same, but both results may be written in the form

$$\frac{\Delta h}{(\Delta h)_{max}} = 1 - \frac{\Gamma}{\Gamma_o} \tag{5.37}$$

The difference between the two propositions is the time required to reach a given value of $\Delta h/\Delta h_{max}$. In Figure 5.6 these times are shown in the nondimensional form $t/(s'_o/q)$.

There are a number of points to be made about this admittedly oversimplified analysis.

1. The constant 0.41 is obviously not sacred, just an order of magnitude guess and is obviously directly related to the constant 0.19.
2. The maximum descent is independent of the span of the aircraft producing the wake. This is related to the assumption of constant q where q is a measure of the total atmospheric turbulent energy.
3. When the integral scale of the atmospheric turbulence is very large compared to s'_o, then some portion of the turbulent energy produces a meandering of the wake while the remaining portion of the turbulent energy can be thought of as being responsible for the instantaneous diffusion of vorticity about the meandered position of the wake. If this effect is to be taken into account, the q used in Eq (5.24) should be taken equal to roughly $(s'/\Lambda)^{1/3}$ times the total value of q.

If we refer to Figure 5.4 and note that the boundary between light and negligible turbulence is taken to be $\varepsilon = 1\ cm^{2/3}sec^{-1}$, we can convert this to q through the use of Eq (5.7). We find for $\varepsilon = 1\ cm^{2/3}sec^{-1}$ that $q = 44.5$ cm/sec or 1.46 ft/sec. Thus a value of 1 ft/sec for q is a small turbulence intensity. Let us then compute the maximum wake descents given by Eq (5.35) for several aircraft under the assumption that $q = 1$ ft/sec. The results are given in the following table:

Aircraft Type	Weight (lbs)	Span (ft)	Flight Velocity (ft/sec)	Γ (ft^2/sec)	Δh_{max} (ft)
Light Single Engine	2000	29	117	315	60
Light Business	7700	46	142	631	120
Light Prop. Transport	27400	95	147	1050	199
DC-9	70000	89	236	1783	339
747 Landing	550000	195	225	6707	1274
747 Climbout	750000	195	320	6430	1222

The wake descents given in this table are in rough agreement with descents that have been observed [54], [82], [83], [84].

Another result of some interest may be obtained from a consideration of Figure 5.6. It has generally been observed that, while there is some growth in the vortex separation $2s'$ during wake decay, the general tendency is for s' not to increase markedly from s'_o. If we make use of this fact by using the curve for $s' \equiv s'_o$ in Figure 5.6, we observe that only 5% of the vorticity originally shed by the wing would remain within the descending bubble at a time equal to

$$t_{.05} \cong 7.35 \frac{s'_o}{q} \tag{5.38}$$

If we substitute Eq (5.7) into Eq (5.38), we obtain

$$t_{.05}(\text{sec}) = 0.165 \frac{s'_o}{\varepsilon^{1/3}} \tag{5.39}$$

where s'_o is in cm and $\varepsilon^{1/3}$ is in $\text{cm}^{2/3}\text{sec}^{-1}$. For the 11 meter wing used by Tombach to produce the data shown in Figure 5.4, we would have $s'_o \cong \pi \times 1100/8 = 432$ cm. Putting this result into Eq (5.39) yields for Tombach's experiment

$$t_{.05}(\text{sec}) \cong \frac{71.3}{\varepsilon^{1/3}(\text{cm}^{3/2}\text{sec}^{-1})} \tag{5.40}$$

This result is in rather remarkable (actually fortuitous) agreement with Tombach's published result of

$$t(\text{sec}) \cong \frac{70}{\varepsilon^{1/3}(\text{cm}^{3/2}\text{sec}^{-1})} \tag{5.41}$$

shown in Figure 5.4.

Although it is not an effect due to atmospheric turbulence, one more analysis related to those just given is probably worth presenting at this point. Suppose the typical turbulent fluctuation in Eq (5.24) was not that due to the atmosphere but was due to the vortex swirling motion itself. Equation (5.24) would then take the form

$$\frac{d\Gamma}{dt} = \alpha \frac{\Gamma^2}{s'^2} \tag{5.42}$$

where α is a constant. Under the assumption $\Gamma s' = \Gamma_o s'_o$, integration of Eq (5.42) and solution for $h_o - h$ yields

$$h_o - h = \frac{s'_o}{4\pi\alpha}\left[\left(1 + \frac{3\alpha\Gamma_o t}{s'^2_o}\right)^{1/3} - 1\right] \tag{5.43}$$

Under the assumption that $s' \equiv s'_o$

$$h_o - h = \frac{s'_o}{4\pi\alpha} \ell n \left(1 + \frac{\alpha\Gamma_o t}{s'^2_o}\right) \tag{5.44}$$

Equations (5.43) and (5.44) show that turbulent transport associated with the vortex motion itself is incapable of stopping the descent of a vortex in a neutrally stable environment. That vortices do reduce their rate and sometimes stop their descent in a neutral environment that has a residual turbulence level has been demonstrated by Brown [87]. It is concluded here that when stopping occurs, it must be the result of the background turbulence in the facility at which the results presented in Ref. 87 were obtained. Experiments such as those reported by Brown, carried out under carefully controlled conditions where the turbulence levels and scales are measured, could be most useful in evaluating the simple theory given above.

5.3 Effects of Stratification

One would think intuitively that the effect of stable atmospheric stratification would be to decelerate the downward motion of a pair of trailing vortices. With the levels of stable stratification that are found in the atmosphere, it is rather surprising to learn that the result of inviscid studies yields quite a different result. Important theoretical studies of inviscid vortex pair descent into stratified media have been carried out by Scorer and Davenport [88], by Tombach [89], by Crow in conjunction with Lissaman, et al. [77], and more recently by Crow [90]. All of these investigators conclude that the result of stable stratification in an inviscid medium is an increase in the rate of descent of a pair of vortices with the passage of time. It is important to understand the nature of this inviscid phenomena. Crow's latest paper on this subject [90] gives a very clear discussion of the physical phenomena involved in the process. In order to obtain simple analytical results, Crow makes use of the fact that the ratio of fluid accelerations resulting from atmospheric stratification

$$a_{strat} = W^* N \tag{5.45}$$

to fluid accelerations due to the circulation

$$a_\Gamma = \frac{W^{*2}}{s'_o} \tag{5.46}$$

is small. In these expressions

$$N = \left(\frac{g}{T}\frac{d\theta}{dh}\right)^{1/2} \quad , \quad W^* = \frac{\Gamma_o}{4\pi s'_o} \tag{5.47}$$

In Eq (5.47), h is the altitude, T is the local temperature, θ is the potential temperature, and g is the acceleration due to gravity. The ratio of accelerations is

$$\frac{a_{strat}}{a_\Gamma} = \frac{4\pi s'^2_o}{\Gamma_o} N = \chi \tag{5.48}$$

To estimate a typical value of N, we note that for an isothermal atmosphere which is stable

$$N \approx 0.02 \text{ sec}^{-1} \tag{5.49}$$

Now for a light single-engine airplane, $4\pi s_o'/\Gamma_o$ is of the order of 5 seconds, while for a 747 in landing condition $4\pi s_o'^2/\Gamma_o$ might be as high as 10 seconds. Thus, the ratio of accelerations due to stratification to those due to circulation is, typically, a number in the range 0.1 to 0.2.

Making use of this fact and assuming that the vorticity is contained in tubes that are small compared to s' at all times, Crow finds that, for stably stratified flows, the descending oval of relatively lighter air is as shown in Figure 5.7. The descending cell contracts as it leaves a trail of lighter fluid moving upwards through a drainage filament. The trajectories of the vortex tubes found by Crow are shown in Figure 5.8 for various values of χ.

Now the inviscid behavior that has been described is just not observed experimentally in any wake of appreciable age [54], [87], [91]. It is possible that for very clean wings with almost rectangular loading, tested in a truly quiescent medium, the behavior predicted by the inviscid theory might be observed for a short time. Such experimental evidence is difficult to come by. In any event, if we are to believe the Betz rollup theory at all, we see that, even for elliptically loaded wings, there is always a small amount of vorticity that is spread almost to the edge of the descending oval. In this case, the existence of any drainage would remove some vorticity from the oval and would certainly change the nature of the problem even in the case of inviscid flow.

The real problem, however, with any inviscid analysis of vortex descent is that it neglects the transport of vorticity across streamlines. This must be the dominant phenomena in considering any aircraft wake of appreciable age. This fact is evident from the experimental studies of Tulin and Schwartz [91], Tombach [54], Maxworthy [85], and Brown [87]. Here we present in Figures 5.9 and 5.10 the results of some measurements of wake descent in stratified media. Figure 5.9 is taken from Ref. 54 and shows the early descent, while Figure 5.10 is taken from Ref. 87 and illustrates the late time behavior of wake descent in stratified media.

A description of the descent of a real wake must take into account at least four effects:

1. The way the vorticity is distributed in the initial process of rollup. To be done properly, account must be taken of both the lift and drag distributions on the wing as well as the existence of any sources of thrust.
2. How much turbulent energy is introduced into the rollup process by wing drag and engine thrust.
3. How much heat has been introduced into the wake by the propulsion system of the aircraft.
4. What is the scale and level of intensity of the ambient turbulence.

Recently, the technology necessary to address the nature of viscous wakes in stratified media has been developed by Lewellen, et al. [68] in connection with another problem. This technology has not yet been applied to the calculation of aircraft wakes, but it would seem that this is the general direction that must be taken if we are to understand the nature of aircraft wakes.

6. AIRCRAFT DESIGN TECHNIQUES TO MINIMIZE WAKE HAZARD

It is only fair to the poor soul who has waded his way through the quasi-learned discussions of the previous sections, hoping to find some information which might allow him to mitigate the hazard posed by aircraft wakes, that the authors now attempt a discussion of the minimization of vortex hazard. We shall draw upon the results that have been presented in the previous sections to give our own ideas as to what appear to be fruitful avenues for the designer of aircraft to follow if he desires to minimize the hazard to other (particularly smaller) aircraft that may have to fly in the wake of the airplane he has on the boards.

The authors wish to point out, before entering into this discussion, that they are fully aware that an aircraft design, in order to be considered successful, has to be such that the resulting airplane is operationally profitable. Thus, any large weight, cost, maintenance, or performance penalties that might be incurred as a result of applying a device to reduce wake hazard will, automatically and quite effectively, bias the designer against the use of such a solution. What we shall seek to do here is to make some observations about aircraft design that will mitigate wake hazard while at the same time result in little, if any, adverse effect on the operational profitability of an aircraft.

6.1 Some Simple Rules to Follow

It has become common practice in the United States to evaluate wake hazard by measuring the maximum rolling moment that will be encountered by a test wing or aircraft in the y-z plane as a function of the distance x of the test wing from the generating aircraft (see, for example, Refs. 75 and 92). Such a measurement is, of course, dependent on the ratio of the span of the test wing to the span of the generating wing, but, nevertheless, such measurements do allow one to evaluate at what distance behind a given airplane another aircraft will encounter rolling moments that exceed its own roll control capabilities. What are the rules to be followed to reduce the rolling moment on any given following aircraft? Since the problem for the trailing airplane is worse the smaller its span,

we will primarily address ourselves to trailing aircraft having spans considerably smaller than those of the generating aircraft.

To reduce the wake hazard to a small aircraft immediately behind a larger one, it is clear that we would want to distribute the vorticity trailed by each wing as widely as possible. To dissipate the wake at large distances from the aircraft, we would want the wake itself to generate or sustain as much turbulence as possible. What are the chances of accomplishing these ends in a way which does not interfere with the profitability of the airplane we wish to design? First of all, since practically all serious problems associated with wake hazard occur in the vicinity of airports, we will address ourselves here to the problems of designing an airplane for low wake hazard when it is in a flaps-extended condition. If we are to improve our present design technique for this case, let us consider the kinds of vortices trailed by some current designs when they are in take-off and landing configurations. Figures 6.1, 6.2, and 6.3, taken from Ref. 13, show the span load distributions on three aircraft in takeoff and landing configurations together with the vortices that are trailed by the wings in these configurations. Figure 6.1 gives this information for the DC-7, Figure 6.2 for the DC-9, and Figure 6.3 for the C-141 cargo airplane. It is important to note that all of these aircraft shed vortices from their flaps that are stronger than their tip vortices. Indeed, in the landing configuration, both the DC-7 and the DC-9 carry almost their entire lift in that part of the span inboard of the flaps. It is clear then, since rolling moments are proportional to Γ, that one could reduce the rolling moments on a test airplane behind these aircraft by a redistribution of the lift on the wings. To get a very quick and approximate number to measure the reduction in rolling moment, consider the two idealized wing loadings shown in Figure 6.4. In this figure we show an unmodified aircraft configuration in which all the lift is carried on the flapped portion of the span b_f and a modified wing designed in such a way that two equal vortices are shed on each side of the aircraft, one from the tip and one from the flap. If the lift or weight of the airplane is fixed, then in the two cases the moments of the trailed vorticity must be equal. Thus,

$$\Gamma_o b_f = \Gamma_m b_f + \Gamma_m b \tag{6.1}$$

or

$$\frac{\Gamma_m}{\Gamma_o} = \frac{b_f/b}{1 + b_f/b} \tag{6.2}$$

For normal aircraft, b_f/b ranges from about 0.6 to 0.75 so that typically

$$\frac{\Gamma_m}{\Gamma_o} \cong \frac{0.65}{1.65} \cong 0.4 \tag{6.3}$$

Equation (6.3) tells us that we should be able to accomplish a large reduction in rolling moment behind an airplane in the landing configuration if we redistribute the load on the wing to carry more load outboard than is customary in many current designs. What is the penalty paid for this reduction? The wing must certainly be designed with effective control of lift over both inboard and outboard wing sections; this is admittedly a penalty of complication and weight. What is the penalty in drag? There will, in general, be none, for the airplane with its redistributed lift performs as an essentially higher aspect ratio wing so that its induced drag is actually less than that of the basic configuration while the profile drag is essentially the same.

What other advantages are inherent in the two equal vortex design criterion? For typical values of b_f/b a glance at Figure 2.2 shows that these two vortices will remain together. In this case, they may strain each other in such a way as to cause the generation of considerable turbulence and an attendant distribution of the vorticity throughout the descending wake of the aircraft, as we have seen in Section 4. This is a most desirable end. One might be tempted to guess that the maximum generation of turbulence would occur when the two vortices are of equal strength, but there is no proof of this intuitive thought. For real aircraft wings, it may not be true; the two vortices trailed from flap and tip will, even if they are of the same total strength, be quite different in structure. This would appear to be a fertile field for research, both experimentally and theoretically.

It is important to note again that real airplanes in the flapped condition do not trail two vortices from each wing. Multiple vortices are trailed and some of these secondary vortices can have a profound effect upon the rate at which the wake develops turbulent transport and a redistribution of vorticity by this mechanism. In order for this mechanism to be most effective, the two principle vortices trailed by the wing must be kept as close together as possible in order that the strain of each on the other is a maximum. What effect do the secondary vortices have upon this process? Let us consider the effect of the negative vortex that is generally trailed from the juncture of the wing root and the fuselage. Figure 6.5 shows the effect of the strength and sign of a fuselage or root vortex upon the trajectories of a tip and a flap vortex. The curves shown were computed for a wing which is configured to shed tip and flap vortices of equal strength $\Gamma = \Gamma_t = \Gamma_f$. These vortices are assumed to be located at $y = y_{t_o} = 0.85(b/2)$ and $y = y_{f_o} = 0.4(b/2)$, respectively, at $x = 0$. A root vortex having strength Γ_r was assumed to be shed from $y = y_{r_o} = 0.15(b/2)$ at $x = 0$. All these vortices were assumed to lie in the plane $z = 0$ at $x = 0$. What is plotted in Figure 6.5 is the separation of the main vortices

$$d = \sqrt{(y_t - y_f)^2 + (z_t - z_f)^2} \tag{6.4}$$

in nondimensional form $2d/b$ versus $2x/b$. For the cases shown, the lift coefficient

of the wing

$$C_L = \frac{\Gamma_t A}{U_\infty b}\left(2.55 + .3\,\frac{\Gamma_r}{\Gamma_t}\right) \tag{6.5}$$

was held constant by changing the strengths of the tip and flap vortices as Γ_r/Γ_t was varied. The results shown in Figure 6.5 were obtained for a lift coefficient of 1.2 and an aspect ratio of 7.

Examination of Figure 6.5 reveals that slightly negative root vortices ($\Gamma_r/\Gamma_t \approx -0.1$), in general, move the main vortices Γ_t and Γ_f a little further apart than they would tend to stay were there no root vortex. Slightly positive root vortices ($\Gamma_r/\Gamma_t \approx +0.1$) tend to keep the vortices a little closer together on the average. It does not seem to be desirable to increase Γ_r/Γ_t much above about 0.1, since the curve for $\Gamma_r/\Gamma_t = 0.3$ shows that the main vortices move further apart again. It is interesting to note that when $\Gamma_r/\Gamma_t = -0.5$ the main vortices Γ_t and Γ_f move very far apart. Because of the low moment of the vorticity trailed at the root, there is very little effect of this vortex on the strengths of the equal tip and flap vortices required to maintain constant lift. This can be seen from the table presented below.

Γ_r/Γ_t	$\Gamma_t/\Gamma_{t_o} = \Gamma_f/\Gamma_{t_o}$
0.5	.944
0.3	.966
0.1	.688
0	1.000
-0.1	1.012
-0.3	1.036
-0.5	1.063

That a strong negative root vortex can cause the tip and flap vortices to separate has been observed in smoke studies of aircraft wakes carried out recently at the Langley Research Center of NASA by Patterson [93]. Figure 6.6 shows wake smoke studies after the passage of a model of the 747 with only its outboard flaps deflected. In this configuration, it is clear that the 747 will shed a very strong negative root vortex. It is also clear from Figure 6.6 that, as time passes, the negative root vortex tends to pair up with the flap vortex in such a way that the tip and the flap vortices are removed from each other.

If the results of Figure 6.5 are to be believed, it should pay one to prevent as much loss of lift at the wing-root juncture as is practical in order to achieve as rapid straining of the tip and flap vortices as is possible. Indeed, the addition of a little additional lift at the fuselage might be helpful. This additional lift might not be worth the complexity of the mechanism required to accomplish this result. It would, of course, be a desirable move from the point of view of induced drag to prevent a negative fuselage vortex from being shed at the wing root.

6.2 The Use of Special Devices

So far in our discussion of design for minimum wake hazard, we have concentrated primarily on slight modifications of existing aircraft design technique so as to take as much advantage of modest changes of wing span load distribution as possible. How far one can go in this direction is moot. Much experimental and theoretical work remains to be done to find an optimum span-load distribution. Should there be two equal vortices from flap and tip with a slightly positive root vortex? Or, can we go even further and trail three or perhaps four equal vortices from each wing? These are questions that can not be answered here, but the direction that research and practical design studies should take is, we believe, quite clear from what has been said above.

What about other schemes for causing rapid dissipation of vortices? A few years ago, there was an avalanche of proposals for quick methods for "getting rid of" the vortex hazard. We may break such proposals down into the following categories according to what the proposers of these schemes thought was the principal cause of their particular system's success.

1. Addition of axial velocity to the core of the vortex
2. Depletion of axial velocity in the core of the vortex
3. Addition of vorticity opposing that of the original vortex or tip load modification
4. Introduction of turbulence into the vortex
5. Span loading variable with time

Method 1 was, as far as the authors are aware, first proposed by Rinehart, Balcerak, and White [94], and many people since that time have studied the effect of mass injection at wing tips as well as into single vortices (see, for example, Refs. 92, 95, 96, 97, and 98).

Method 2 has been studied extensively by NASA starting with the work of Corsiglia, Jacobsen, and Chigier [99]. Studies have been carried out on the use of drag splines by Hastings, et al. [100], Patterson [101], and Dunham [75].

Of course, with either Method 1 or Method 2, one cannot help but introduce turbulence when a turbulence-producing flow, a jet or a wake, is introduced into the vortex. Thus, these methods really contain Method 4.

We shall consider as fitting in Method 3 all devices that tend to resist the normal rotation that starts its rollup at the wing tip. In this category, we include straightening vanes and vanes used to induce opposite rotation (see Uzel and Marchman [102]), as well as end plates and schemes for blowing air at the wing tip so as to oppose the natural circulation (see Yuan [103]).

Introduction of "turbulence" into the vortex, Method 4, through the use of spoilers at locations other than the tip has been tried by Croom [104]. It must be recognized that when "turbulence" is introduced by spoilers a major effect on the wake may be a change in the wing load distribution which alters the mean structure of the wake more than the introduction of "turbulence." Although there has been much talk of introducing turbulence into the wake in the past, the authors know of no experimental study where this effect has been studied in isolation from other effects.

Finally, Method 5, the use of time-varying span load to excite the Crow instability, has been studied experimentally by Chevalier [56] and Bilanin and Widnall [58].

One of the troubles with evaluating the effectiveness of all devices used to change the nature of a tip vortex is the fact that almost any gadget added to the tip of a wing will greatly alter the lift distribution on that portion of the wing. This, as we have seen, greatly modifies the tip rollup and it is difficult to separate out just what any given device does. Does it affect primarily the lift distribution? Does it affect primarily the axial velocity profile? Does it produce multiple vortices? Or does it temporarily produce a single centered vortex with a change in sign of circulation (a highly unstable situation)? There is no question but what such devices can and do produce large changes in the near wakes of aircraft trailing a single pair of vortices. It is also true that they do not affect greatly the total flux of angular momentum in the near wake. They do tend to increase the rate of diffusion of vorticity at larger distances from the generating aircraft, but the drag or power penalties for greatly modifying the roll power contained in the far wake seem to be fairly large, as we shall presently see.

It is also not clear that these devices are relatively anywhere nearly as effective for aircraft in the flapped condition as they are when the airplane is clean. As we have said before, the slow-flying, flapped, heavy aircraft is the real operational problem so that, to a certain extent, this operational fact tends to downgrade the usefulness of specialized tip devices.

Method 5, the use of time-varying load distributions, can be effective in causing vortex linking and a subsequent very rapid diffusion and/or annihilation of vorticity for the case of clean wings. It is not yet clear that, for the case of flapped wings, the linking mechanism is effective. At the present time, studies currently underway in the NASA laboratories or sponsored by NASA are concerned primarily with alleviating the wake hazard of flapped aircraft. To date they have not been concerned with the linking instability per se but instead have considered the relative merits of several devices that have been proposed for wake hazard alleviation when compared with what can be accomplished by optimizing wing load distribution for the minimization of wake hazard.

6.3 Recent NASA Studies

Recently a rather extensive experimental program has been carried out by NASA in order to compare the relative effectiveness of "devices" for the alleviation of wake hazard with the effectiveness of wing span load revision as a means to accomplish the same end. This is a continuing program and involves the use of similar models in several different facilities, as well as flight tests of like configurations to check the validity of wind tunnel and towing tank tests of scaled models.

Typical of these tests is a program, centered about the reduction of the wake hazard of the 747 aircraft, that has been carried out at the Langley Research Center of NASA. In one series of tests conducted by Dunham [75], a model characteristic of the 747 was tested in a water towing tank in four configurations. The first configuration was the basic 747 landing-approach configuration, with flaps and leading edge slats extended, and flown (towed) at a lift coefficient of 1.2. The second and third configurations are shown in Figure 6.7. One "device," configuration (a) in Figure 6.7, represented a drag spline located at 80% of the semispan of the model. The other "device," configuration (b), represented a spoiler device running from 50% to 70% of the semispan. Both of the configurations were also flown (towed) at $C_L = 1.2$. The final configuration was with the wing in its usual landing-approach configuration but with the outboard flaps removed. This configuration was also flown (towed) at $C_L = 1.2$.

It should be pointed out here that the results we will present below are not to be taken as gospel for the 747 or for any other real airplane. The NASA tests have shown, as we might expect from our discussion of vortex rollup and geometry in Sections 1 and 2 and the effect of secondary vortices discussed in this section, that the exact nature of the wake of an airplane is very sensitive to configuration. This is particularly so in the case of models which must be mounted in their test environment with the consequent possibility of secondary vortices and turbulence being shed as a result of the mounting struts. Nevertheless, the general character of the results that we will present is believed to be correct.

We will present some results obtained by Dunham for the case of a rectangular trailing test wing representative of a trailing aircraft having a span of 0.182 that of the generating aircraft. The results are the maximum rolling moments C_ℓ^* experienced by the trailing wing in three y-z planes behind the generating aircraft, namely,

$x/b \approx 15$, $x/b \approx 30$, and $x/b \approx 45$. We will make these rolling moments nondimensional with respect to the level of maximum rolling moment incurred by the test wing at $x/b = 15$ for the unmodified generating aircraft. This level we give the symbol $C^*_{\ell_o}$. Typical results are given in the table of values of $C^*_\ell/C^*_{\ell_o}$ below.

x/b	Basic Model	Spoiler Model	Spline Model	Modified Lift Model
15	1.0	.39	.65	.64
30	.92	.29	.56	.47
45	.79	.16	.47	.35

It is clear from this table that large reductions in rolling moment can be accomplished through the use of spoilers. It is also interesting to note that we can accomplish more in this particular case through the redistribution of lift than we can through the use of the spline device. This table is not the whole story, however. We must also inquire as to what penalty in drag must be paid for the above reduction. If we make the drag of each configuration dimensionless by dividing by the drag of the basic model, we get a measure of the drag penalty paid for the cure we have effected. The results of such a calculation are shown below.

	Basic Model	Spoiler Model	Spline Model	Modified Lift Model
C_D/C_{D_o}	1.0	1.6	1.2	0.9

These results are interesting. They show that while the spoiler configuration was most effective in reducing the rolling moment on the following model, one had to pay for the reduction with a 60% increase in drag. For the splined configuration which was not quite as effective in reducing rolling moment as was the redistributed lift, the drag penalty was a 20% increase. As anticipated earlier in this section, redistributing the lift actually reduced the drag of the generating aircraft by some 10%. This is, indeed, pleasing to the designer, for although some additional complexity might be required to design for wake alleviation, he actually does not have to pay a drag penalty for the reduction.

The authors should point out again that results such as those presented above are, in detail, very dependent on the precise configuration being tested. Nevertheless, it is the opinion of the authors that, at the present time, research on the vortex alleviation problem must start with a complete understanding of what can be accomplished in the way of vortex hazard elimination by proper wing span-load design. This developmental research must include an understanding of the role played not only by the primary vortices trailed by an airplane but by root and other secondary (tail) vortices as well. It must also consider the way in which flap vortices should be trailed in conjunction with the placement of any wing-mounted propulsion devices.

The laboratories of NASA are well started on a program of this type and the results will, we are sure, be of great interest and importance to aeronautical engineers.

6.4 Tail Design

We have just concluded a brief review of some recent research at NASA on vortex hazard alleviation with the admonition that the detailed behavior of the wake of a wing is enormously sensitive to the lift and drag distributions on the wing and to any secondary vortices that might be shed by mounting struts or other surfaces generating lift or drag in the vicinity of the wing. It is therefore necessary to say something about the effect of tails on wakes and, as we shall see, perhaps more importantly on the effects of the wakes of wings on tails.

It is clear that the vortices shed by the tail of an airplane represent important secondary vortices. For stable aircraft of conventional configuration, the tail vortex shed on the same side of an airplane is of opposite sign from that trailed by the wing. A brief look at Figure 2.2 shows that a pair of negative vortices may be captured by a pair of stronger positive vortices for quite a range of separations if the vortices are initially coplanar. The same is true for noncoplanar vortices. When a wing is trailing a strong vortex pattern and the tail trim lift is not too large, the negative tail vortices can be "captured" by the wing vortex pattern and can interact strongly with this pattern. On the other hand, if the tail lift is large enough, the tail vortices "escape" the field of the wing vortices and rise above the aircraft. The case when tail vortices are most important is when they are reasonably strong compared to the main wing vortices but are still not strong enough to escape a strong interaction with the wing vortices. It thus happens that changes in airplane trim can, under certain circumstances, have a powerful effect on the structure of an aircraft's wake.

There is only one thing to be said about this. That is, before one can truly say anything about the wake of an airplane, he must have a complete knowledge of the lift, drag, and thrust distributions on the aircraft in question. It may be possible to classify the kind of wake behavior that will be observed behind an aircraft on the basis of inviscid considerations, i.e., do the vortices stay together and interact strongly or do they tend to draw apart and interact less strongly, following a scheme such as that set forth in Section 2. However, if one really desires precise answers, it is going to be necessary to compute in detail the viscous interactions that take place in a wake. In other words, the wake of an airplane is not a simple thing, and the authors do not believe that one should make more than <u>qualitative</u> generalities about the behavior of wakes. If one insists upon making <u>quantitative</u> generalities, that person should realize that very large error bounds must be placed on the numbers that he generates.

We have just noted the fact that the tail of an airplane can, under the proper circumstances, exert a strong effect upon the details of the behavior of an aircraft's wake. The converse is also true. If the model we have been discussing of the wake of a wing is correct, then it is possible for the details of vortex trailing to have a profound effect upon the effectiveness of a tail design. Nowhere is this more true than in the design of V/STOL aircraft. To illustrate this phenomenon, we consider the STOL aircraft configuration shown in Figure 6.8. This configuration was tested by NASA [105] for its aerodynamic characteristics at various levels of engine blowing coefficient C_μ to induce extra lift over the inboard flaps mounted just aft of the engines. These aerodynamic coefficients are shown in Figure 6.9. It may be seen from this figure that at high blowing coefficients the airplane is unstable at high lift. The explanation of this instability as given in Ref. 105 was that the tip vortex was driven to a location near the tail by the very high lift on the inboard flaps induced on the inboard flaps by blowing. Figure 6.10 is a photograph reproduced from Ref. 105 to illustrate this conjecture.

Let us reconsider the tail design problem in the light of the type of inviscid wake analysis considered in Section 2. An idealized lift distribution of the aircraft in the configuration represented in Figure 6.10 is given in Figure 6.11. In this figure, the vortex lift coefficient was taken to be $C_{L_\Gamma} = 3.5$. The effective direct lift coefficient due to engine thrust deflection was taken to be 1.1, so that the total lift coefficient was $C_L = 4.6$. In Figure 6.12 we show two views of the vortices that would be shed by this idealized wing lift distribution. There are three vortices shed from each side, a tip vortex, an outboard flap vortex, and an inboard flap vortex. If one compares the trajectories of these vortices with the smoke pattern shown in Figure 6.10, it is clear that one can distinguish both the tip and the outboard flap vortex. Both move in a pattern very much like that predicted by the simple theory for the idealized lift distribution. It appears from a comparison of Figures 6.10 and 6.12 that the biggest contributors to the instability of the aircraft in question at high C_L and C_μ are the outboard flap vortices.

It is clear from the preceding discussions of tail design that not only does the tail affect the far wake but that strongly flapped high lift wings can also have a very powerful effect upon those surfaces that fly very closely behind the wing, namely, the tails that trim the aircraft. In view of the new insights gained in Sections 1 and 2 on the rollup and motion of vorticity trailed behind wings, it is now possible to reëxamine the methods used for the preliminary design of the tails of conventional aircraft.

7. CONCLUDING REMARKS

For the reader who has followed us this far, it must be obvious that, although much has been learned in the past few years, we have only begun the task of gathering the necessary information that would enable an aircraft designer to design for low wake hazard. To be able to predict in detail and with any degree of confidence the degree of wake hazard posed by an airplane at various distances under various atmospheric conditions is still an undeveloped technology. Nevertheless, the authors believe that the corner of rationality has been turned and that the technical tools necessary to think constructively about wake problems have been developed or are under development. What we have tried to do in this monograph is to bring together in one place a description of these tools and the use to which they might be put. It is, perhaps, appropriate to remark that many, many people have in some way contributed to the writing of this monograph. The authors would like to acknowledge the support of both the United States Air Force and the National Aeronautics and Space Administration. Their support has made possible the authors' continued study of the wake problem for the past few years. Although many people contributed to making this monograph possible, there are two persons to whom the authors feel particularly indebted. First, Dr. Milton Rogers of the U.S. Air Force Office of Scientific Research which originally sponsored our work in this area and, second, we must mention Mr. R. Earl Dunham, Jr. of NASA's Langley Research Center with whom we have enjoyed a very constructive interaction in relation to NASA's test programs for the last year and a half.

8. REFERENCES

1. Lanchester, F.W.: *Aerodynamics*. Second Edition, London, Constable & Company Ltd., 1909, p. 178.
2. Westwater, F.L.: Rolling Up of the Surface of Discontinuity Behind an Aerofoil of Finite Span. A.R.C. R&M 1962, 1935.
3. Takami, H.: A Numerical Experiment with Discrete Vortex Approximation with Reference to the Rolling Up of a Vortex Sheet. Stanford University Department of Aeronautics and Astronautics Report No. 202, 1964.
4. Hackett, J.E. and M.R. Evans: Vortex Wakes Behind High Lift Wings. J. Aircraft 8, 5, May 1971, pp. 334-340.
5. Chorin, A.J. and P.S. Bernard: Discretization of a Vortex Sheet, with an Example of Roll-Up. J. Comp. Physics 13, 1973, pp. 423-429.
6. Moore, D.W.: A Numerical Study of the Roll-Up of a Finite Vortex Sheet. J. Fluid Mech. 63, 2, 1974, pp. 225-235.
7. Bloom, A.M. and H. Jen: Roll-Up of Aircraft Trailing Vortices Using Artificial Viscosity. J. Aircraft 11, 11, November 1974, pp. 714-716.
8. Rossow, V.J.: Theoretical Study of Lift-Generated Vortex Sheets Designed to Avoid Roll-Up. NASA TM X-62,304, September 1973.
9. Kaden, H.: Augwicklung einer un-stabilen Unstetigkeitsflache. Ingenieur Archiv. Bd. II, 1931, pp. 140-168.
10. Durand, W.F. (editor): *Aerodynamic Theory*. Volume II, Division E, California, Durand Reprinting Committee, 1943, pp. 328-330.

11. Betz, A.: Behavior of Vortex Systems. NACA TM 713 (trans. from ZAMM, Vol. XII.3, 1932).
12. Howard, L.N.: Divergence Formulas Involving Vorticity. Arch. Rational Mech. Anal. 1, 1, 1957, pp. 113-123.
13. Donaldson, C. duP., R.S. Snedeker, and R.D. Sullivan: A Method of Calculating Aircraft Wake Velocity Profiles and Comparison with Full-Scale Experimental Measurements. J. Aircraft 11, 9, September 1974, pp. 547-555.
14. Rossow, V.: On the Inviscid Rolled-Up Structure of Lift-Generated Vortices. J. Aircraft 10, 11, November 1973, pp. 647-650.
15. Jordan, P.: Structure of Betz Vortex Cores. J. Aircraft 10, 11, November 1973, pp. 691-693.
16. Verstynen, H.A.,Jr., and R.E. Dunham, Jr.: A Flight Investigation of the Trailing Vortices Generated by a Jumbo Jet Transport. NASA TN D-7172, April 1973.
17. Yates, J.E.: Calculation of Initial Vortex Roll-Up in Aircraft Wakes. J. Aircraft 11, 7, July 1974, pp. 397-400.
18. Brown, C.E.: Aerodynamics of Wake Vortices. AIAA Journal 11, 4, April 1973, pp. 531-536.
19. Bilanin, A.J. and C.duP. Donaldson: Estimation of Velocities and Roll-Up in Aircraft Vortex Wakes. Aeronautical Research Associates of Princeton, Inc. Report No. 214, May 1974 (J. Aircraft - to be published).
20. Donaldson, C.duP.: A Brief Review of the Aircraft Trailing Vortex Problem. AFOSR-TR-71-1910, May 1971 (presented at Nat'l Aerospace Electronics Conf., Dayton, Ohio, May 1971).
21. McCormick, B.W., J.L. Tangler, and H.E. Sherrieb: Structure of Trailing Vortices. J. Aircraft 5, 3, May-June 1968, pp. 260-267.
22. Grow, T.L.: Effect of a Wing on Its Tip Vortex. J. Aircraft 5, 2, March-April 1968, pp. 37-41.
23. Dosanjh, D.S., E.P. Gasparek, and S. Eskinazi: Decay of a Viscous Trailing Vortex. Aero. Quarterly, May 1962.
24. Garodz, L.J.: Federal Aviation Administration Full-Scale Aircraft Vortex Wake Turbulence Flight Test Investigations: Past, Present, Future. AIAA Preprint 71-97, AIAA 9th Aerospace Sciences Meeting, 1971.
25. Bilanin, A.J., C.duP. Donaldson, and R.S. Snedeker: An Analytic and Experimental Investigation of the Wakes Behind Flapped and Unflapped Wings. AFFDL-TR-74-90, May 1974.
26. Mason, W.H. and J.F. Marchman, III: Farfield Structure of an Aircraft Trailing Vortex. J. Aircraft 10, 2, February 1973, pp. 86-92.
27. Orloff, K.L. and G.R. Grant: The Application of a Scanning Laser Doppler Velocimeter to Trailing Vortex Definition and Alleviation. AIAA Paper No. 73-680, AIAA 6th Fluid and Plasma Dynamics Conference, 1973.
28. Reed, Robert E., Jr.: Properties of the Lateral Random Oscillations of Trailing Vortices Observed in Wind Tunnel Tests. Nielsen Engineering and Research, Inc. Technical Report 47, January 1973.
29. Baker, G.R., S.J. Barker, K.K. Bofah, and P.G. Saffman: Laser Anemometer Measurements of Trailing Vortices in Water. J. Fluid Mech. 65, 2, 1974, pp. 325-336.
30. Lin, C.C.: *On the Motion of Vortices in Two Dimensions*, Toronto, University of Toronto Press, 1943, pp.
31. MacCready, P.B., Jr.: An Assessment of Dominant Mechanisms in Vortex-Wake Decay. In *Aircraft Wake Turbulence and Its Detection* (J.H.Olsen, A.Goldburg, M.Rogers, eds.), New York, Plenum Press, 1971, pp. 289-304.
32. Crow, S.C.: Stability Theory for a Pair of Trailing Vortices. AIAA Journal 8, 12, December 1970, pp. 2172-2179.
33. Widnall, S.E., D.B. Bliss, and A. Zalay: Theoretical and Experimental Study of the Stability of a Vortex Pair. In *Aircraft Wake Turbulence and Its Detection* (J.H. Olsen, A.Goldburg, M. Rogers, eds.), New York, Plenum Press, 1971, pp. 305-329.
34. Moore, D.W.: Finite Amplitude Waves on Aircraft Trailing Vortices. Aero. Quarterly 23, 1972.
35. Lord Kelvin: Vibrations of a Columnar Vortex. Mathematical and Physical Papers 4, Cambridge University Press, 1910.
36. Peckham, D.H. and S.A. Atkinson: Preliminary Results of Low Speed Wind Tunnel Tests on a Gothic Wing of Aspect Ratio 1.0. ARC C.P. 508, 1960.
37. Smith, T.B. and K.M. Beesmer: Contrail Studies for Jet Aircraft. Meteorology Research, Inc., 1959 (AD 110 278).
38. Hall, M.G.: Vortex Breakdown. In *Annual Review of Fluid Mechanics* (M. Van Dyke, W.G.Vincenti, J.V.Wehausen, eds.), Palo Alto, Annual Reviews, Inc., 1972, pp. 195-218.
39. Landahl, M.T.: Wave Mechanics of Breakdown. J. Fluid Mech. 56, 4, 1972, pp. 775-802.
40. Bilanin, A.J.: Wave Mechanics of Line Vortices. Ph.D. Thesis, Massachusetts Institute of Technology, June 1973.
41. Randall, J.D. and S. Leibovich: The Critical State - A Trapped Wave Model of Vortex Breakdown. J. Fluid Mech. 58, 3, 1973, pp. 495-515.
42. Chandrasekhar, S.: *Hydrodynamic and Hydromagnetic Stability*. London, Oxford University Press, 1961, pp. 366-371
43. Moore, D.W. and P.G. Saffman: The Motion of a Vortex Filament with Axial Flow. Phil. Trans. Royal Soc. London 272, 1972,
44. Krishnamurthy, V.: Vortex Breakdown and Measurements of Pressure Fluctuations Over Slender Wings. Ph.D. Thesis, Southampton University, 1966.
45. Widnall, S.E. and D.R. Bliss: Slender-Body Analysis of the Motion and Stability of a Vortex Filament Containing an Axial Flow. J. Fluid Mech. 50, 2, 1971, pp. 335-353.
46. Benjamin, T.B.: Theory of the Vortex Breakdown Phenomenon. J. Fluid Mech. 14, 4, 1962, pp. 593-629.
47. Squire, H.B.: Analysis of the Vortex Breakdown Phenomenon. Part 1. Imperial College London, Aero. Dept. Report 102, 1960.

48. Jones, J.P.: A Note on Professor Squire's Analysis of the Vortex Breakdown Phenomenon. ARC 22, 1960.
49. Kantrowitz, A.: The Formation and Stability of Normal Shock Waves in Channel Flows. NACA TN 1225, 1947.
50. Sarpkaya, T.: On Stationary and Travelling Vortex Breakdowns. J. Fluid Mech. 45, 3, 1971, pp. 545-559.
51. Landahl, M.T. and S.E. Widnall: Vortex Control. In *Aircraft Wake Turbulence and Its Detection* (J.H.Olsen, A.Goldburg, M.Rogers, eds.), New York, Plenum Press, 1971, pp. 137-155.
52. Mager, A.: Dissipation and Breakdown of a Wing-Tip Vortex. J. Fluid Mech. 55, 4, 1972, pp. 609-628.
53. Lakshmikantha, H.: Investigation of Two-Phase Vortex Flows with Applications to a Cavity Nuclear Rocket. Ph.D. Thesis, Massachusetts Institute of Technology, September 1973, Appendix C, pp. 275-314.
54. Tombach, I.: Observations of Atmospheric Effects of Vortex Wake Behavior. J. Aircraft 10, 11, November 1973, pp. 641-647.
55. Bossel, H.H.: Vortex Breakdown Flowfield. Phy. Fluids 12, 3, March 1969, pp. 498-508.
56. Chevalier, H.: Flight Test Studies of the Formation and Dissipation of Trailing Vortices. J. Aircraft 10, 1, January 1973, pp. 14-18.
57. Crow, S.C.: Panel Discussion in *Aircraft Wake Turbulence and Its Detection* (J.H. Olsen, A. Goldburg, M.Rogers, eds.), New York, Plenum Press, 1971, pp. 577-583.
58. Bilanin, A.J. and S.E. Widnall: Aircraft Wake Dissipation by Sinusoidal Instability and Vortex Breakdown. AIAA Paper 73-107, 11th Aerospace Sciences Meeting, January 1973.
59. Kolmogoroff, A.N.: Equations of Turbulent Motion of an Incompressible Fluid. Izv. Akad. Nauk, SSSR, Ser. Fiz. VI, Nos. 1-2, 1942, pp. 56-58.
60. Prandtl, L. and K. Wieghardt: Uber ein neuses Formelsystem für die ausgebeldte Turbulenz. Nach. Akad. Wiss. Goettingen 19, 6, 1945.
61. Rotta, J.: Statistische Theorie nichthomogener Turbulenz. Z. Phys. 129, 1951, p. 547.
62. Rodi, W. and D.B. Spalding: A Two-Parameter Model of Turbulence and Its Application to Free Jets. Warme-und Stoffubertragung 3, 1970, pp. 85-95.
63. Donaldson, C.duP.: A Progress Report on an Attempt to Construct an Invariant Model of Turbulent Shear Flows. AGARD CP-93, September 1971.
64. Hoffman, E.R. and P.N. Joubert: Turbulent Line Vortices. J. Fluid Mech. 16, 3, July 1963, pp. 395-411.
65. Iversen, J.: Inviscid to Turbulent Transition of Trailing Vortices. University of Iowa ERI Technical Report, November 1974.
66. Donaldson, C.duP. and R. D. Sullivan: An Invariant Second-Order Closure Model of the Compressible Turbulent Boundary Layer on a Flat Plate. Aeronautical Research Associates of Princeton, Inc. Report No. 178, June 1972.
67. Lewellen, W.S., M.E. Teske, and C.duP. Donaldson: Turbulent Wakes in a Stratified Fluid. Aeronautical Research Associates of Princeton, Inc. Report No. 226, September 1974.
68. Lewellen, W.S., M.E. Teske, R.M. Contiliano, G.R. Hilst, and C.duP. Donaldson: Invariant Modeling of Turbulent Diffusion in the Planetary Boundary Layer. EPA Report EPA-650/4-74-035, September 1974.
69. Lewellen, W.S., M.E. Teske, and C.duP. Donaldson: Prediction of the Monin-Obukhov Similarity Functions from an Invariant Model of Turbulence. J. Atmos. Sciences 30, 7, October 1973, pp. 1340-1345.
70. Donaldson, C.duP. and R.D. Sullivan: Decay of an Isolated Vortex. In *Aircraft Wake Turbulence and Its Detection* (J.H.Olsen, A.Goldburg, M.Rogers, eds.), New York, Plenum Press, 1971, pp. 389-411.
71. Donaldson, C.duP.: The Relationship Between Eddy Transport and Second-Order Closure Models for Stratified Media and for Vortices. NASA SP-216, July 1972, pp. 233-255.
72. Aris, R.: *Vectors, Tensors, and the Basic Equations of Fluid Mechanics*. Englewood Cliffs, NJ, Prentice-Hall, Inc., 1962, pp. 176-181.
73. Sullivan, R.D.: A Program to Compute the Behavior of a Three-Dimensional Turbulent Vortex. ARL-TR-74-0009, December 1973.
74. Taylor, G.I.: Stability of a Viscous Liquid Contained Between Two Rotating Cylinders. Proc. Roy. Soc. London 223, 1923, pp. 289-343.
75. Dunham, R.E., Jr.: Model Tests of Various Vortex Dissipation Techniques in a Water Towing Tank. NASA LWP-1146, January 1974.
76. Lewellen, W.S., M.E. Teske, and C.duP. Donaldson: Turbulence Model of Diurnal Variations in the Planetary Boundary Layer. Proc. 1974 Heat Transfer and Fluid Mechanics Institute (L.R.Davis and R.E.Wilson, eds.), Stanford University Press, 1974, pp. 301-319.
77. Lissaman, P.B.S., S.C.Crow, P.B.MacCready, Jr., I.H.Tombach, and E.R.Bate,Jr.: Aircraft Vortex Wake Descent and Decay Under Real Atmospheric Effects. FAA-RD-73-120, October 1973.
78. Harvey, J.K. and F.J.Perry: Flowfield Produced by Trailing Vortices in the Vicinity of the Ground. AIAA Journal 9, 8, August 1971, pp. 1659-1660.
79. Burnham, D.C.: Effect of Ground Wind Shear on Aircraft Trailing Vortices. AIAA Journal 10, 8, August 1972, pp. 1114-1115.
80. Brashears, M.R. and J.N.Hallock: Aircraft Wake Vortex Transport Model. J.Aircraft 11, 5, May 1974, pp. 265-272.
81. Crow, S.C.: Vortex Wakes of Large Aircraft, Sections 9, 10. Notebook for AIAA Professional Study Seminar, Palo Alto, Calif., June 1974.
82. Smith, T.B. and P.B. MacCready, Jr.: Aircraft Wakes and Diffusion Enhancement. Meteorology Research, Inc., 1963, Part A
———— and M.A. Wolf: Vertical Diffusion from an Elevated Line Source Over a Variety of Terrains. Meteorology Research, Inc., 1963, Part B.

83. Condit, P.M. and P.W. Tracy: Results of the Boeing Company Wake Turbulence Test Program. In *Aircraft Wake Turbulence and Its Detection* (J.H.Olsen, A.Goldburg, M.Rogers, eds.), New York, Plenum Press, 1971, pp. 473-508.
84. FAA Task Force: Vortex Wake Turbulence Flight Tests Conducted During 1970. FAA Report No. FAA-FS-71-1, 1971.
85. Maxworthy, T.: The Structure and Stability of Vortex Rings. J. Fluid Mech. 51, 1, 1972, pp. 15-32.
86. Donaldson, C.duP.: Construction of a Dynamic Model of the Production of Atmospheric Turbulence and the Dispersal of Atmospheric Pollutants. In *Workshop on Micrometeorology* (D.A.Haugen, ed.), Ephrata, Pa., Science Press, 1973, pp. 371-372.
87. Brown, C.E. and K.Kirkman: Simulation of Wake Vortices Descending in a Stably Stratified Atmosphere. FAA Report No. FAA-RD-74-116, July 1974.
88. Scorer, R.S. and L.J.Davenport: Contrails and Aircraft Downwash. J. Fluid Mech. 43, 3, 1970, pp. 451-464.
89. Tombach, I.: Transport of a Vortex Wake in a Stably Stratified Atmosphere. In *Aircraft Wake Turbulence and Its Detection* (J.H.Olsen, A. Goldburg, M.Rogers, eds.) New York, Plenum Press, 1971, pp. 41-56.
90. Crow, S.C.: Motion of a Vortex Pair in a Stably Stratified Fluid. Poseidon Research Report No. 1, May 1974.
91. Tulin, M.P. and J.Schwartz: The Motion of Turbulent Vortex-Pairs in Homogeneous and Density Stratified Media. Hydronautics, Inc. Tech. Report 231-15, 1971.
92. Snedeker, R.S.: The Effect of Air Injection on the Torque Produced by a Trailing Vortex. J. Aircraft 9, 9, September 1972, pp. 682-684.
93. Patterson, J.C., Jr.: private communication
94. Rinehart, S.A., J.C. Balcerak, and R.P. White, Jr.: An Experimental Study of Tip Vortex Modifications by Mass Flow Injection. Rochester Applied Science Associates, Inc. Report RASA 71-01, January 1971.
95. Poppleton, E.D.: A Preliminary Experimental Investigation of the Structure of a Turbulent Trailing Vortex. McGill University, Mech. Eng. Res. Labs. Report No. TN 71-1, March 1971.
96. Poppleton, E.D.: Effect of Air Injection into the Core of a Trailing Vortex. J. Aircraft 8, 8, August 1971, pp. 672-673.
97. Mason, W.H. and J.F. Marchman, III: Farfield Structure of an Aircraft Trailing Vortex, Including Effects of Mass Injection. NASA CR-62078, April 1972.
98. Snedeker, R.S.: A Comparison of the Trailing Vortex Measurements of Poppleton with Invariant Modeling Computations. Aeronautical Research Associates of Princeton, Inc. Tech. Memo. 72-5, November 1972.
99. Corsiglia, V.R., R.A.Jacobsen, and N.Chigier: An Experimental Investigation of Trailing Vortices Behind a Wing with a Vortex Dissipator. In *Aircraft Wake Turbulence and Its Detection* (J.H.Olsen, A.Goldburg, M.Rogers, eds.), New York, Plenum Press, 1971, pp. 229-242.
100. Hastings, E.C, Jr., R.E.Shanks, R.A.Champine, W.L.Copeland, and D.C.Young: Preliminary Results of Flight Tests of Vortex Attenuating Splines. NASA TM X-71928, March 1974.
101. Patterson, J.C., Jr.: Lift-Induced Wing-Tip Vortex Attenuation. AIAA Paper No. 74-38, AIAA 12th Aerospace Sciences Meeting, 1974.
102. Uzel, J.N. and J.F.Marchman, III: The Effect of Wing-Tip Modifications on Aircraft Wake Turbulence. Virginia Polytechnic Institute, College of Engineering Report VPI-E-72-8, July 1972.
103. Yuan, S.W. and A.M. Bloom: Experimental Investigation of Wing-Tip Vortex Abatement. Paper No. 74-35, Inter'l Council of Aero. Sci. Congress, Haifa, August 1974.
104. Croom, Delwin: private communication
105. Parlett, L.P. and J.P. Shivers: Wind Tunnel Investigation of an STOL Aircraft Configuration Equipped with an External-Flow Jet Flap. NASA TN D-5364, August 1969.

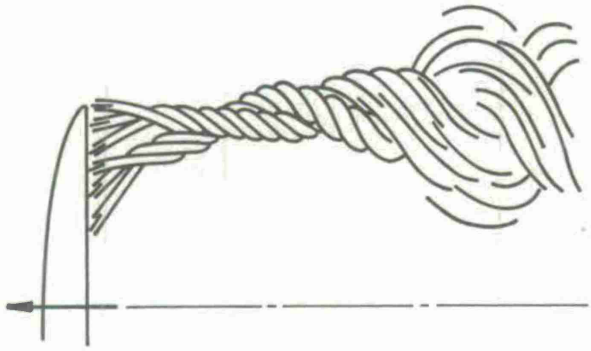

Figure 1.1 Lanchester's concept of tip vortex rollup [1]

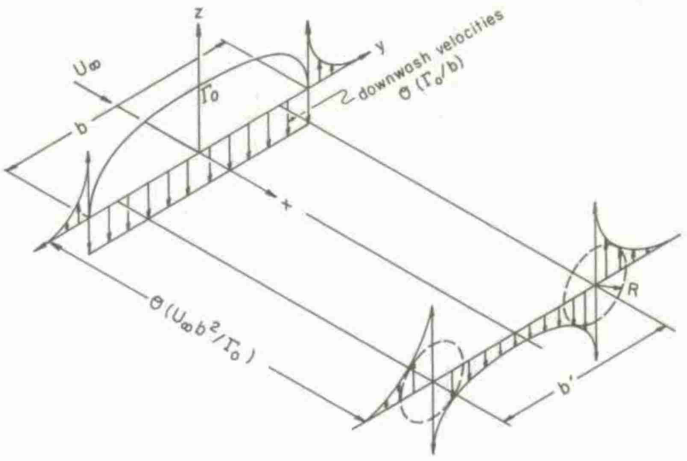

Figure 1.2 The near wake of a simply loaded wing

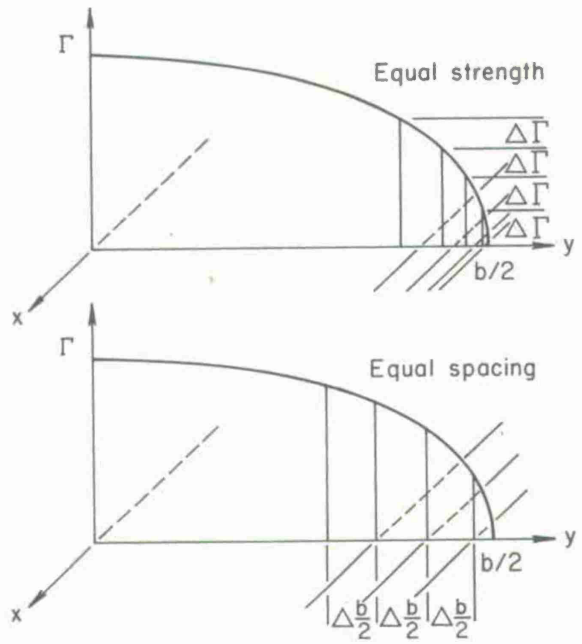

Figure 1.3 Discretization of the trailed axial vorticity

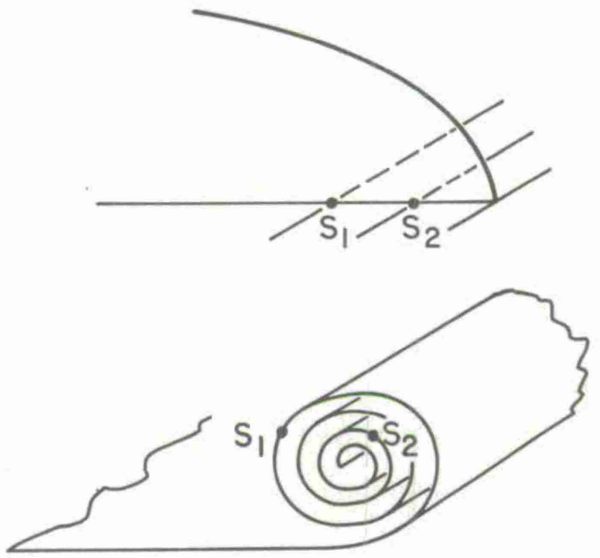

Figure 1.4 Stretching of the vortex sheet during rollup

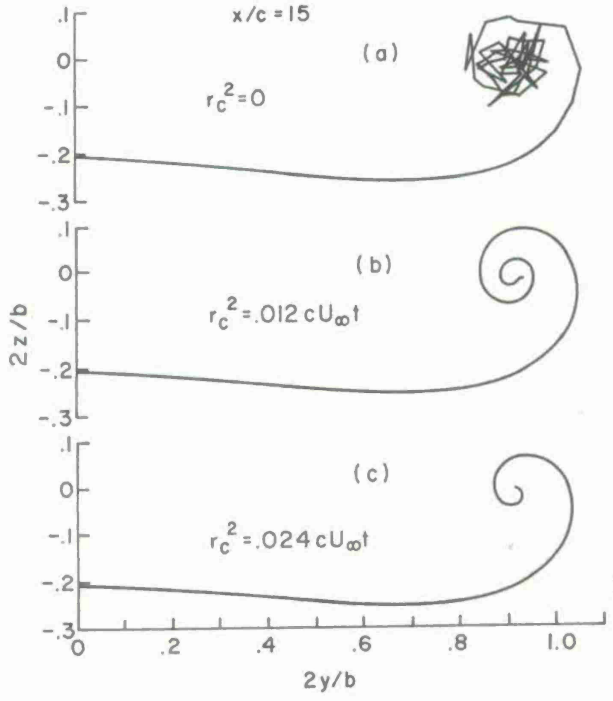

Figure 1.5 The effect of artificial viscosity on the rollup of discrete vortices [7]

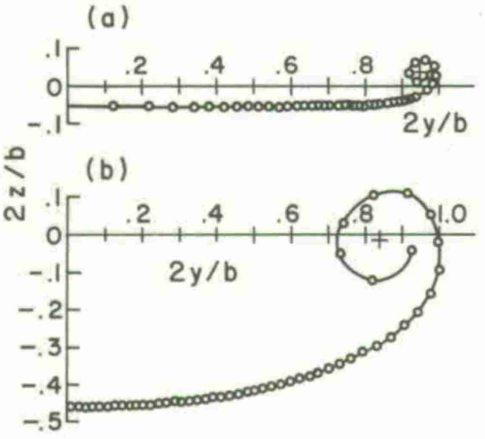

Figure 1.6 Point vortex computations by Moore [6] where the tip spiral structure is modeled by a single point vortex

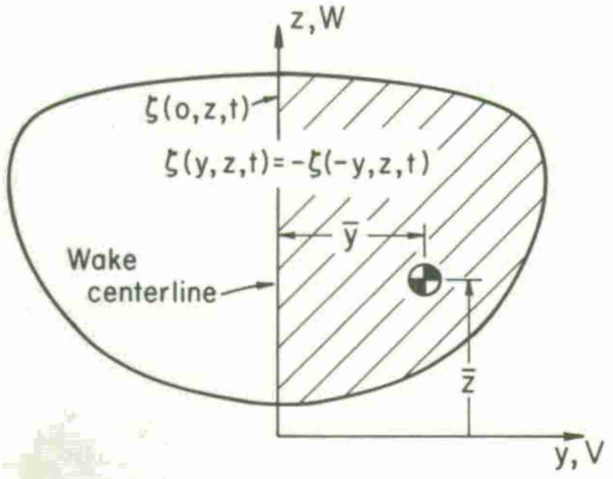

Figure 1.8 The flowfield in a plane normal to the flight direction

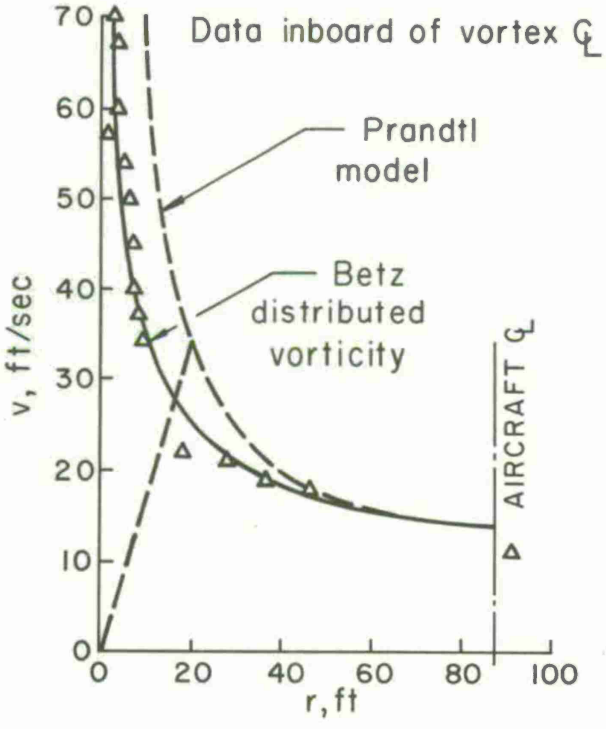

Figure 1.10 Comparison of the Betz and Prandtl models with measurement made in the wake of a C5 aircraft [16]

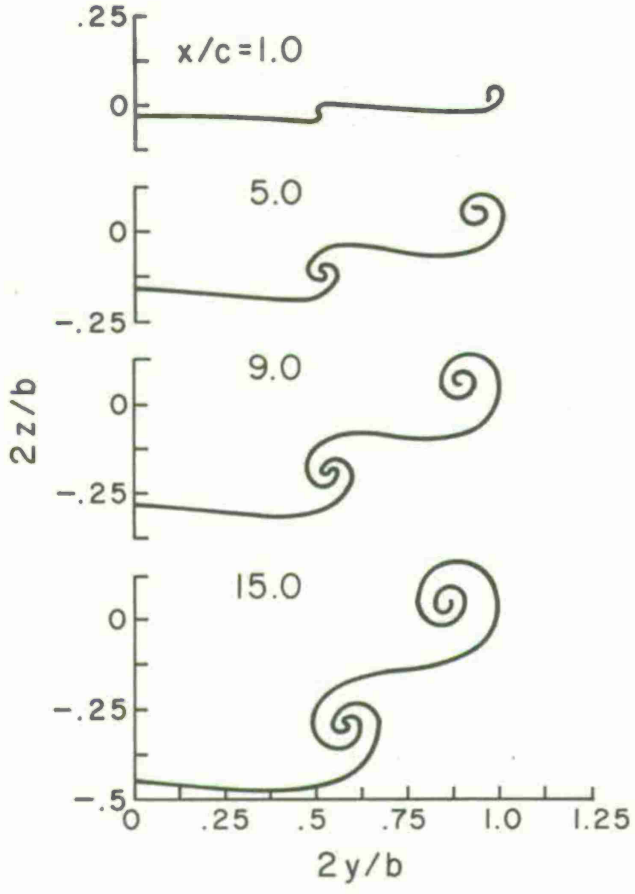

Figure 1.7 The rollup of a tip and flap vortex [7]

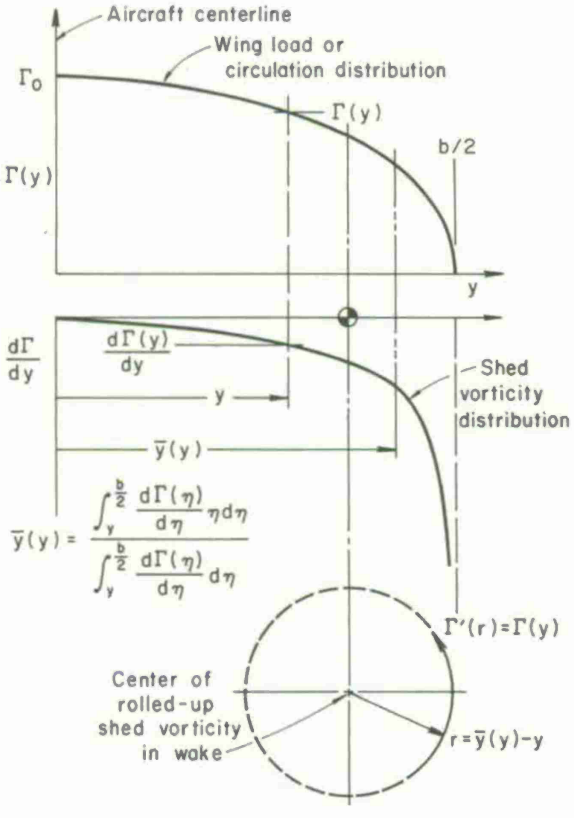

Figure 1.9 The Betz rollup relations for a simply loaded wing [13]

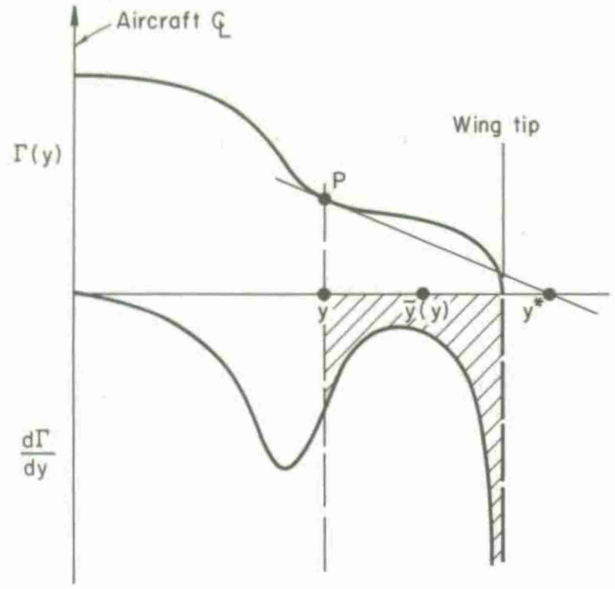

Figure 1.11 Representative load distribution of a flapped wing Γ(y), upper curve, and distribution of shed vorticity dΓ/dy from same wing, lower curve [13]

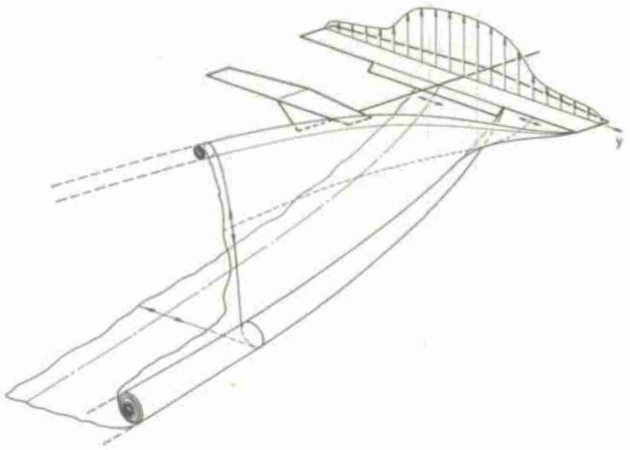

Figure 1.12 The wake of a flapped wing

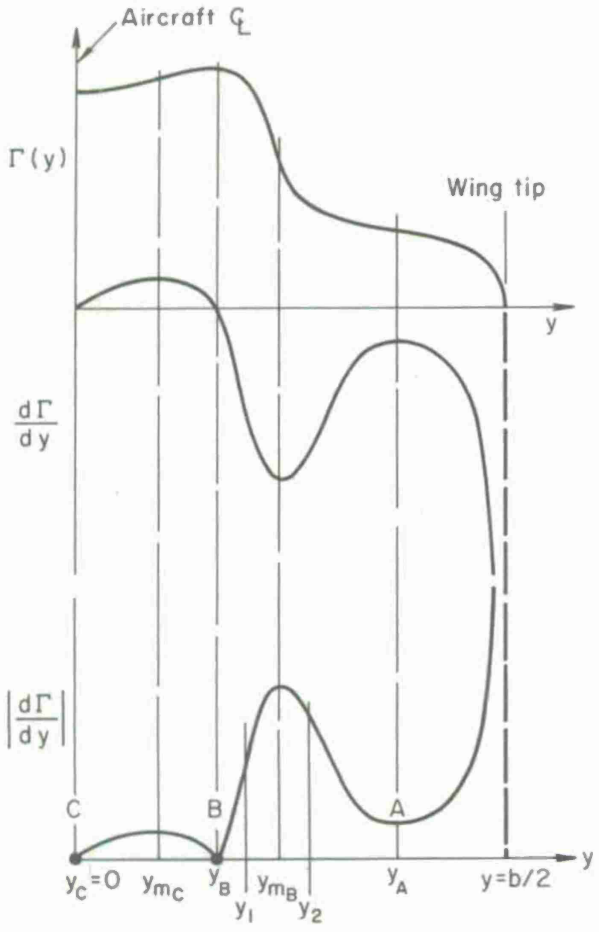

Figure 1.13 Load distribution which will produce three vortices [13]

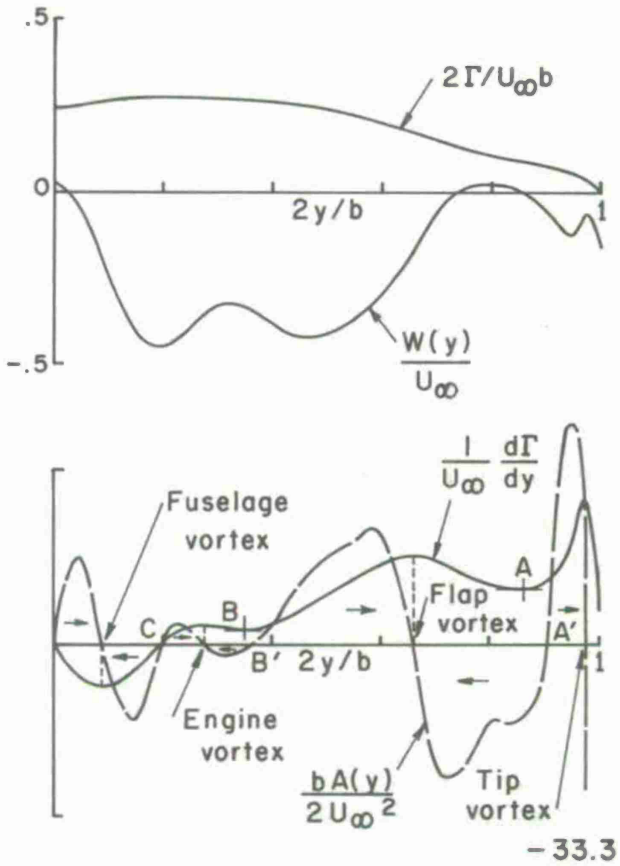

Figure 1.14 Normalized load ($2\Gamma/U_\infty b$), down wash [$W(y)/U_\infty$], sheet strength ($1/U_\infty(d\Gamma/dy)$), and acceleration function ($bA/2U_\infty^2$) distributions for a C-141 aircraft in the take-off configuration [17]

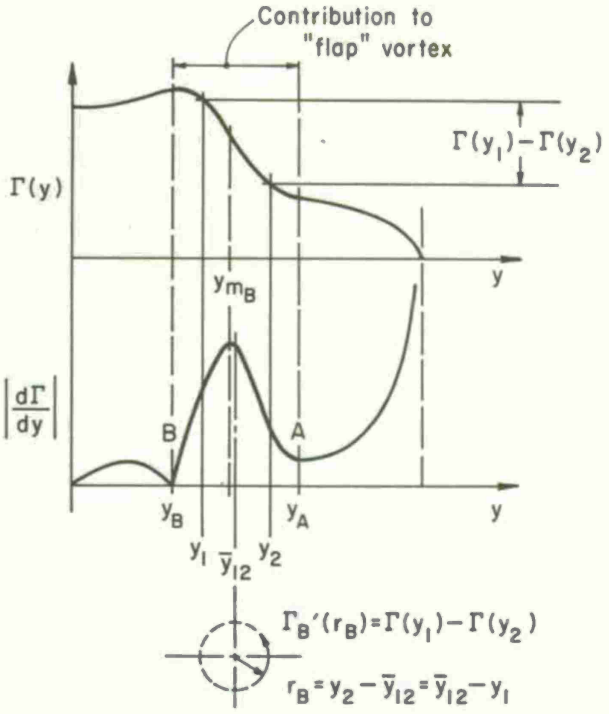

Figure 1.15 The rollup relations for an "interior" vortex [13]

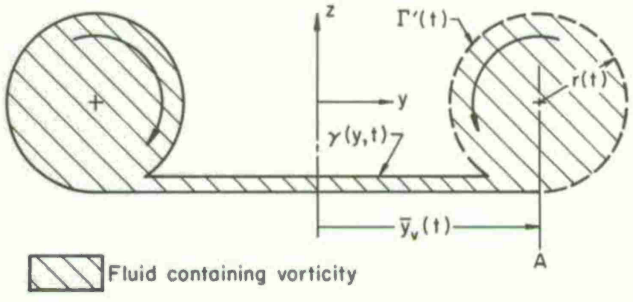

Figure 1.17 A simple two-dimensional rollup model [19]

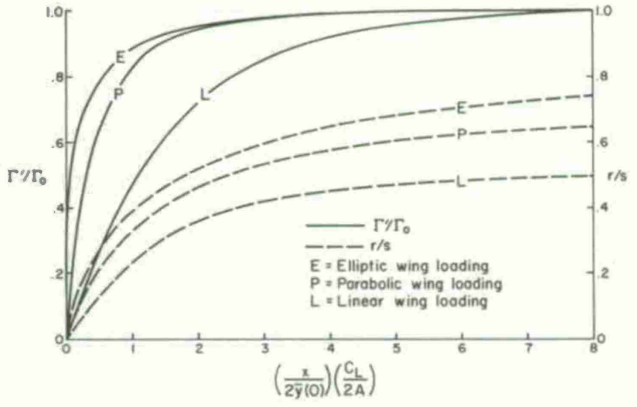

Figure 1.18 Vortex circulation and radius as a function of downstream distance (time has been replaced by x/U_∞) [19]

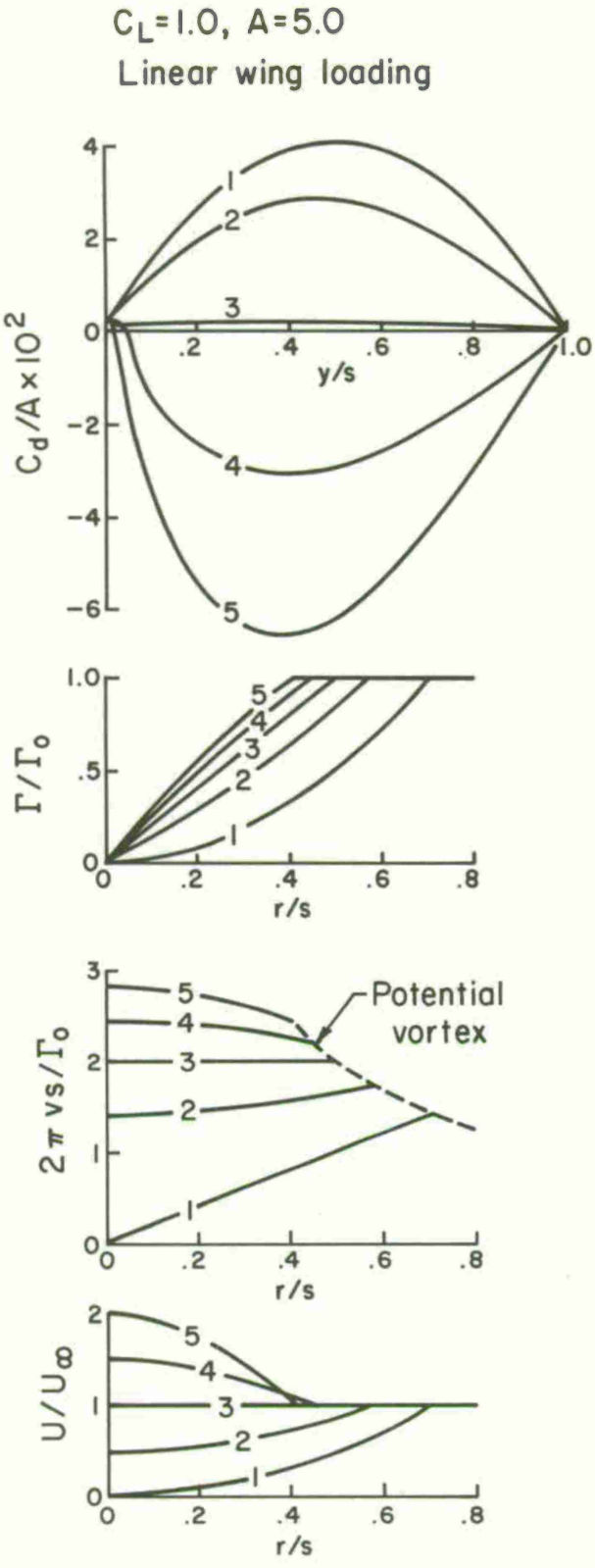

Figure 1.16 The vortex wake structure for a linearly loaded wing [19]

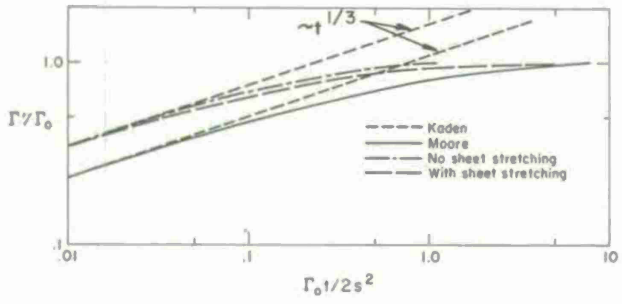

Figure 1.19 Comparison of the simple rollup model with the calculation of Moore [6]. The constant in Kaden's solution [9] has been adjusted to give agreement at $\Gamma_o t/2s^2 = 10^{-2}$. [19]

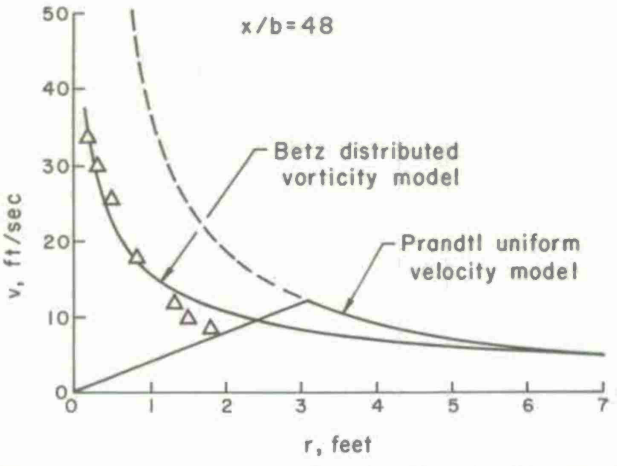

Figure 1.20 Tangential velocity in the vortex wake of an Army O-1 aircraft [21]

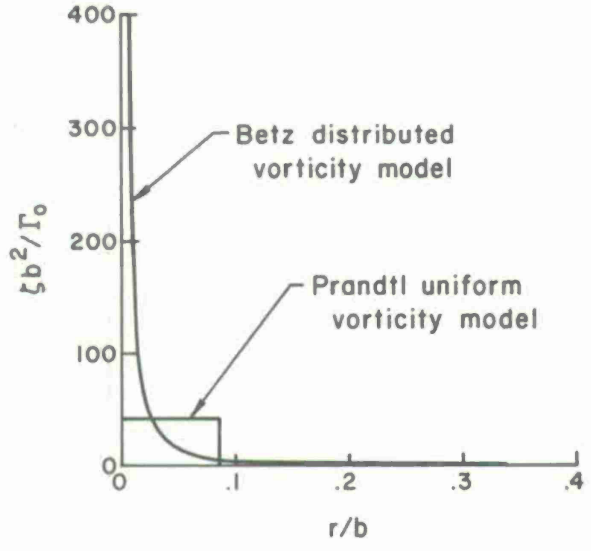

Figure 1.21 The vorticity distribution for the vortex velocities shown in Figure 1.20

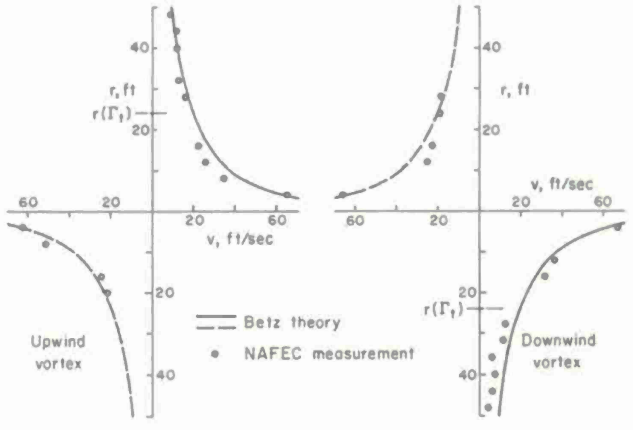

Figure 1.22 Comparison of computed and measured tangential velocity profiles in a wake vortex. DC-7, landing configuration. NAFEC test run 74 [13]

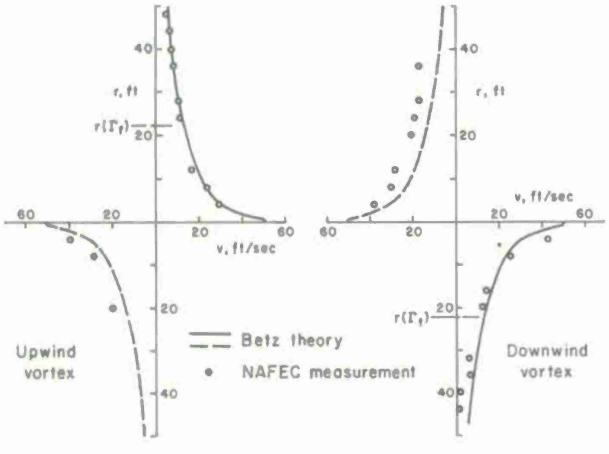

Figure 1.23 Comparison of computed and measured tangential velocity profiles in a wake vortex. DC-7, takeoff configuration. NAFEC test run 82 [13]

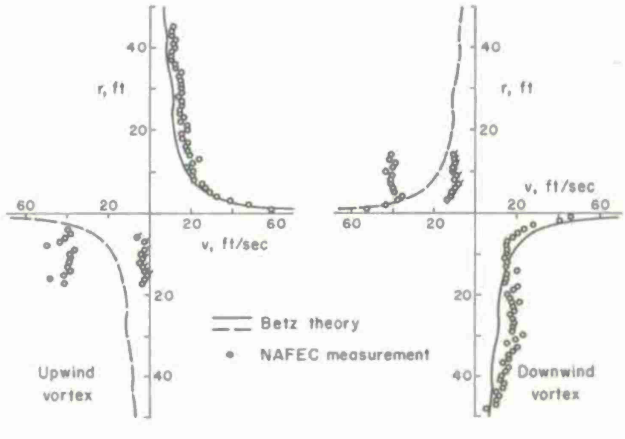

Figure 1.24 Comparison of computed and measured tangential velocity profiles in a wake vortex. C-141, holding configuration. NAFEC test run 22 [13]

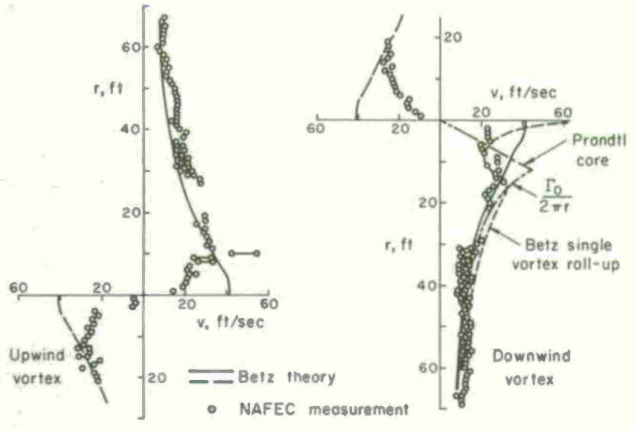

Figure 1.25 Comparison of computed and measured tangential velocity profiles in a wake vortex. C-141, landing configuration. NAFEC test run 2 [13]

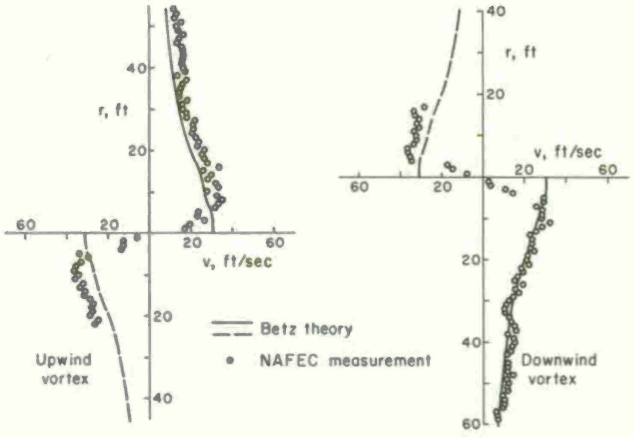

Figure 1.26 Comparison of computed and measured tangential velocity profiles in a wake vortex. C-141, takeoff configuration. NAFEC test run 14 [13]

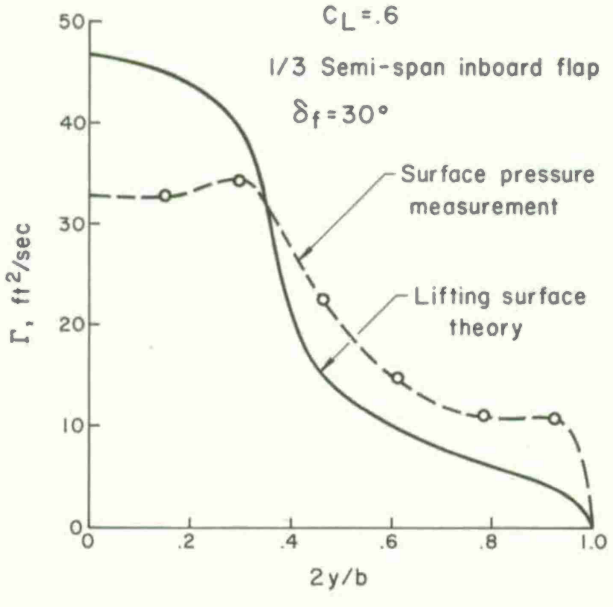

Figure 1.27 Lift distribution on a flapped wing as determined from lifting surface theory and surface pressure taps [25]

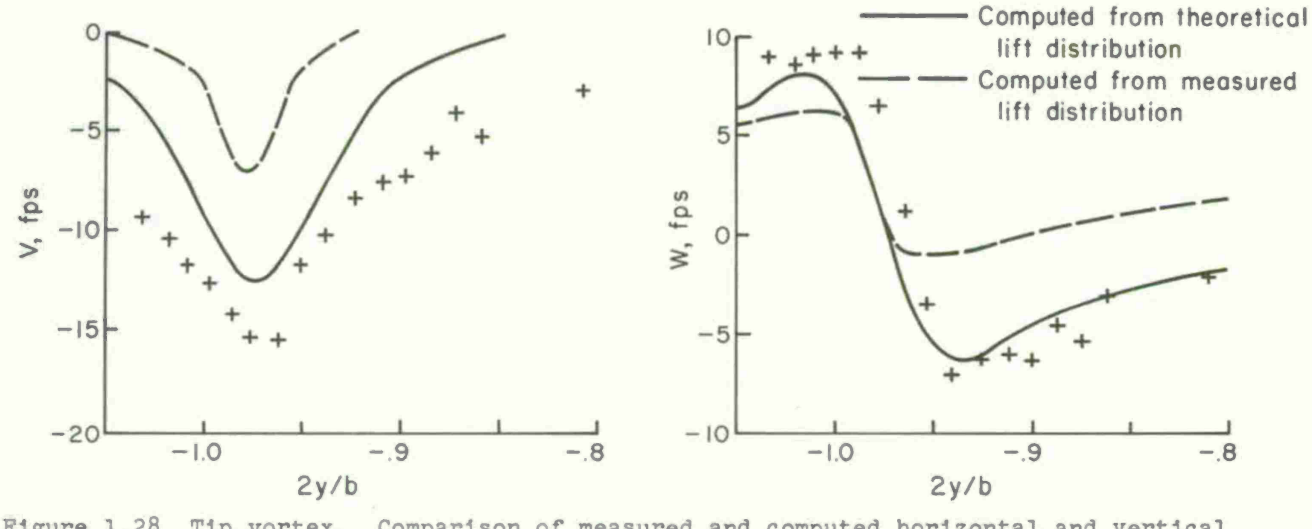

Figure 1.28 Tip vortex. Comparison of measured and computed horizontal and vertical velocities (x/c = 10, z/c = 7.05). Computed vortex center from measured lift distribution y/c = -3.85, z/c = 7.24; from theoretical lift distribution y/c = -3.92, z/c = 7.24 (b/c ≒ 10) [25]

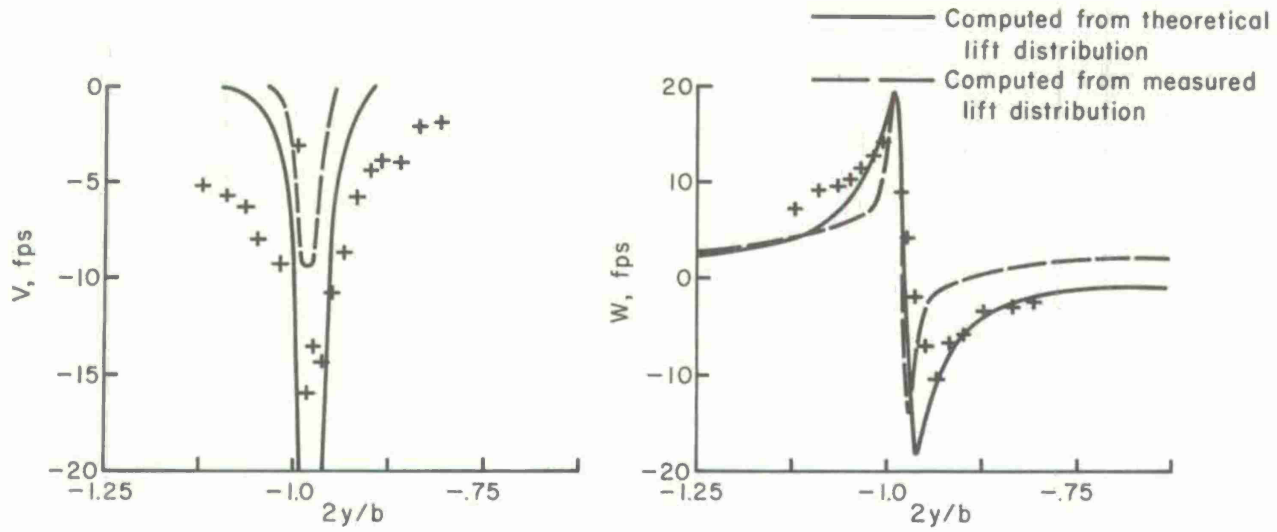

Figure 1.29 Tip vortex. Comparison of measured and computed horizontal and vertical velocities (x/c = 10, z/c = 7.15); vortex center as in Figure 1.28 [25]

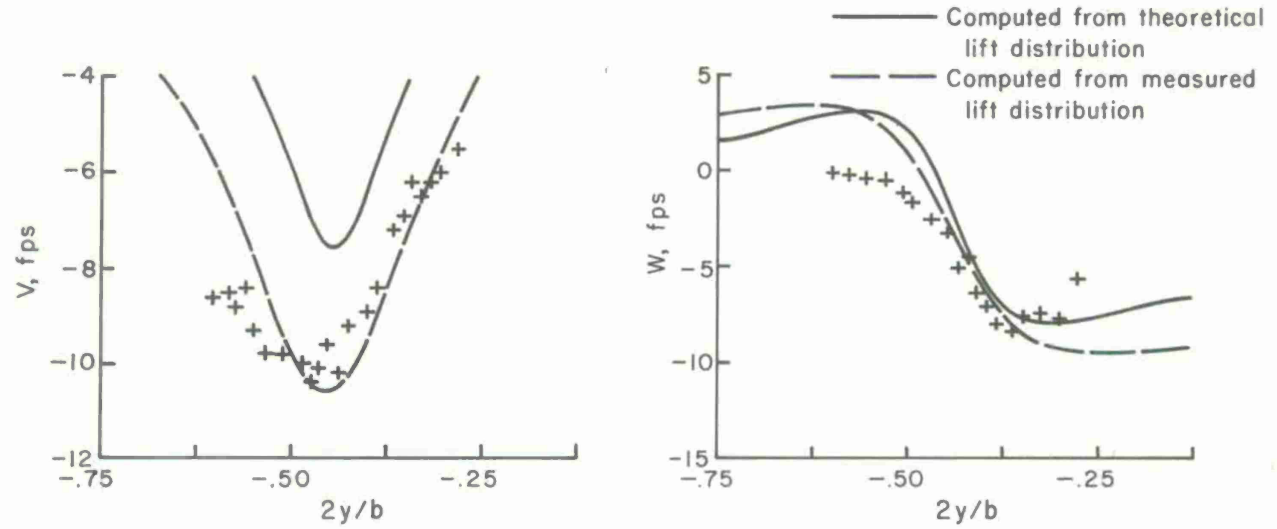

Figure 1.30 Flap vortex. Comparison of measured and computed horizontal and vertical velocities (x/c = 10, z/c = 5.85). Computed vortex center from measured lift distribution y/c = -1.98, z/c = 6.24; from theoretical lift distribution y/c = -2.2, z/c = 6.43 [25]

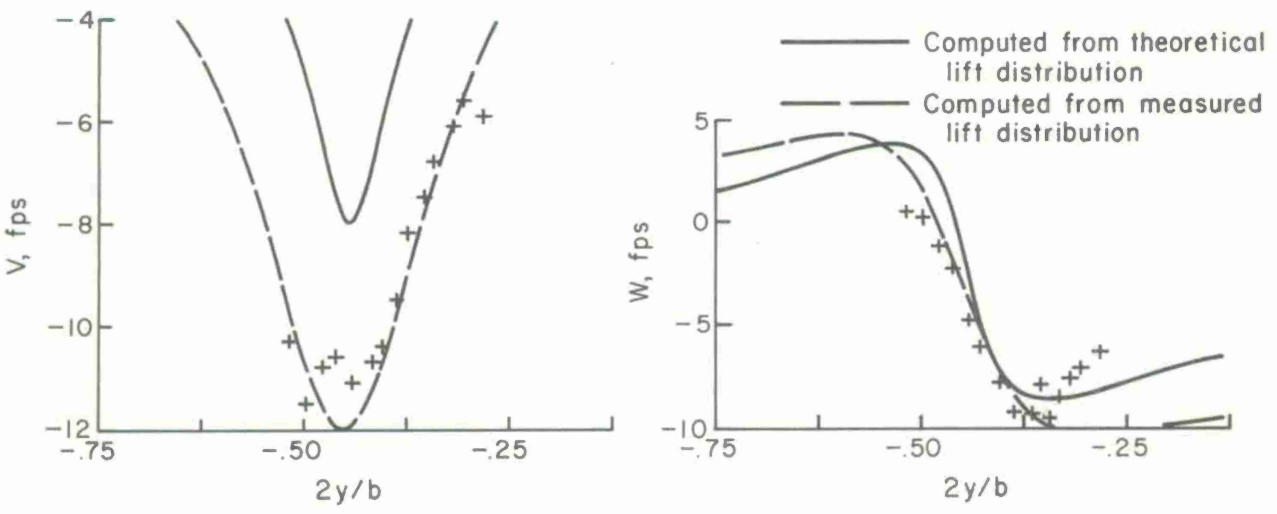

Figure 1.31 Flap vortex. Comparison of measured and computed horizontal and vertical velocities (x/c = 10, z/c = 5.95); vortex center as in Figure 1.30 [25]

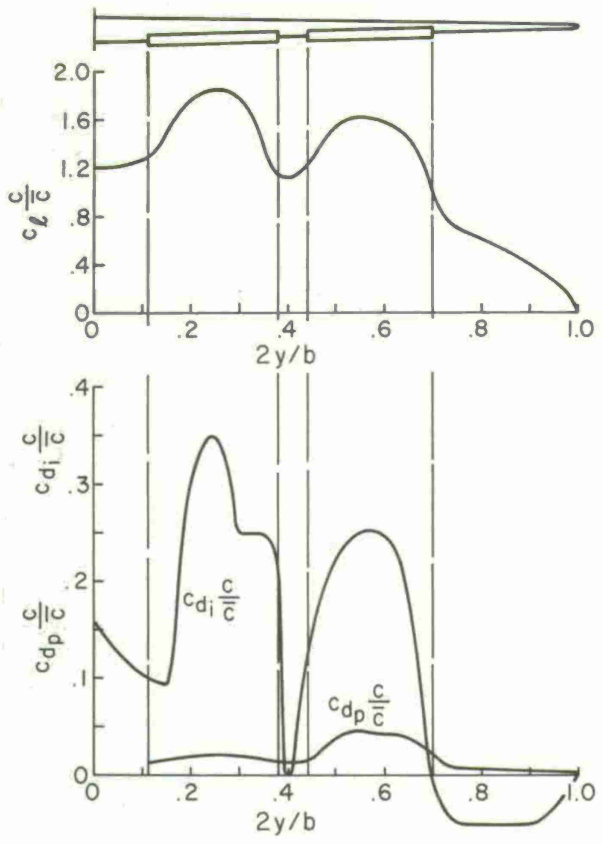

Figure 1.32 Wing lift and drag distribution of the 747 aircraft in the landing configuration (C_L = 1.2)

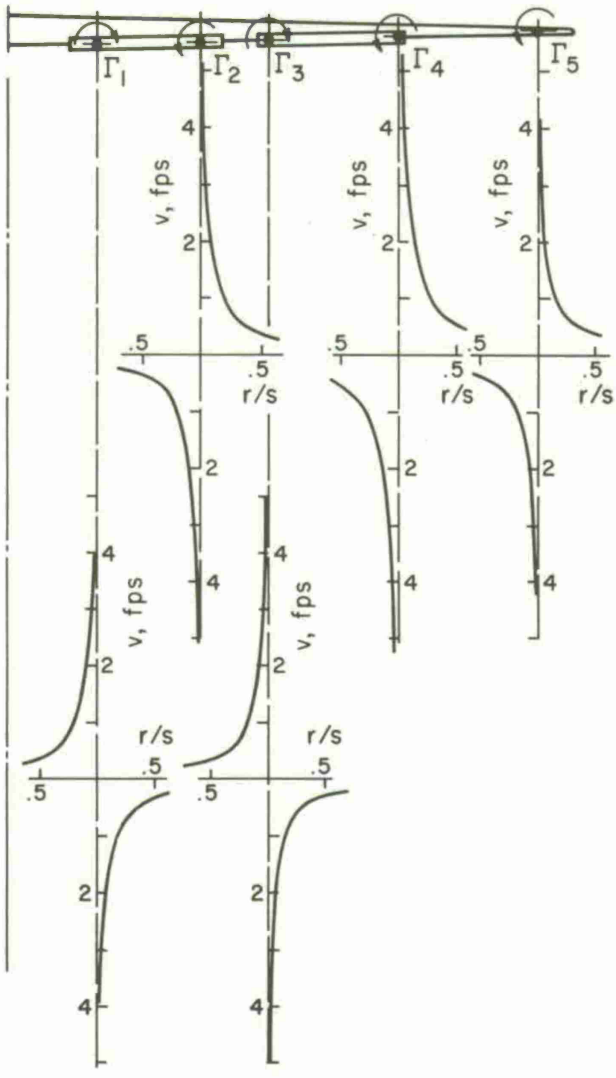

Figure 1.33 Vortex swirl velocity distributions with uniform axial velocity

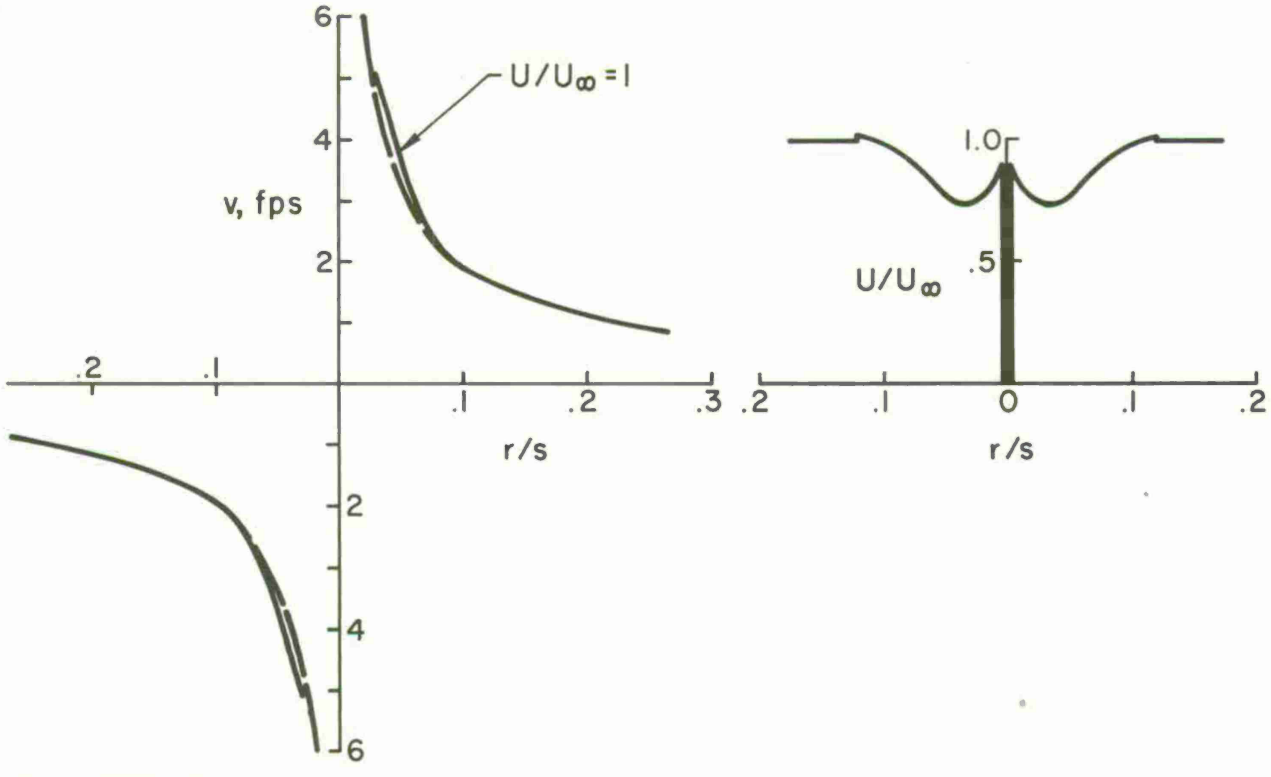

Figure 1.34 Vortex swirl and axial velocity distributions for vortex 2

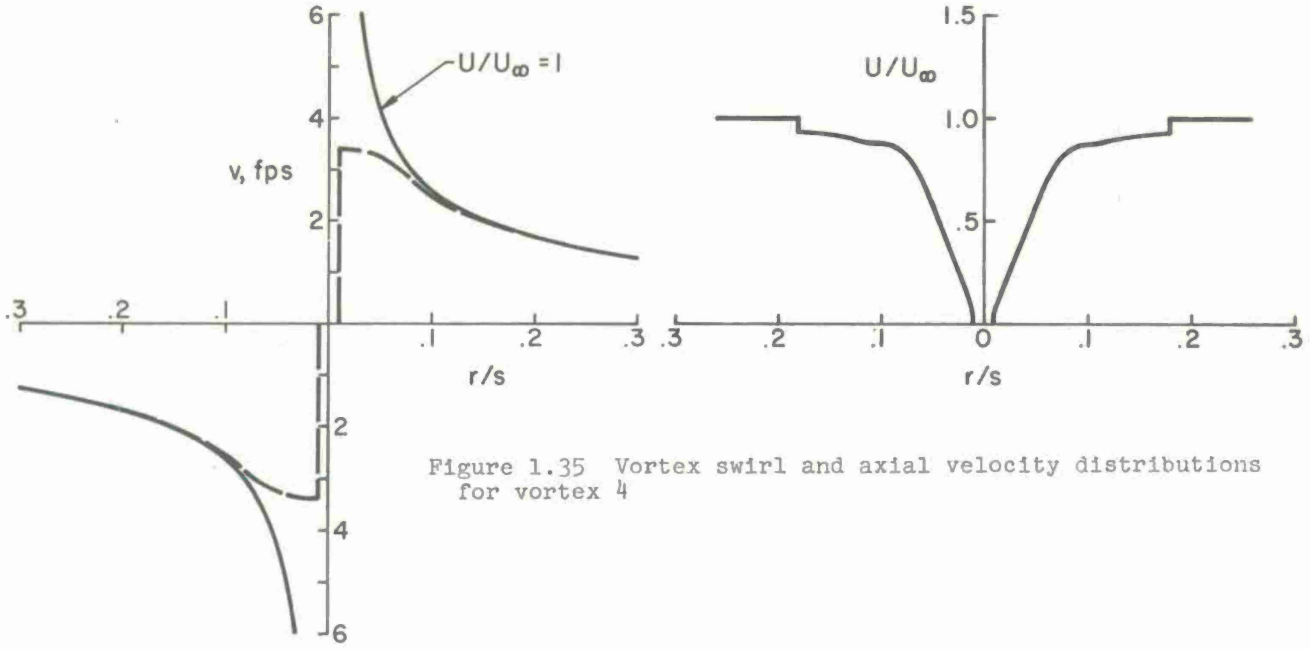

Figure 1.35 Vortex swirl and axial velocity distributions for vortex 4

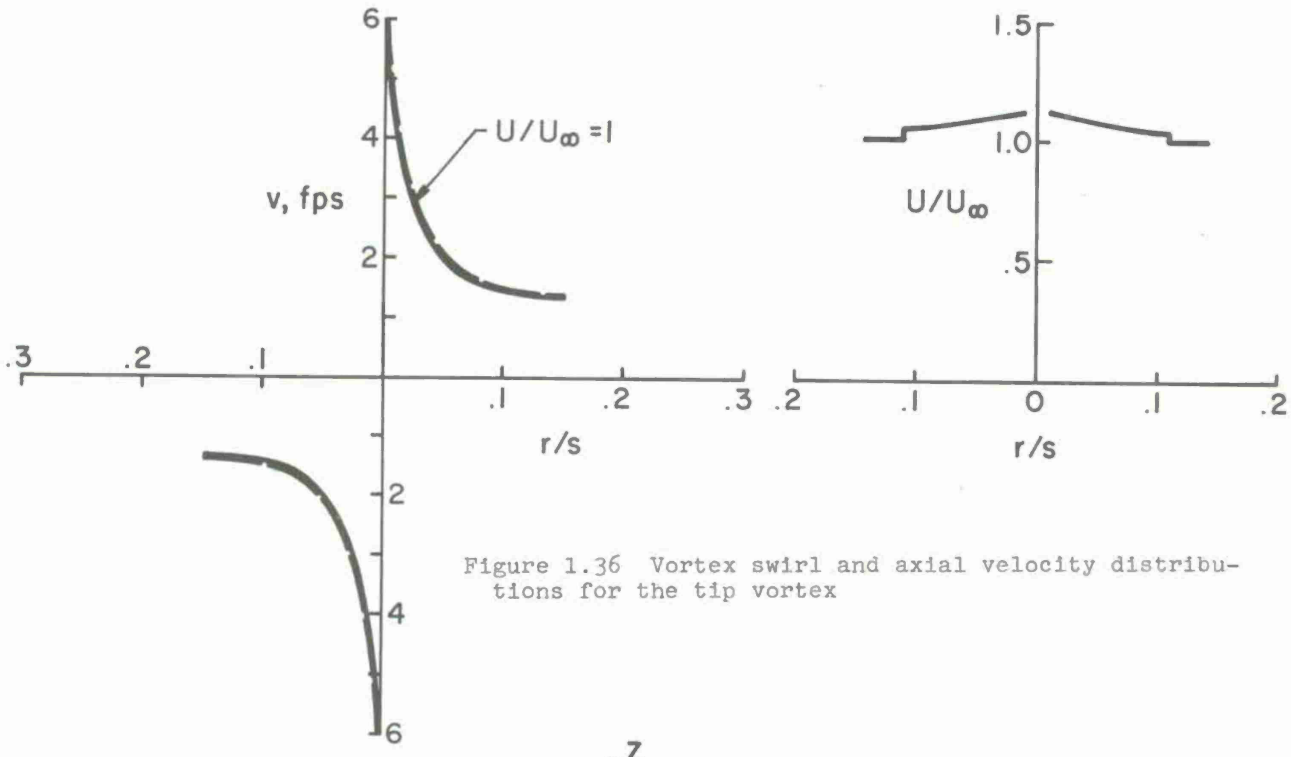

Figure 1.36 Vortex swirl and axial velocity distributions for the tip vortex

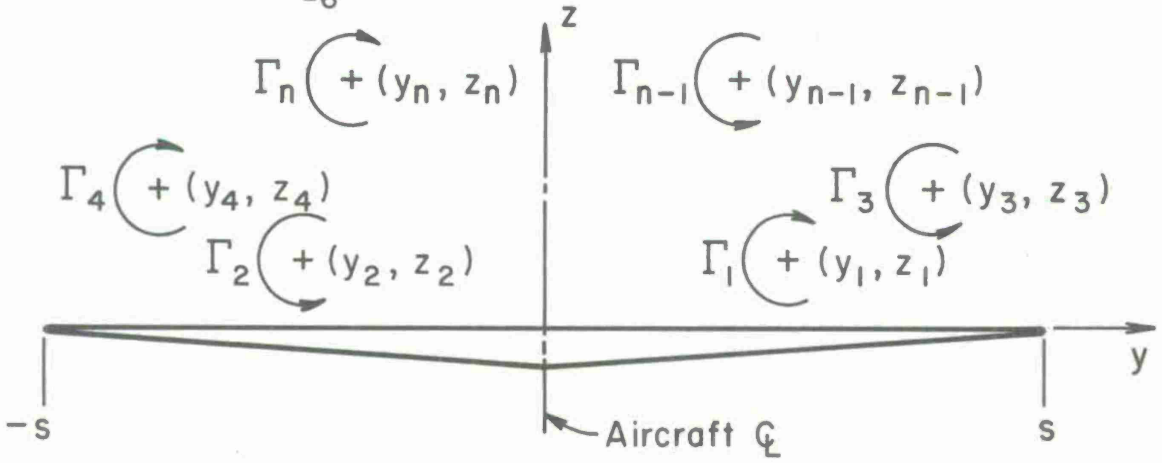

Figure 2.1 Geometry for the calculation of the downstream location of vortex centroids

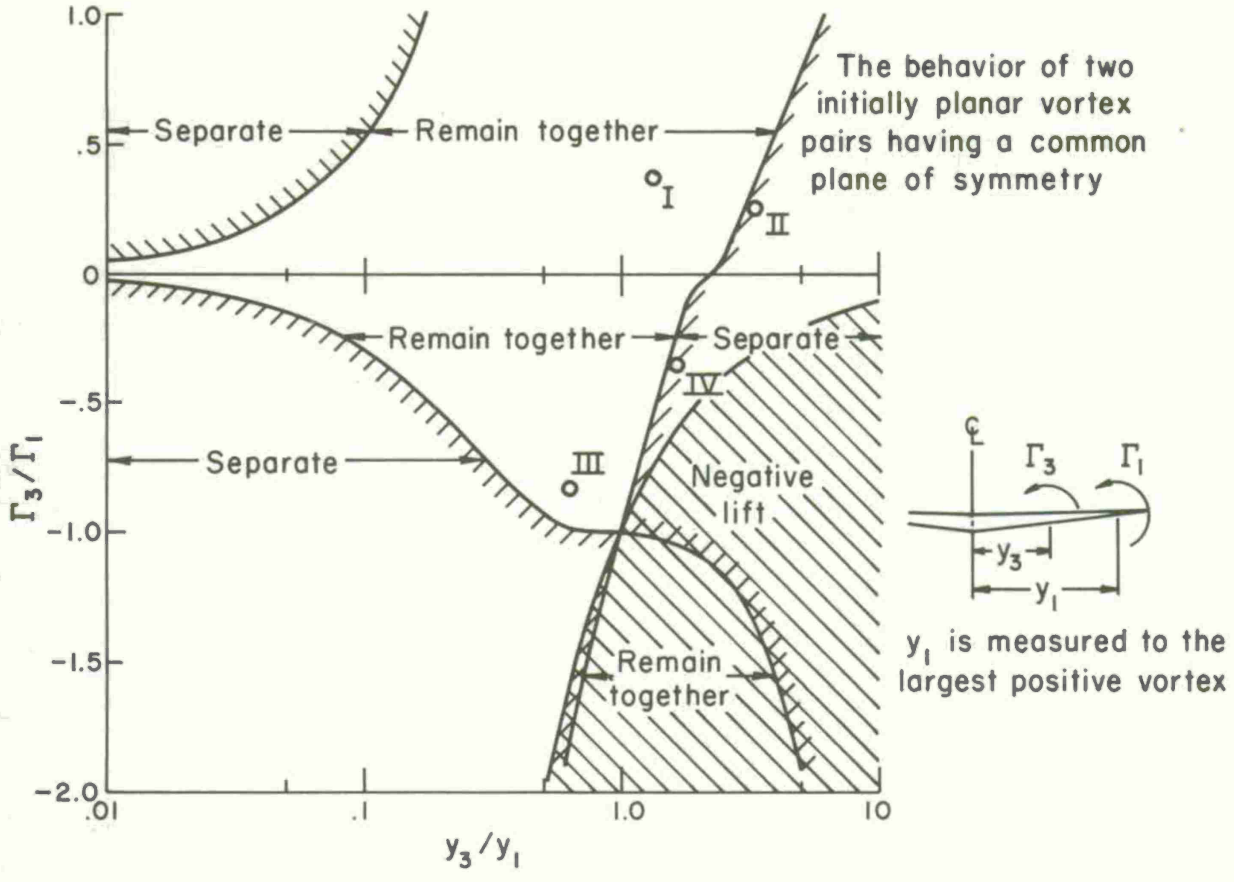

Figure 2.2 Wake classification for two-vortex-pair wakes [25]

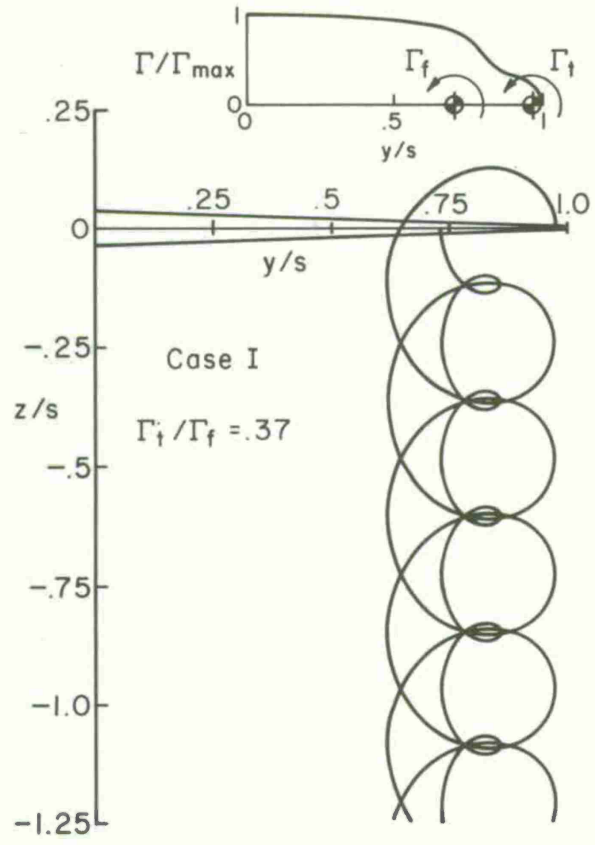

Figure 2.3 Vortex centroid locations as seen from downstream with strong interaction between neighboring vortices [25]

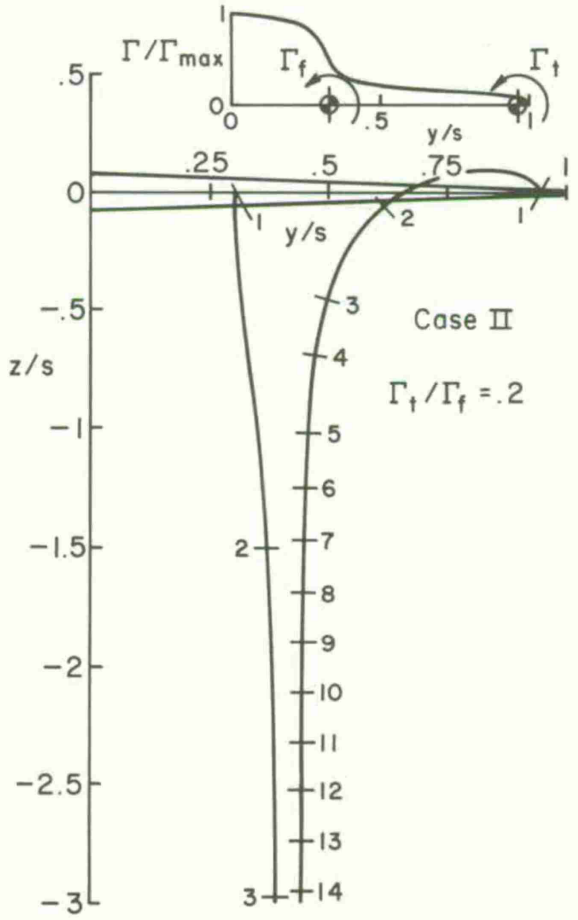

Figure 2.4 Vortex centroid locations as seen from downstream with weak interaction between vortex pairs; pairs diverge. The time interval between consecutive integers is a constant [25].

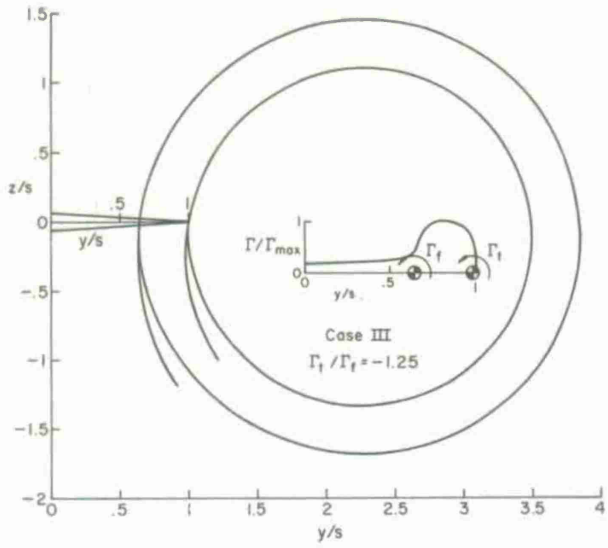

Figure 2.5 Vortex centroid locations as seen from downstream with strong interaction between neighboring vortices

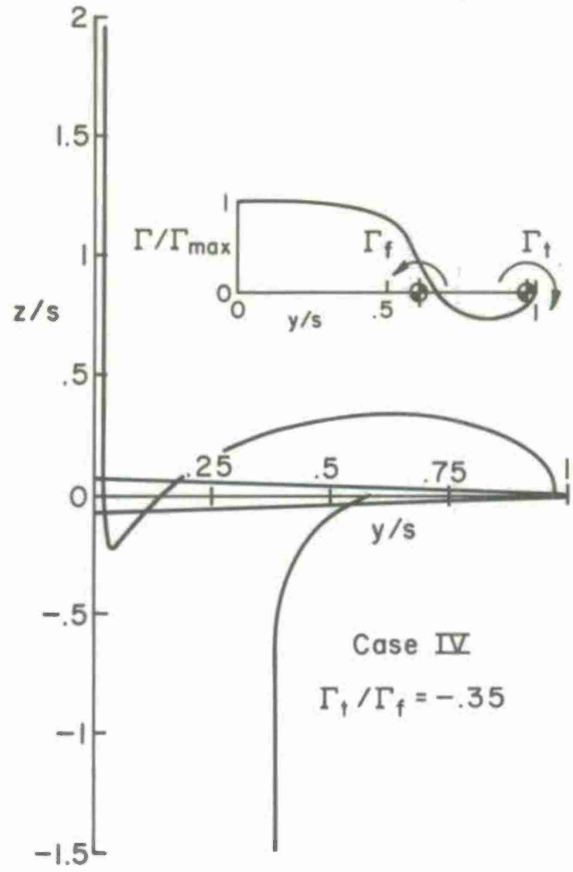

Figure 2.6 Vortex centroid locations as seen from downstream; pairs of opposite sign. Weak interaction between pairs; pairs diverge [25]

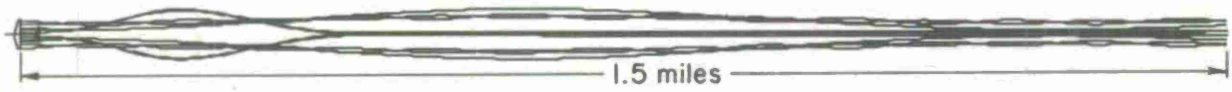

Figure 2.7 Top view of computed wake geometry for wing loading shown in Figure 1.32

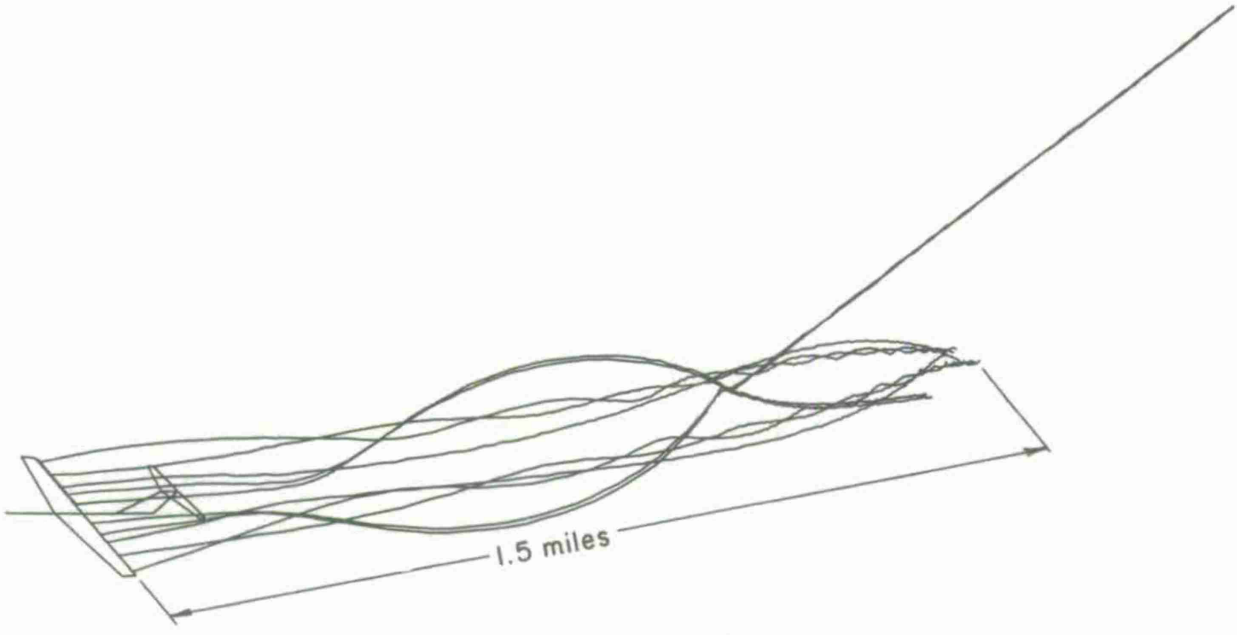

Figure 2.8 Oblique view of computed wake geometry for wing loading shown in Figure 1.32

Figure 2.9 Side view of computed wake geometry for wing loading shown in Figure 1.32. Fuselage and inboard engine vortices are vortices 1 and 2 in Figure 1.33, respectively.

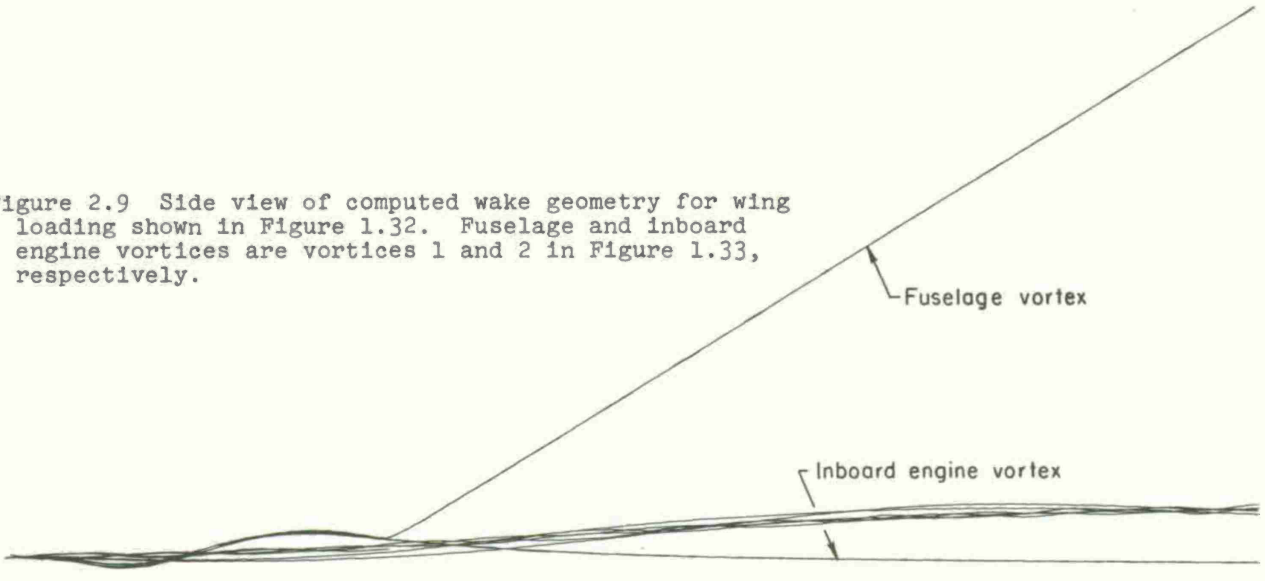

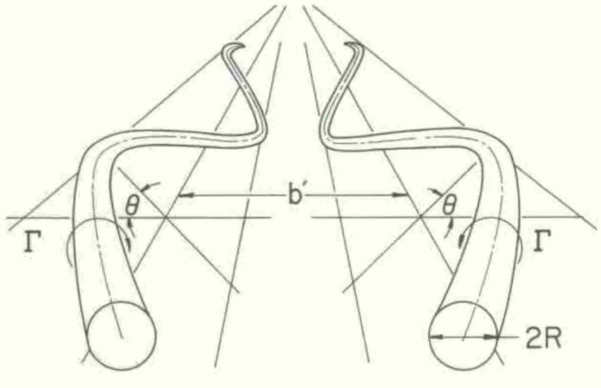

Figure 3.1 The geometry of sinusoidal instability

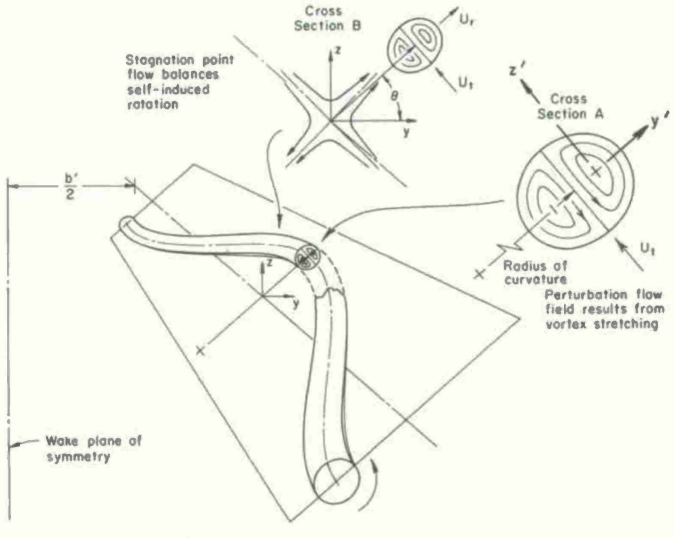

Figure 3.2 Schematic of the mechanisms responsible for sinusoidal instability

Axial velocity in the vortex tube $U(r) = U_m(1 - r^2/R^2)$; Swirl velocity in the vortex tube $v(r) = v_m r/R$; $\bar{U} = U_m/v_m$

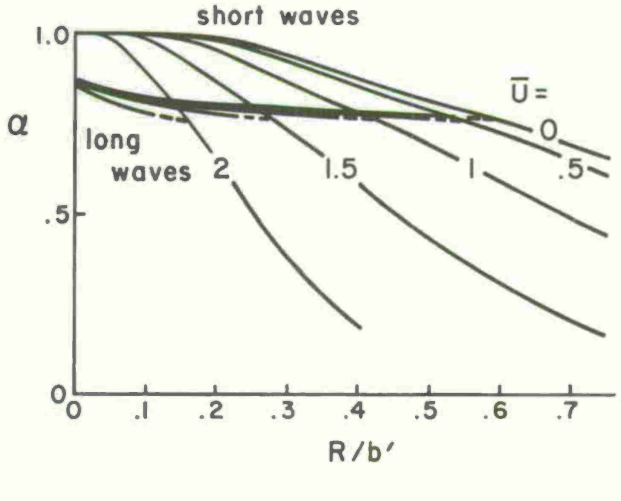

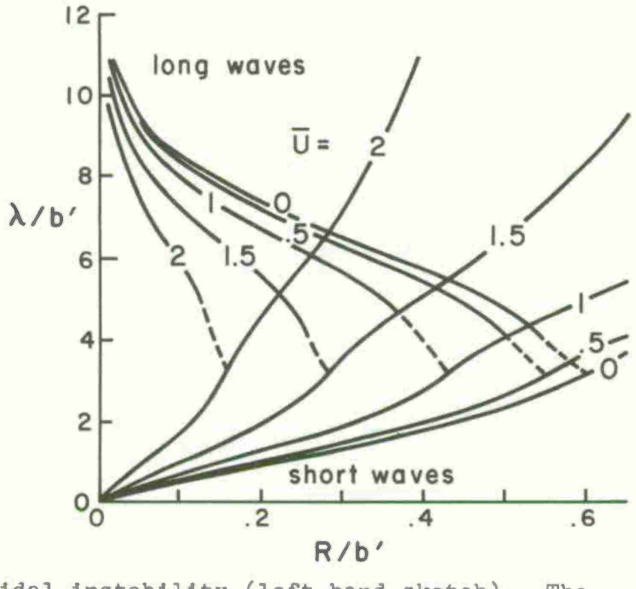

Figure 3.3 Amplification rate α for sinusoidal instability (left-hand sketch). The divergence of the trailing vortices is proportional to $\exp(\alpha\Gamma t/2\pi b'^2)$. The most unstable wavelength is shown as a function of vortex tube radius (right-hand sketch) [33]

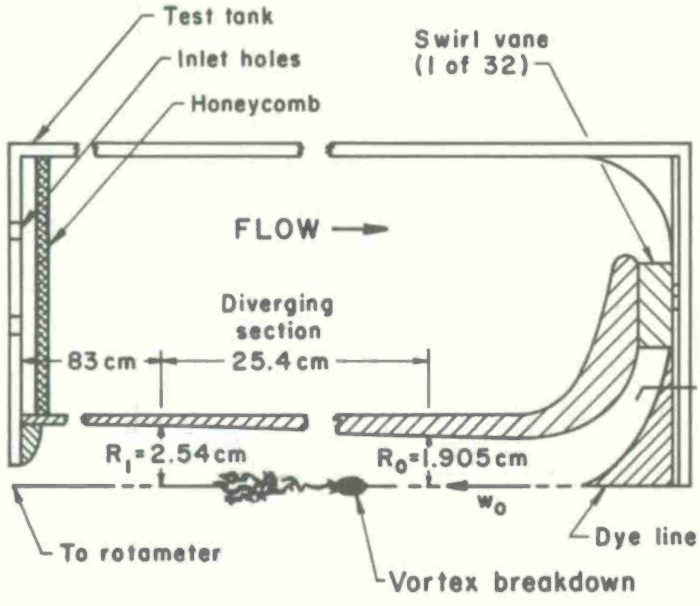

Figure 3.4 Top half of Sarpkaya's experimental apparatus [50]

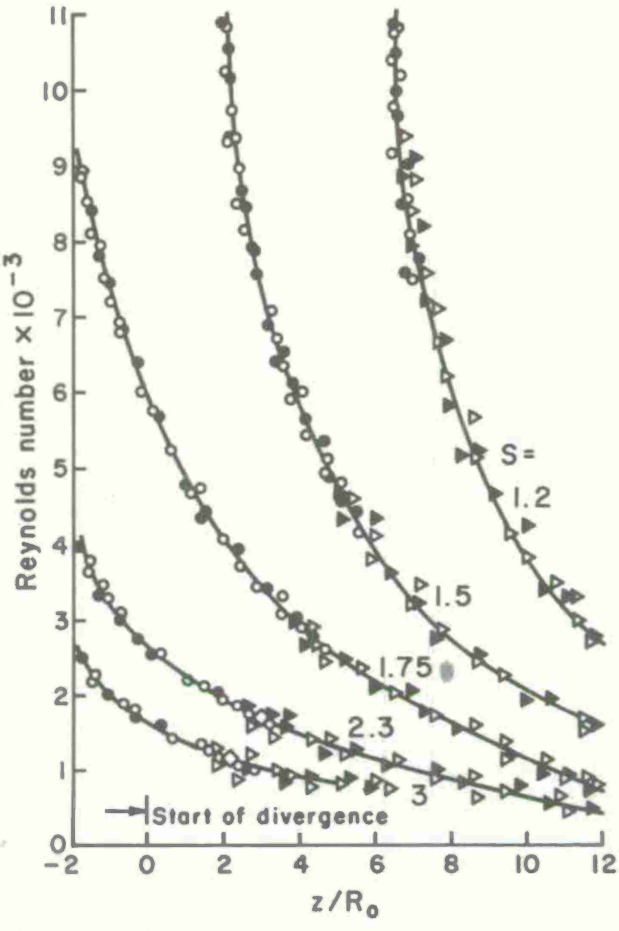

Figure 3.5 Vortex breakdown position as a function of Reynolds number, $2w_0R_0V$, and circulation number $S = \Gamma/2w_0R_0$.
O,● - axisymmetric breakdown; Δ,▲ - spiral breakdown; ◇ - double helix breakdown.
z is measured from the start of the diverging tube (see Figure 3.4) [50]

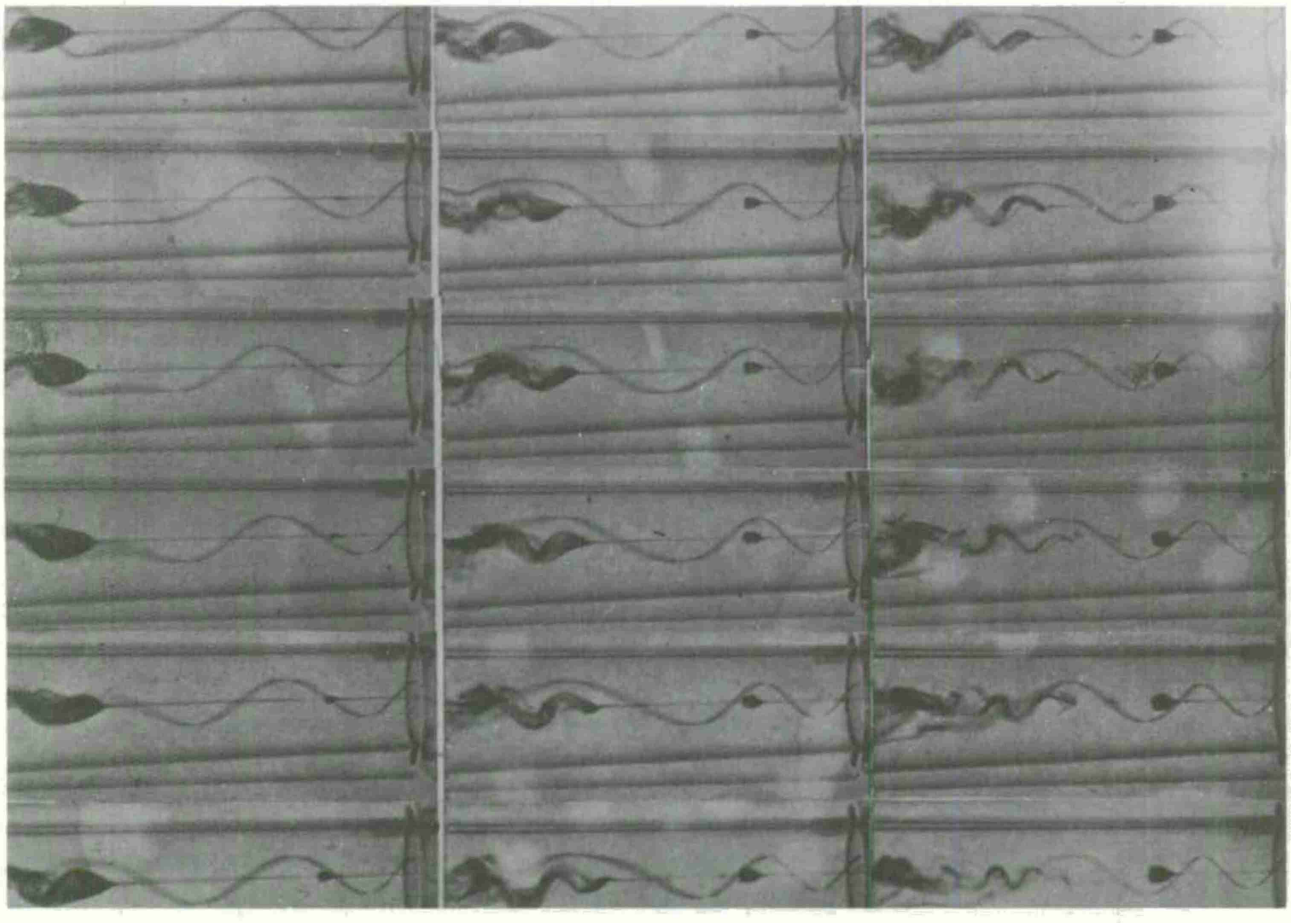

Figure 3.6 Birth and growth of a bubble and the propagation upstream of a traveling breakdown. The Axial symmetry of the initial disturbance, evolution of the streamlines between the two disturbances, and the inability of the waves to propagate into the supercritical flow are clearly visible [50].

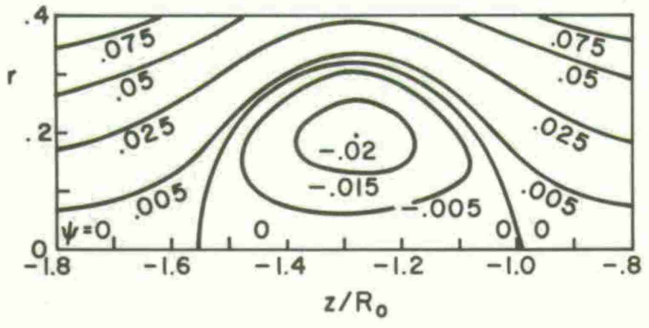

Figure 3.7 Streamline pattern in neighborhood of equilibrium position using final wave profile. Numbers are stream-function values [40]

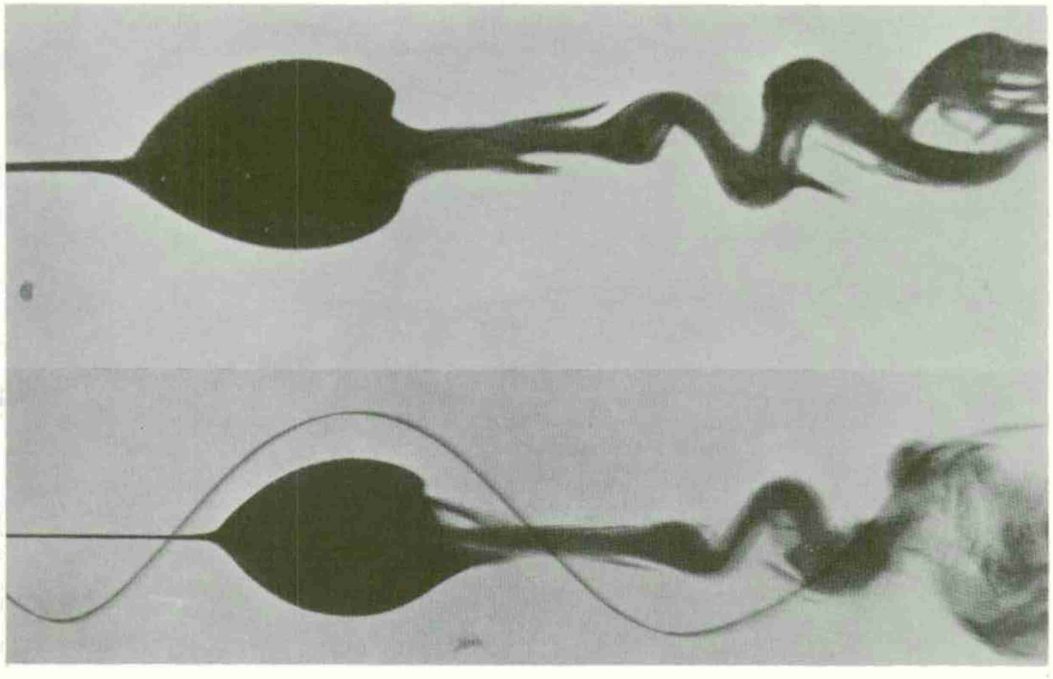

Figure 3.8 Axisymmetric breakdown made visible by dye [50]

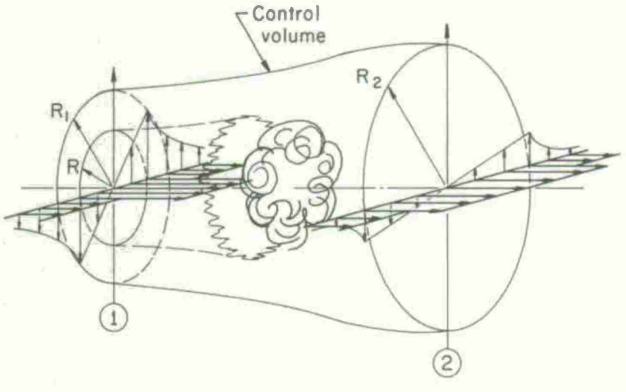

Figure 3.9 Control volume for simple breakdown model

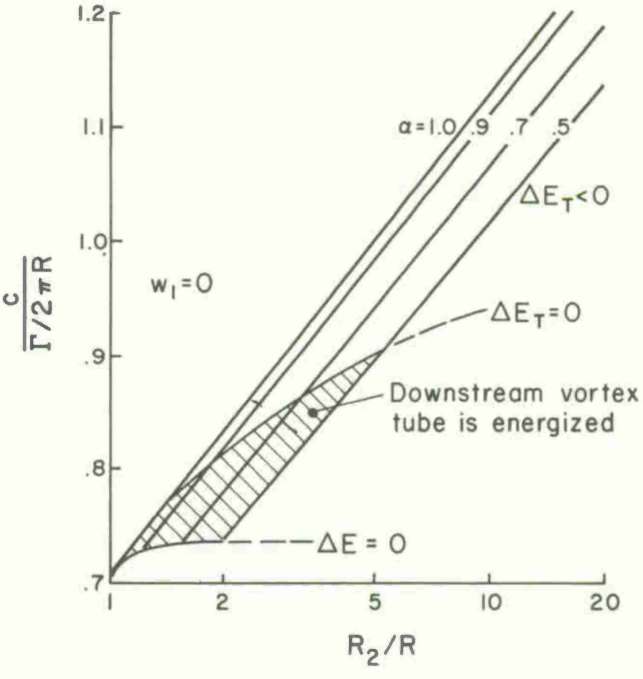

Figure 3.10 Vortex jump conditions for $w_1 = 0$ [40]

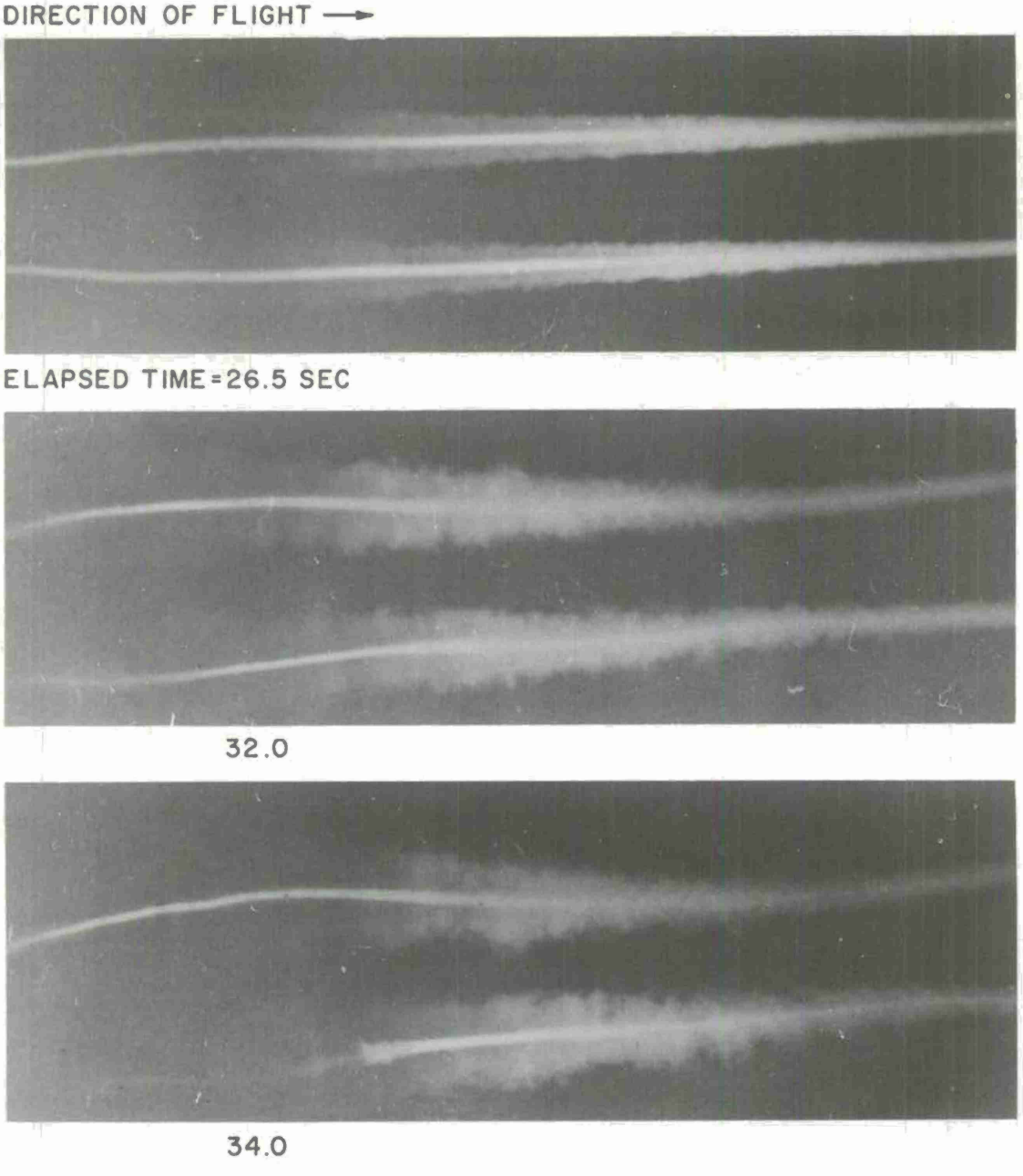

Figure 3.11 Trailing pair undergoing both vortex breakdown and Crow instability [56]

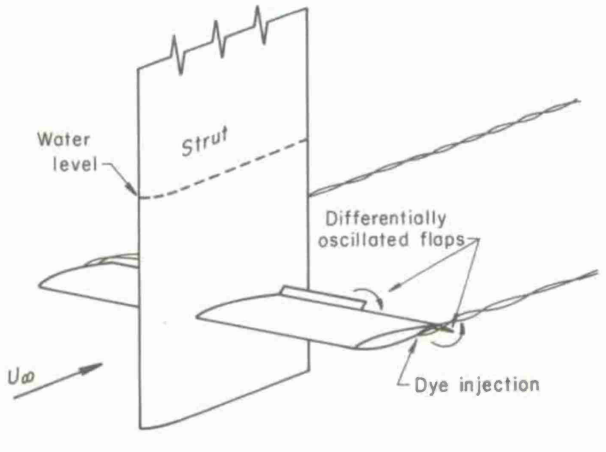

Figure 3.12 Model wing used to excite Crow instability [58]

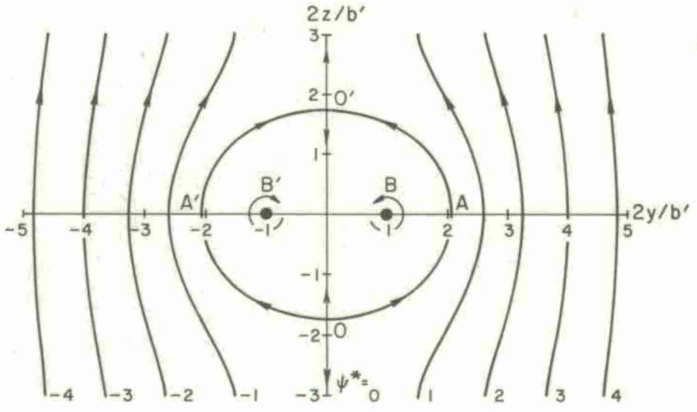

Figure 4.1 Streamlines in the vicinity of a vortex pair. The observer is at rest relative to the two vortices.

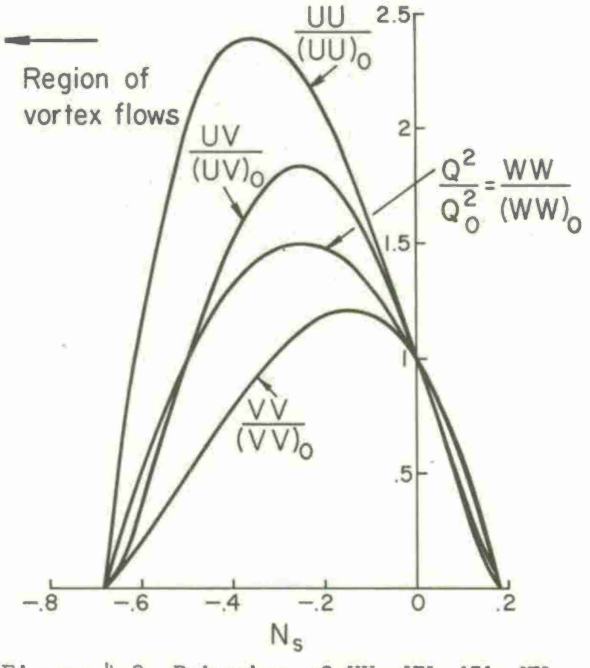

Figure 4.2 Behavior of UU, VV, WW, UV and Q^2 as functions of the stability parameter N_s for b = 0.125, β = 0

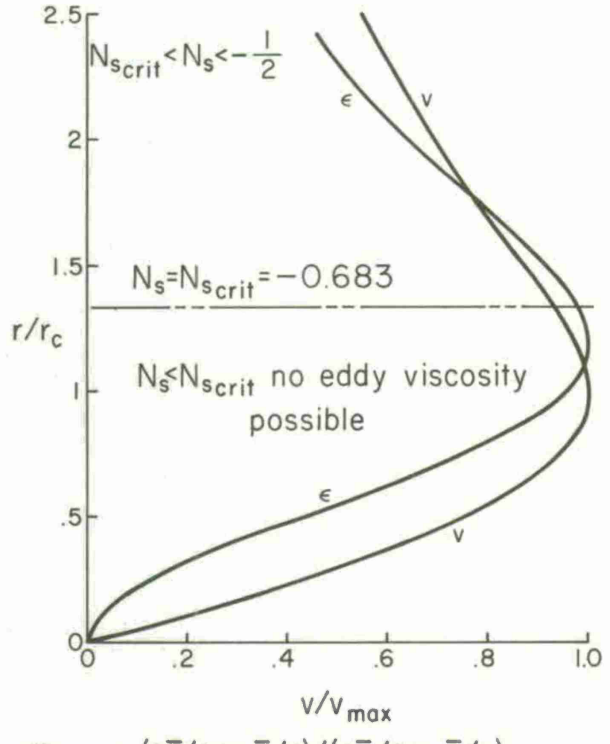

$$\epsilon/\epsilon_{max} = (\partial\bar{v}/\partial r - \bar{v}/r)/(\partial\bar{v}/\partial r - \bar{v}/r)_{max}$$

Figure 4.3 Behavior of deformation rate and stability in a classical vortex

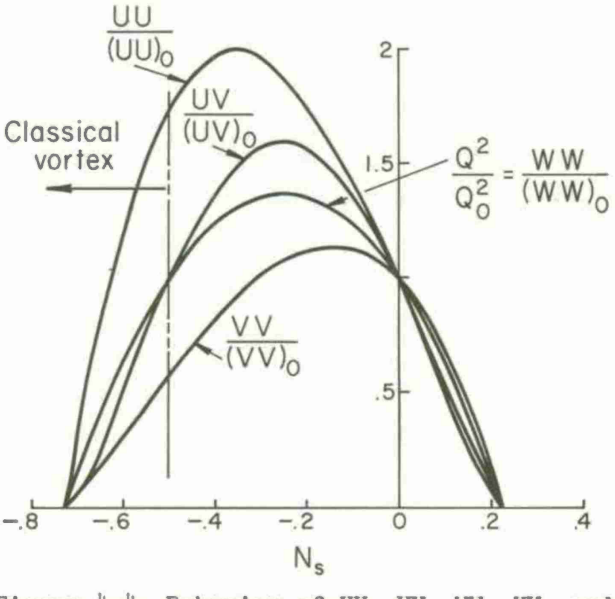

Figure 4.4 Behavior of UU, VV, WW, UV, and Q^2 as functions of the stability parameter N_s for b = 0.125, β = 1

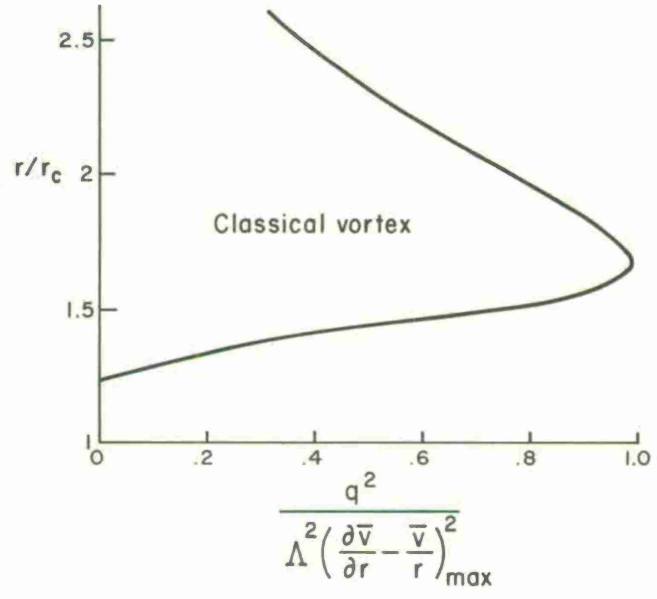

Figure 4.5 Hypothetical distribution of turbulent energy in a classical vortex according to superequilibrium theory

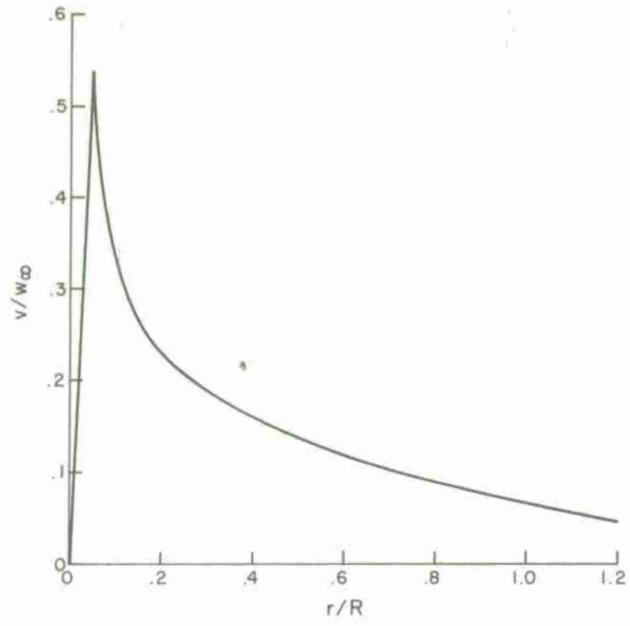

Figure 4.6 Swirl velocity distribution from an elliptically loaded wing [11]. A vortex core is added to facilitate numerical computations.

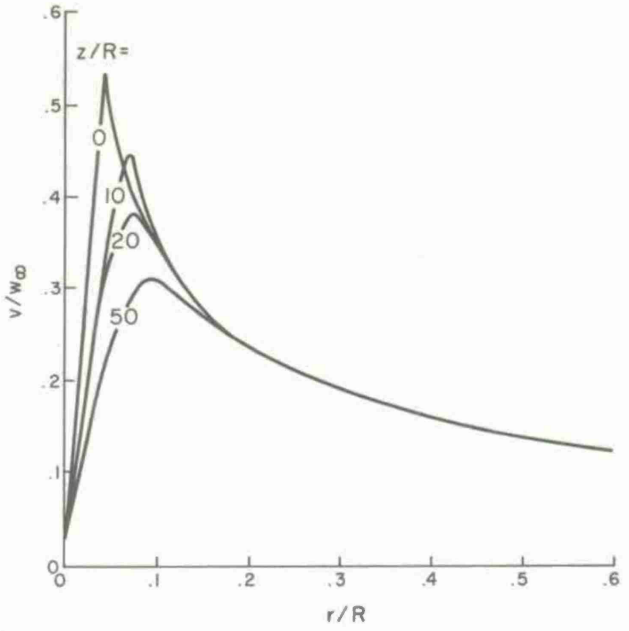

Figure 4.7 Laminar decay of the tangential velocities in a Betz-like vortex for $Re = \rho w_\infty R/\mu = 5 \times 10^4$

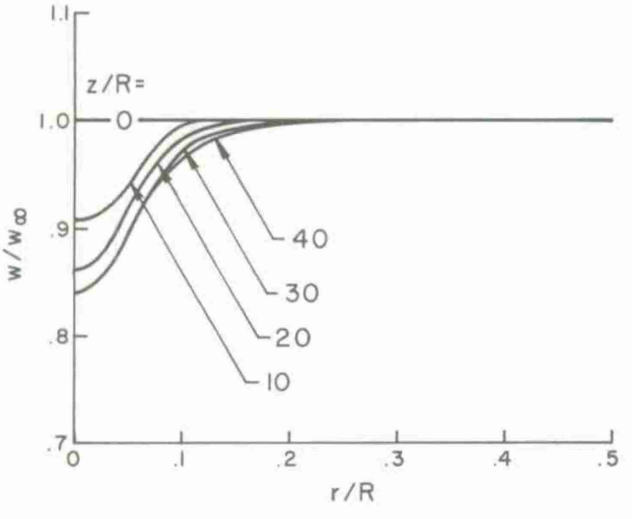

Figure 4.8 Effect of variations of tangential velocity shown in Figure 4.7 on the axial velocities in a Betz-like vortex

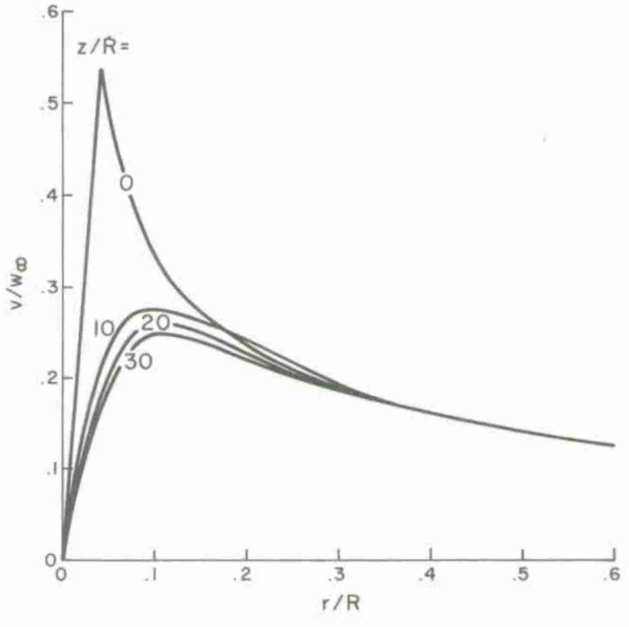

Figure 4.9 Effect of turbulence introduced at the center of a Betz-like vortex on tangential velocity

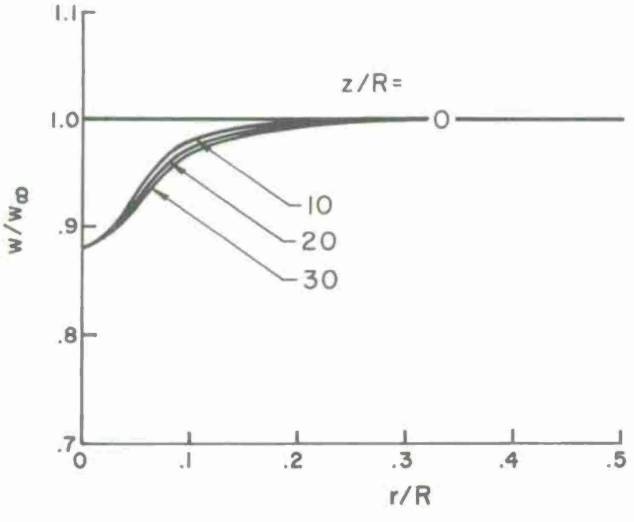

Figure 4.10 Behavior of the axial velocities in a Betz-like vortex when turbulence is introduced into the center of the vortex

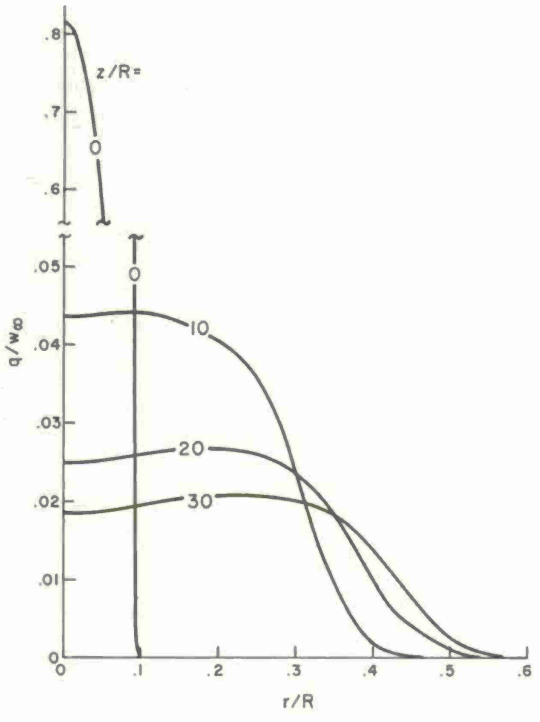

Figure 4.11 Behavior of the turbulent energy introduced at the center of a Betz-like vortex

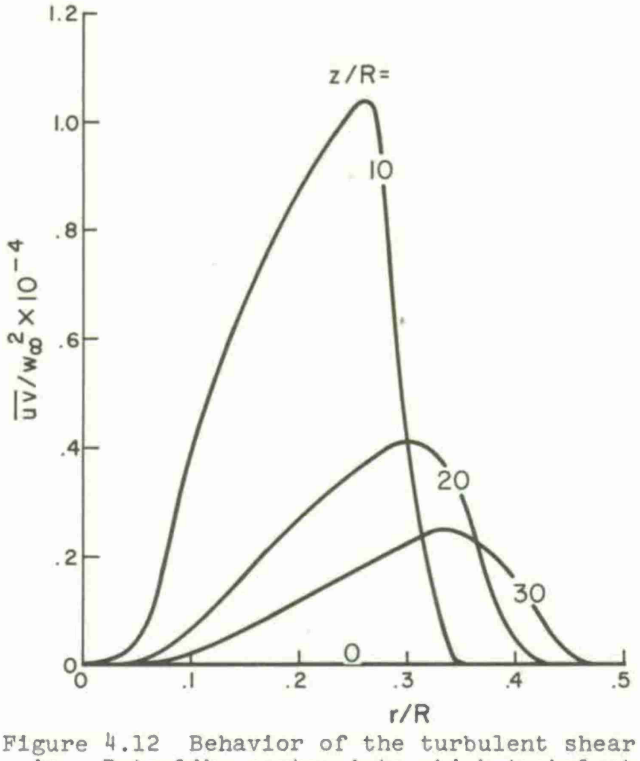

Figure 4.12 Behavior of the turbulent shear in a Betz-like vortex into which turbulent energy has been introduced at the center of the vortex

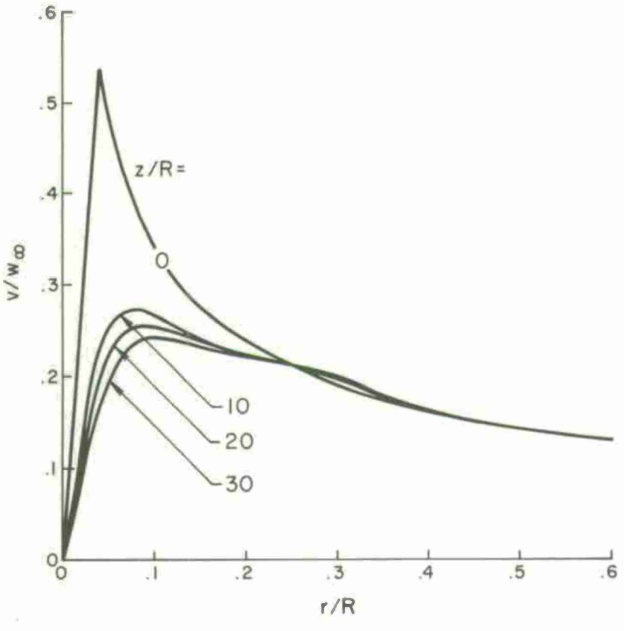

Figure 4.13 Effect of turbulence introduced at r/R = 0.2 in a Betz-like vortex on tangential velocity

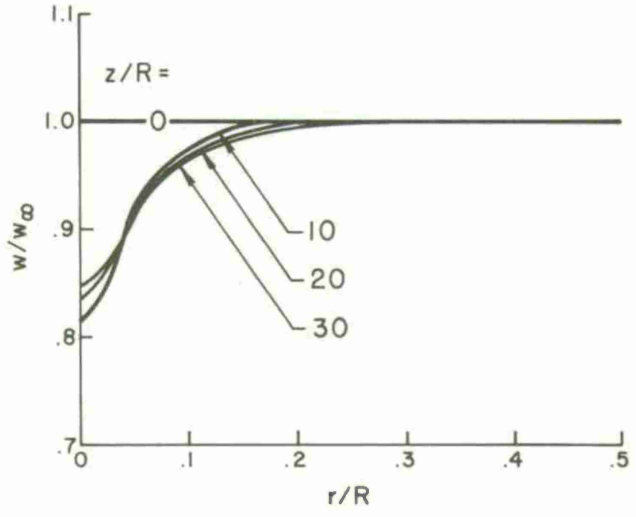

Figure 4.14 Behavior of the axial velocities in a Betz-like vortex when turbulence is introduced at r/R = 0.2

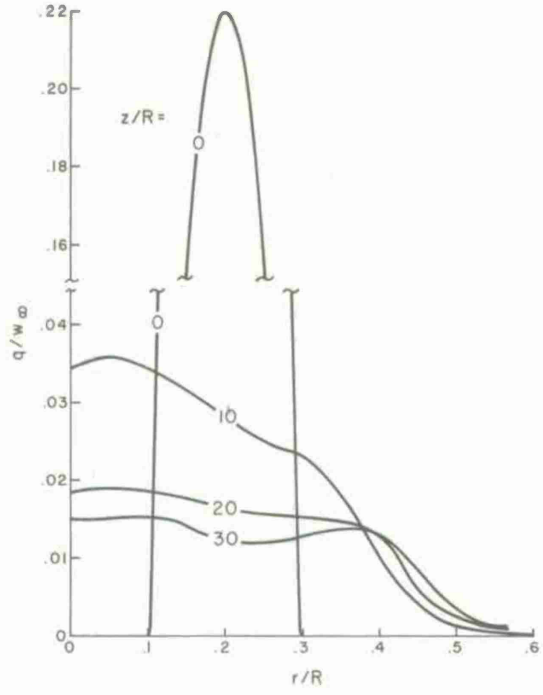

Figure 4.15 Behavior of turbulent energy introduced into a Betz-like vortex at r/R = 0.2

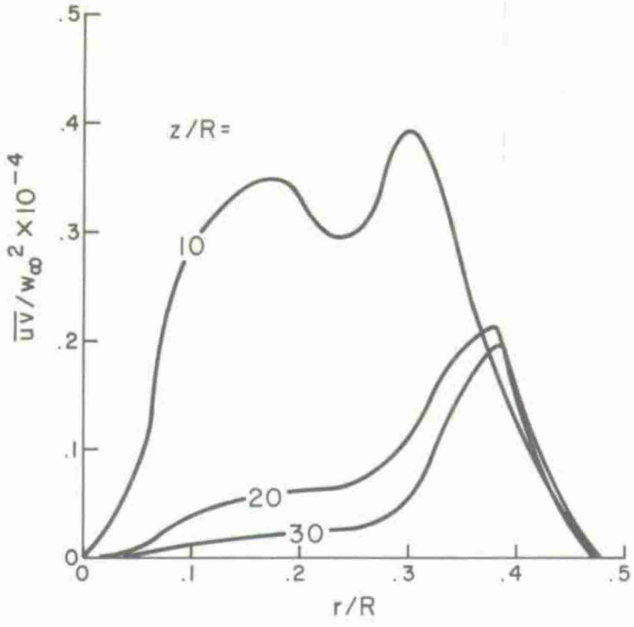

Figure 4.16 Behavior of turbulent shear in a Betz-like vortex into which turbulence has been introduced at r/R = 0.2

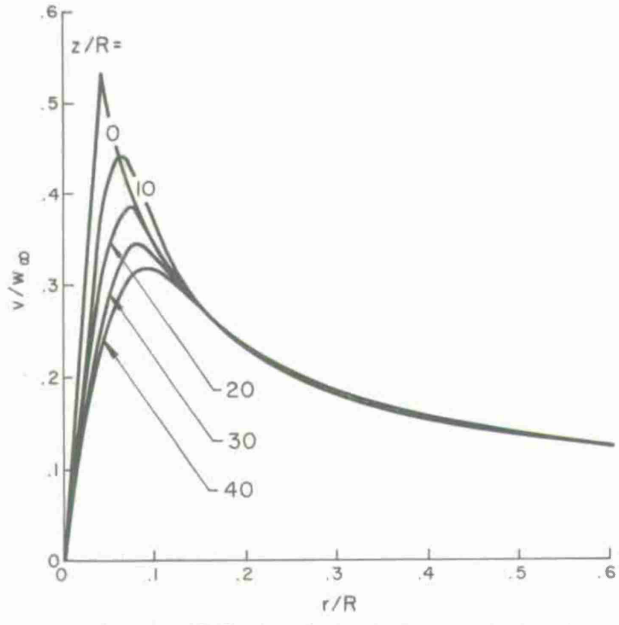

Figure 4.17 Effect of turbulence introduced at r/R = 0.8 in a Betz-like vortex on tangential velocity

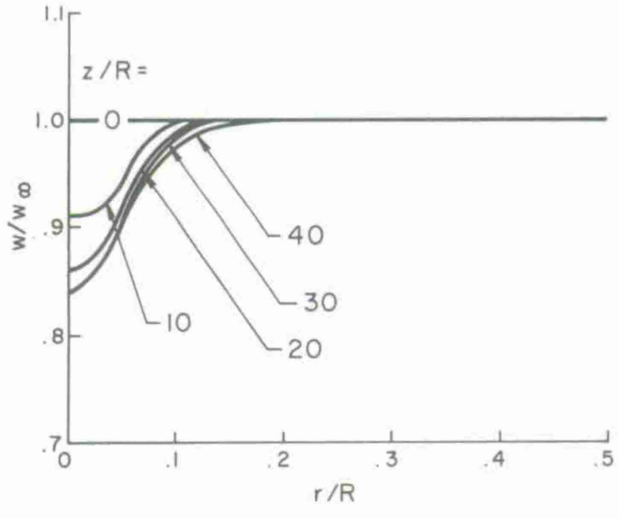

Figure 4.18 Behavior of the axial velocities in a Betz-like vortex into which turbulence has been introduced at r/R = 0.8

Figure 4.19 Behavior of turbulent energy introduced into a Betz-like vortex at r/R = 0.8

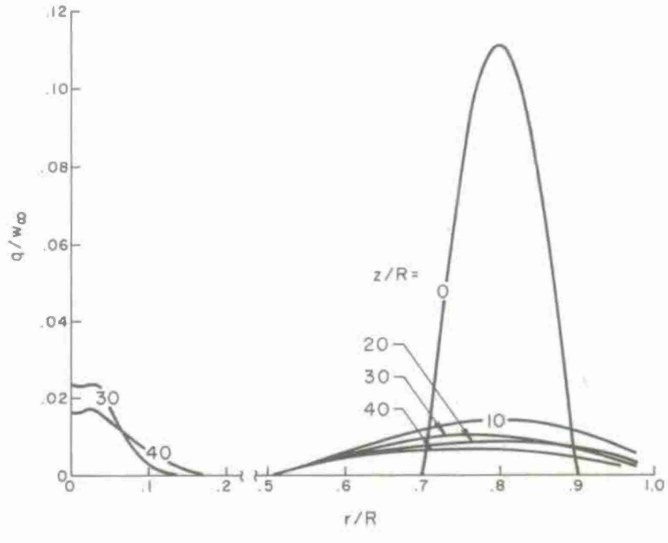

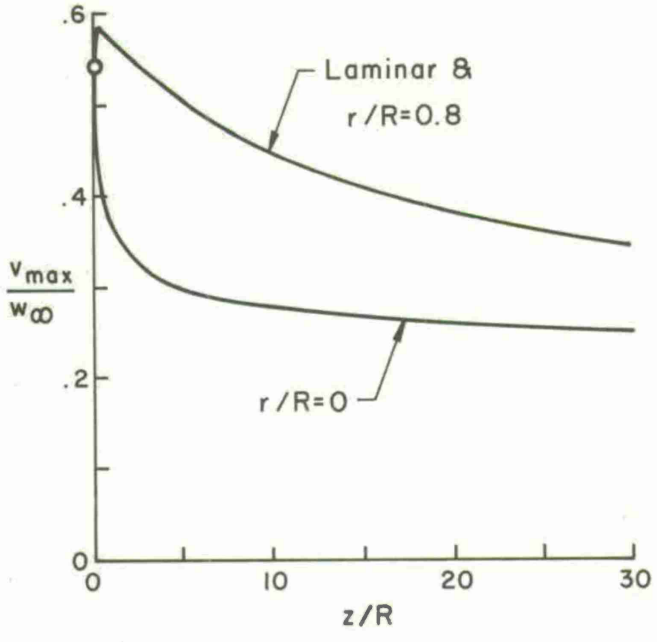

Figure 4.20 Comparison of behavior of maximum tangential velocities for a laminar Betz-like vortex and two cases where turbulence has been introduced into the vortex

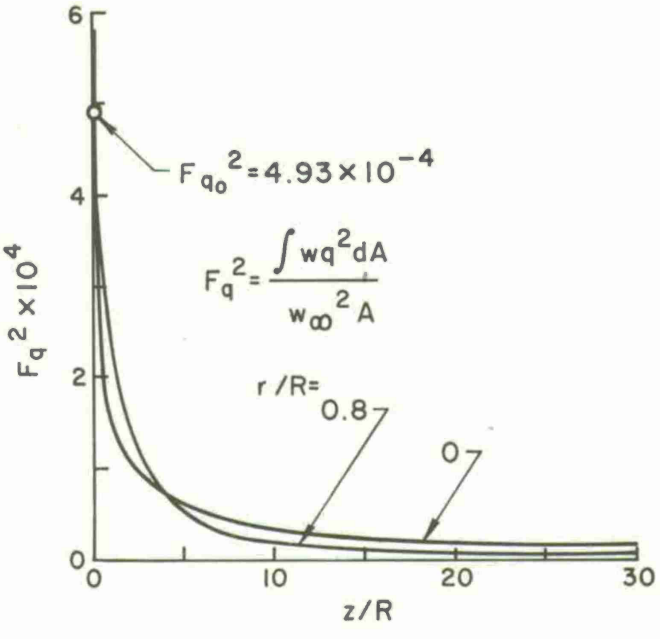

Figure 4.21 Decay of turbulent energy flux in a Betz-like vortex into which a given flux of turbulent energy was introduced at two locations

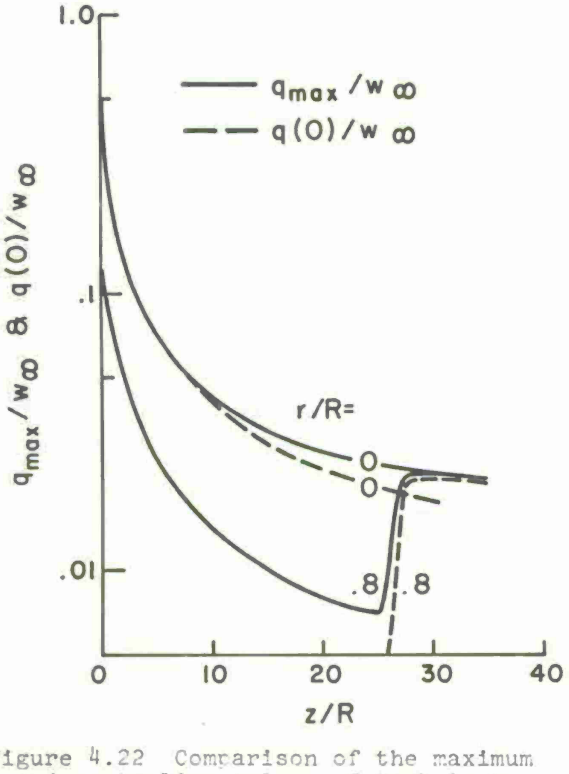

Figure 4.22 Comparison of the maximum and centerline values of turbulent kinetic energy for two Betz-like vortices into which a given flux of turbulent energy was introduced at two locations

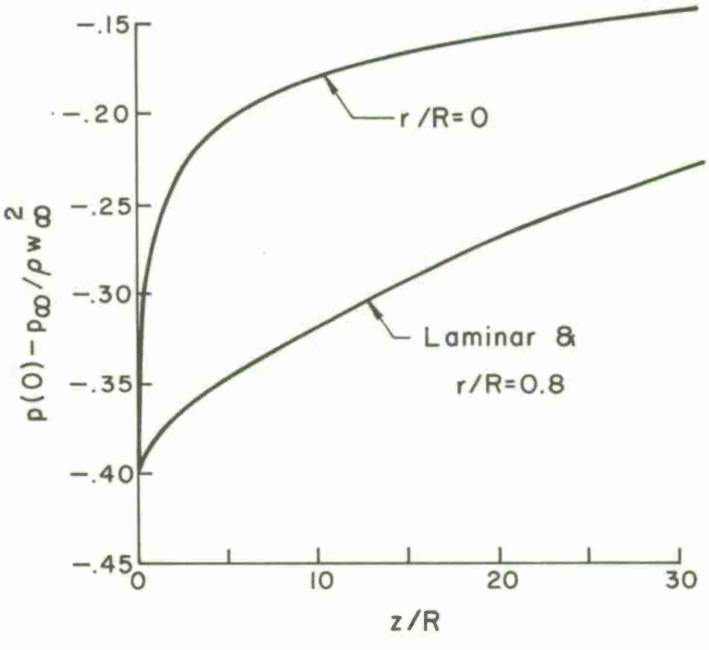

Figure 4.23 Comparison of the centerline pressures for a laminar Betz-like vortex and for two cases when a given flux of turbulent energy was introduced at different locations

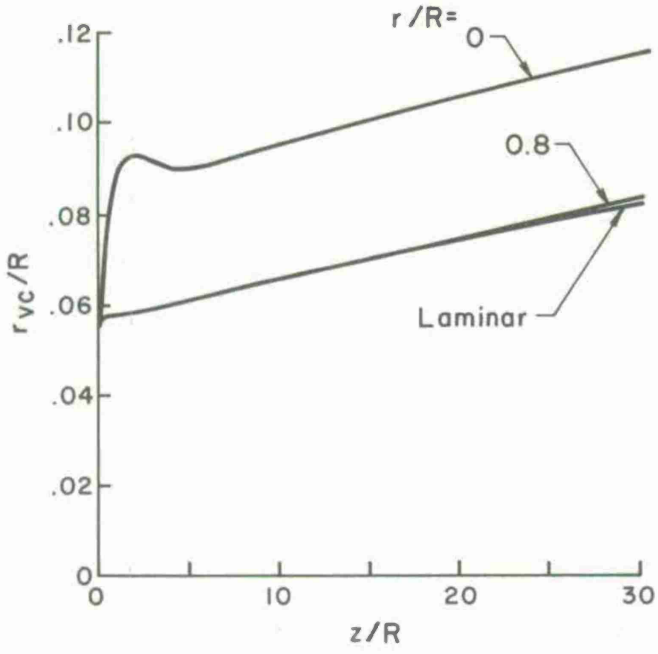

Figure 4.24 Comparison of the viscous core sizes of a laminar Betz-like vortex and for two cases when a given flux of turbulent energy was introduced at different locations

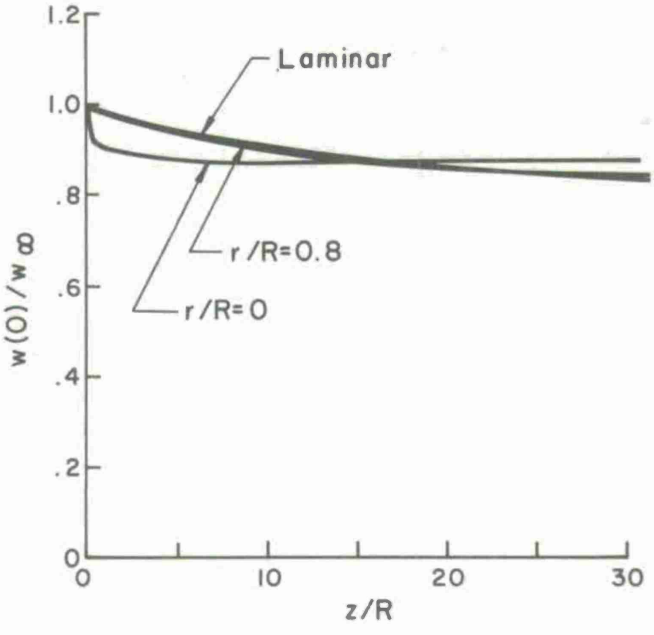

Figure 4.25 Comparison of centerline axial velocities for a laminar Betz-like vortex and for two cases when a given flux of turbulent energy was introduced at two locations

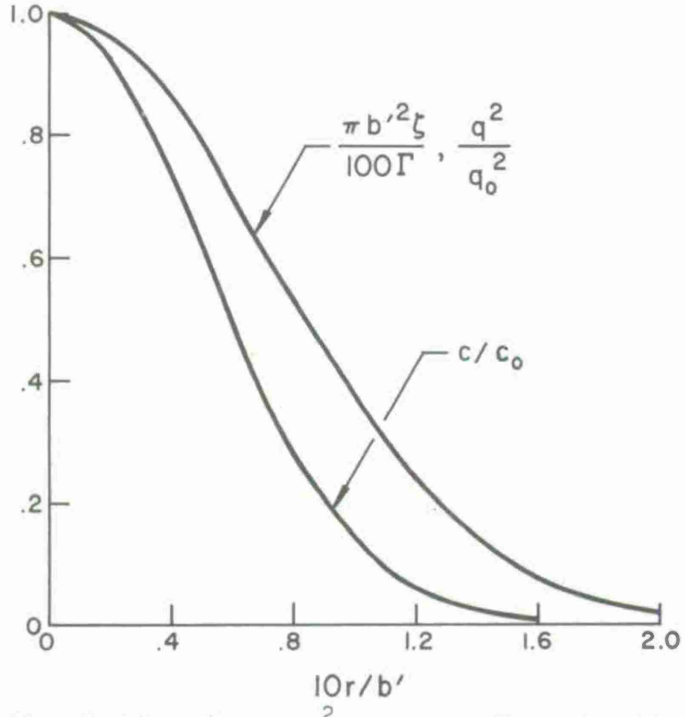

Figure 4.26 Initial distribution of ζ, q^2, and c for a hypothetical pair of vortices behind a wing

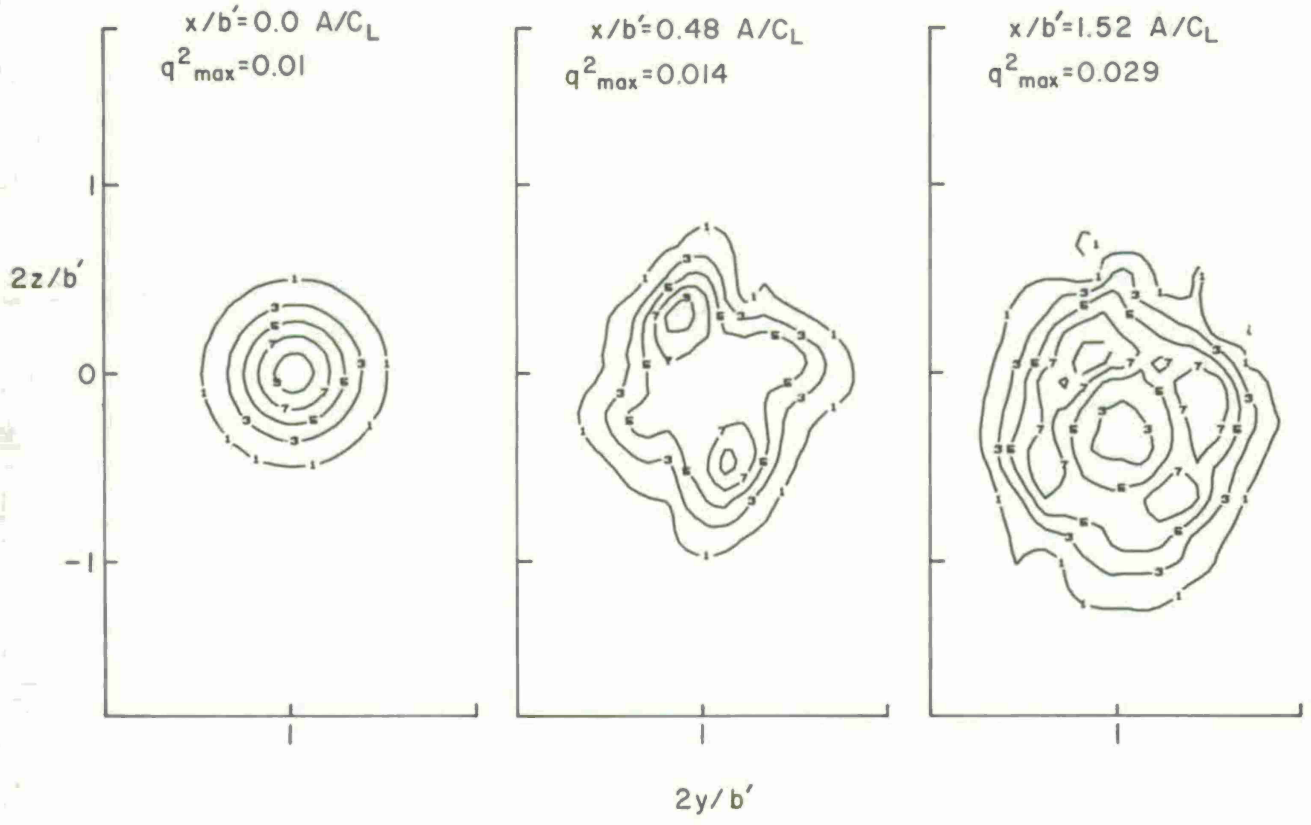

Figure 4.27 Turbulent kinetic energy isopleths as a function of downstream distance for a one-pair wake

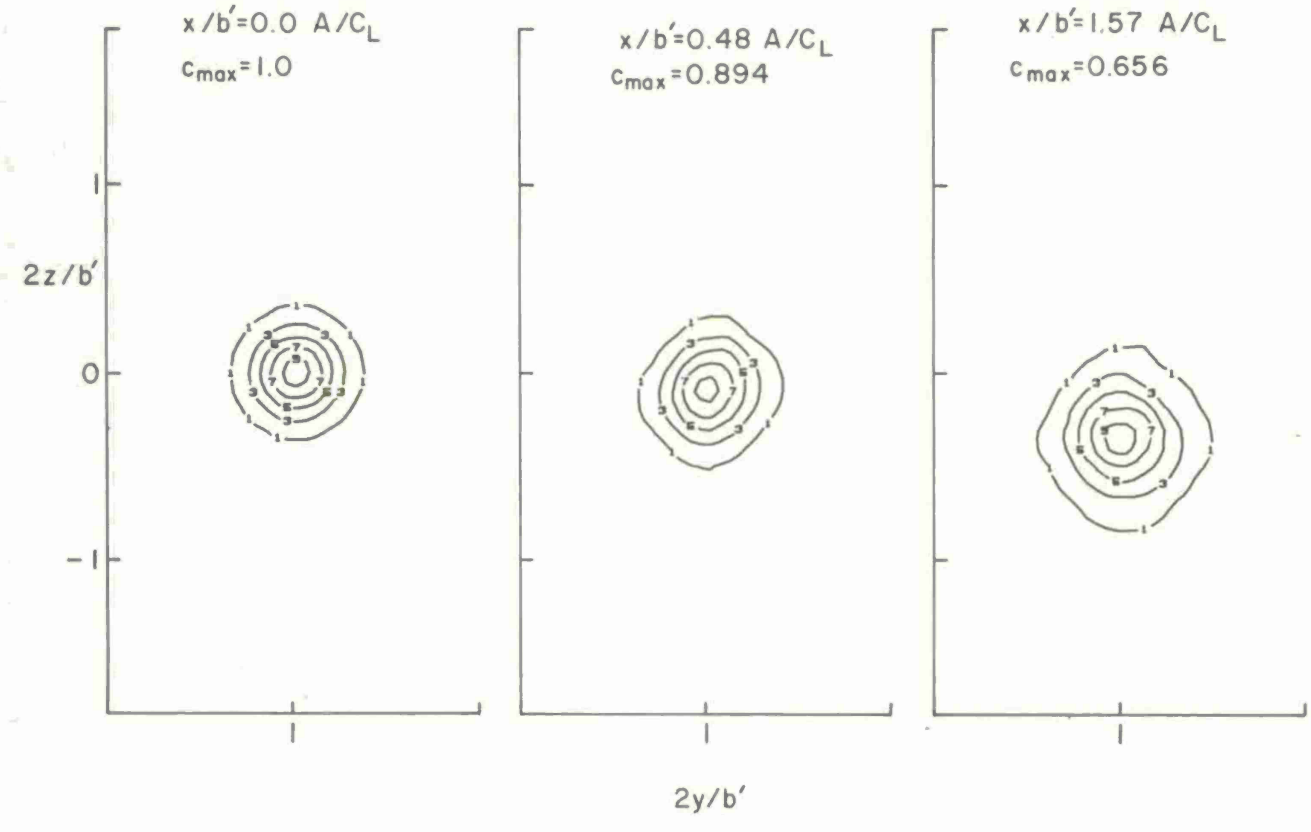

Figure 4.28 Smoke concentration isopleths as a function of downstream distance for a one-pair wake

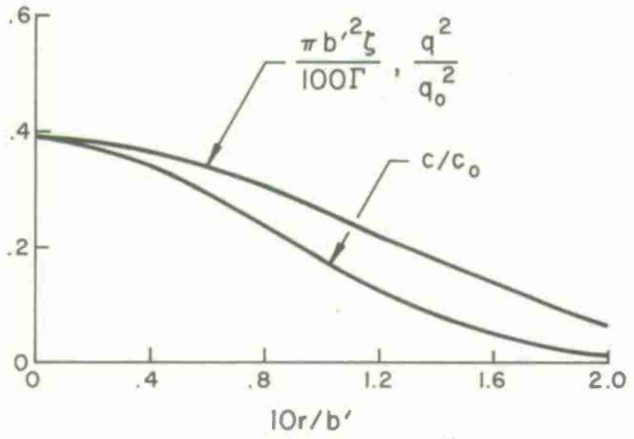

Figure 4.29 Initial distribution of ζ, q^2, and c for each vortex for the case of two pairs of hypothetical vortices behind a wing

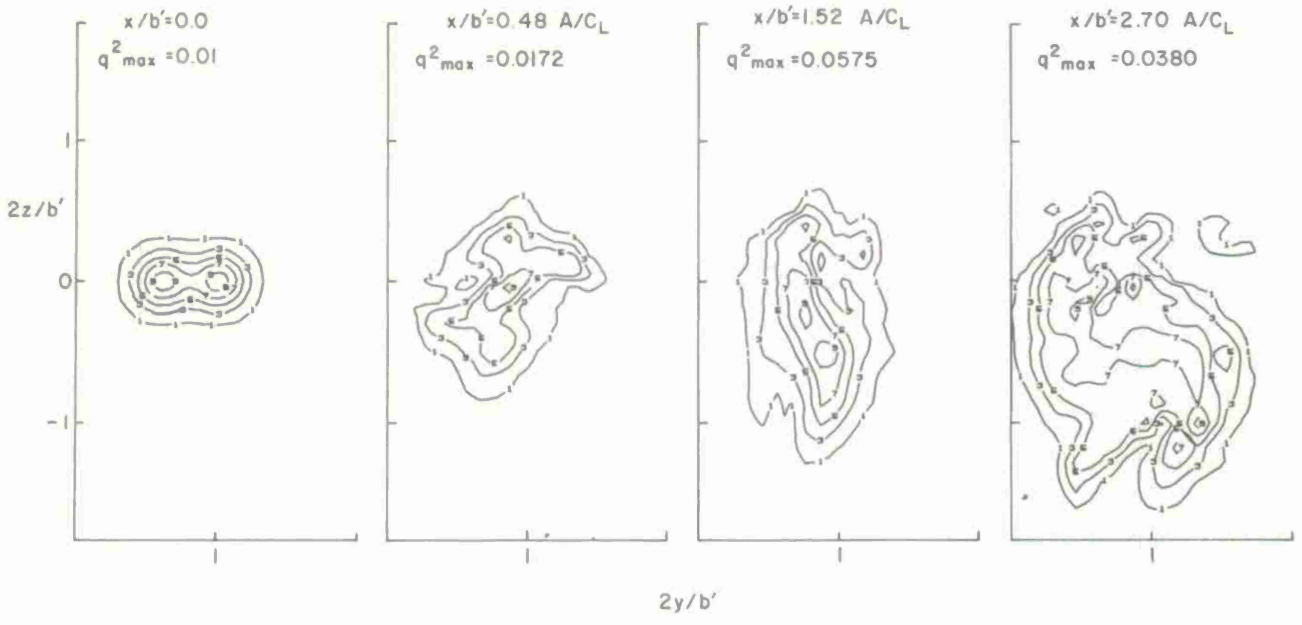

Figure 4.30 Turbulent kinetic energy isopleths as a function of downstream distance for a two-vortex-pair wake

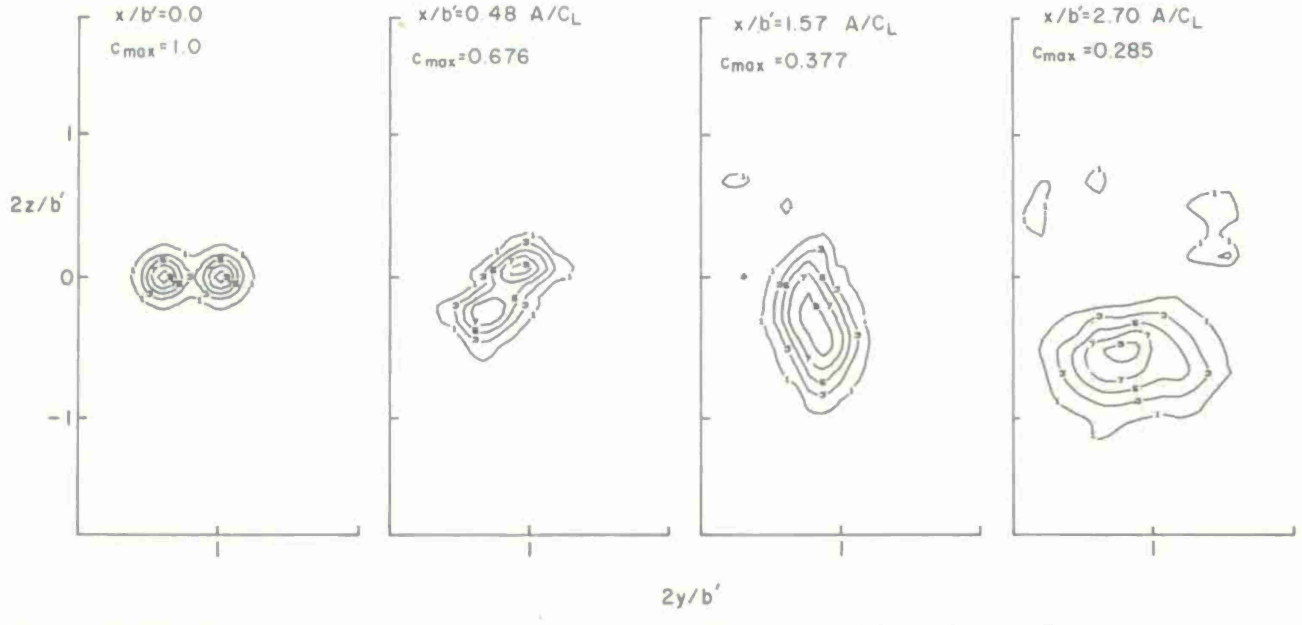

Figure 4.31 Smoke concentration isopleths as a function of downstream distance for a two-vortex-pair wake

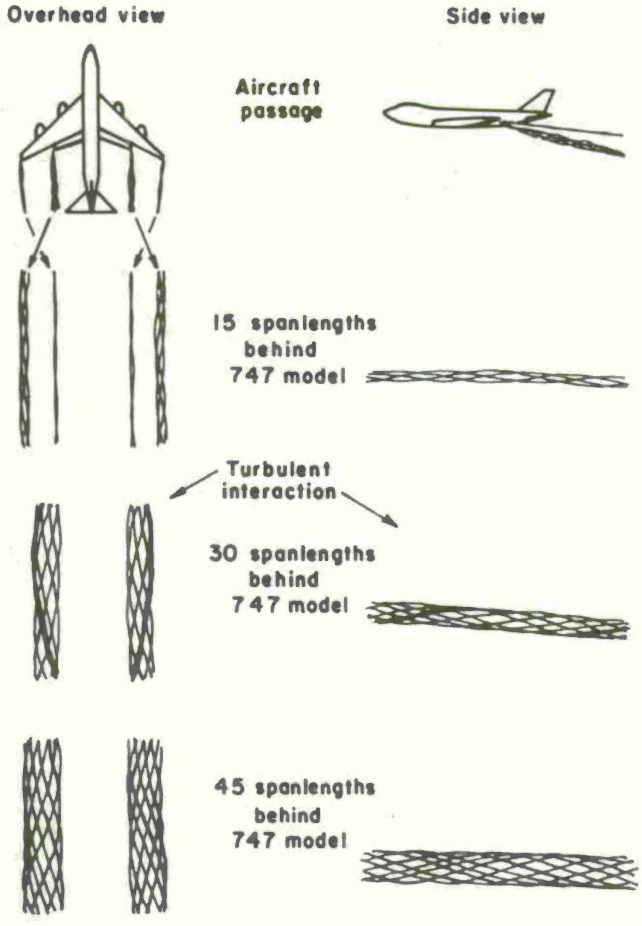

Figure 4.32 Interaction of a tip and a flap vortex as sketched by Dunham [75]

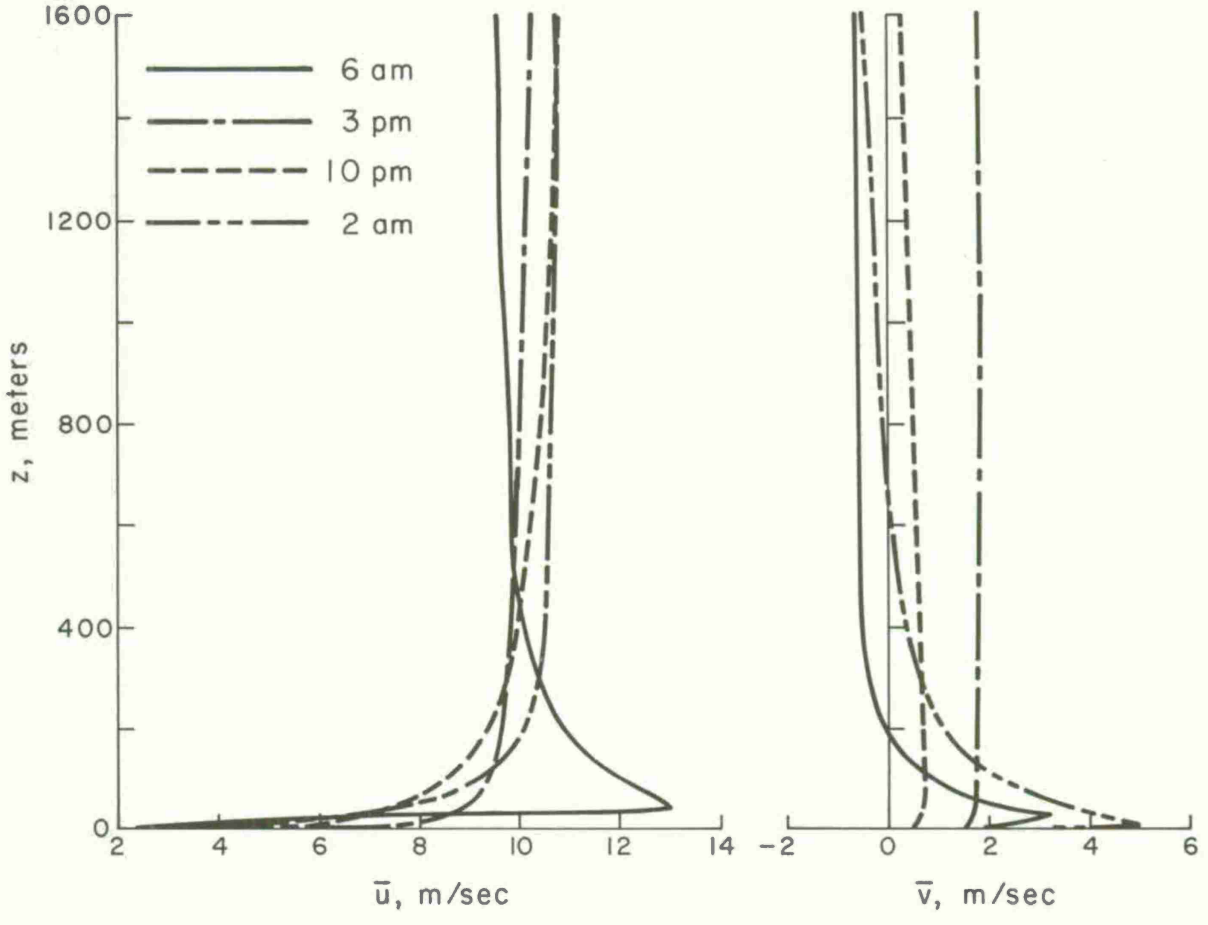

Figure 5.1 Variation of wind speed with altitude under conditions of strong diurnal heating and cooling over smooth terrain. $\bar{u}$ is velocity in the direction of the geostrophic wind, $\bar{u}$ = 10 m/sec, and $\bar{v}$ is velocity perpendicular to the geostrophic wind [76]

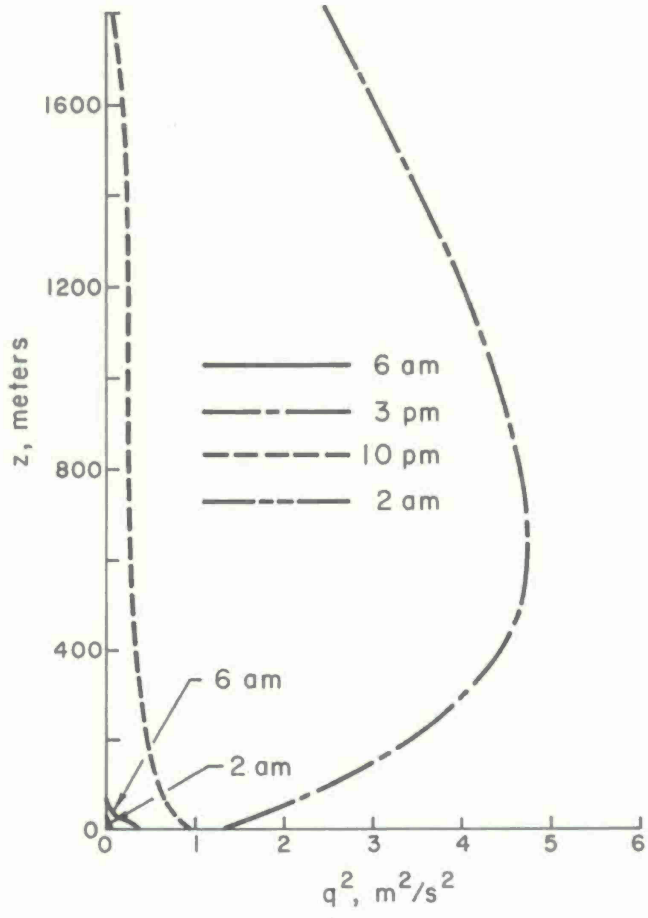

Figure 5.2 Turbulence levels q^2 as a function of altitude and time of day generated by velocity profiles shown in Figure 5.1 [76]

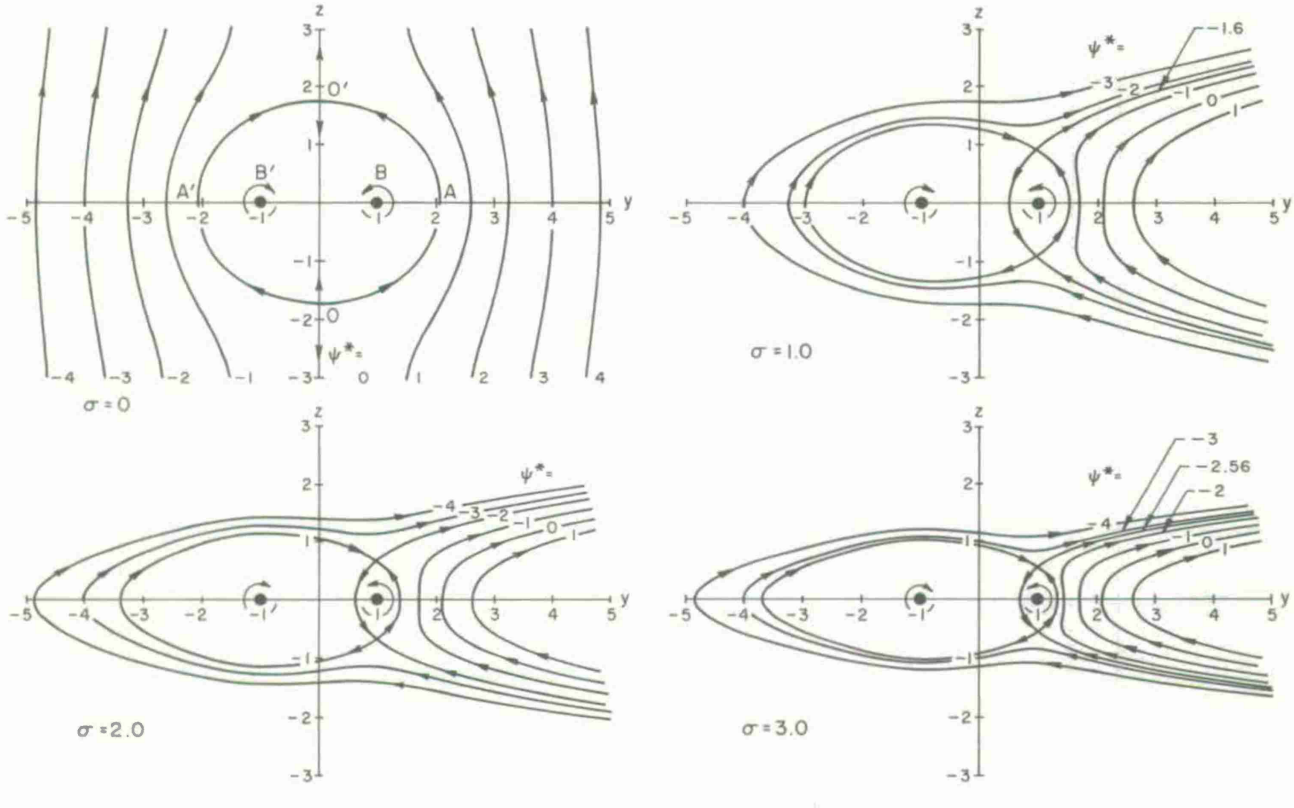

Figure 5.3 Effect of constant shear on the streamlines about an ideal vortex pair in two dimensions [77]

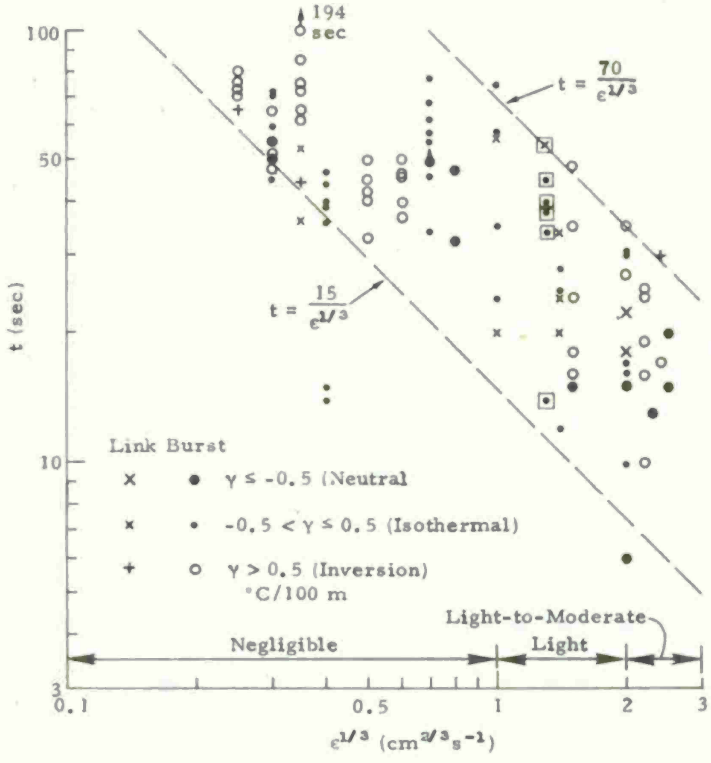

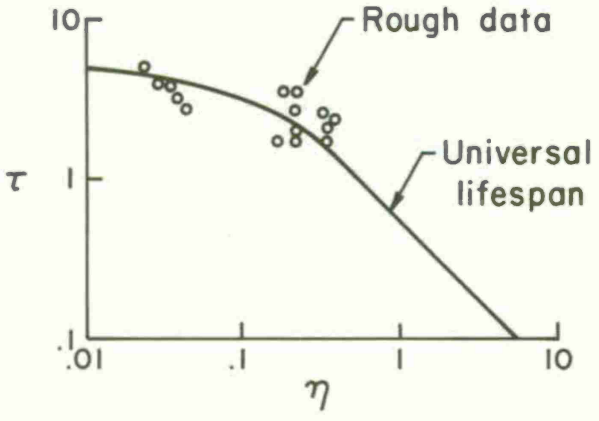

Figure 5.5 Form of Crow's universal lifespan function. The figure is from Ref. 81; the data are from Ref. 54.

Figure 5.4 Time of occurrence of observed instabilities as a function of turbulence. Γ_o = 16m²/sec for the boxed points; otherwise $\Gamma_o \sim$ 30m²/sec. The two arrowheads indicate that the point indicated was the last observed instability but that data are not available to give the time of final decay. (This figure is a reproduction of Figure 9 of Ref. 54.)

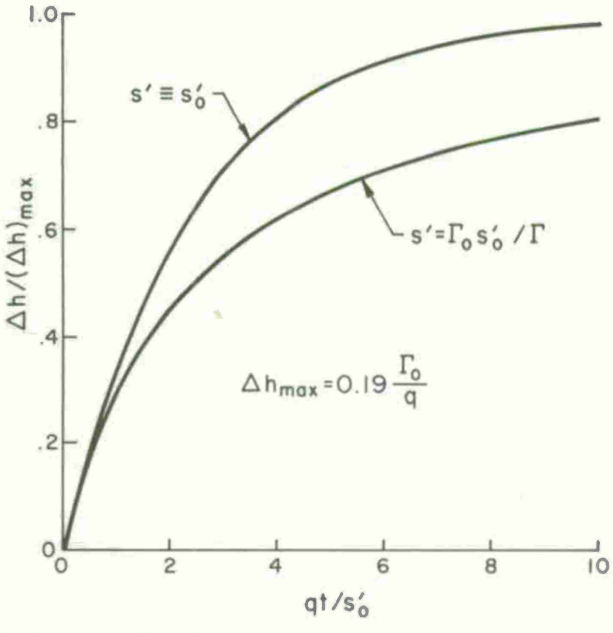

Figure 5.6 Nondimensional time to descend to a given fraction of maximum possible wake altitude changes given by Eqs (5.34) and (5.36)

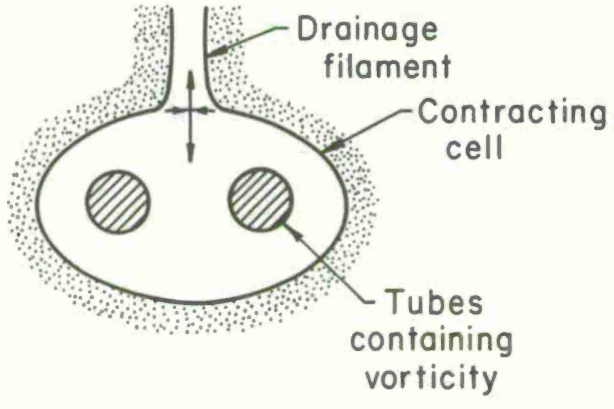

Figure 5.7 Nature of a descending vortex pair in a stably stratified medium as given by Crow [90]

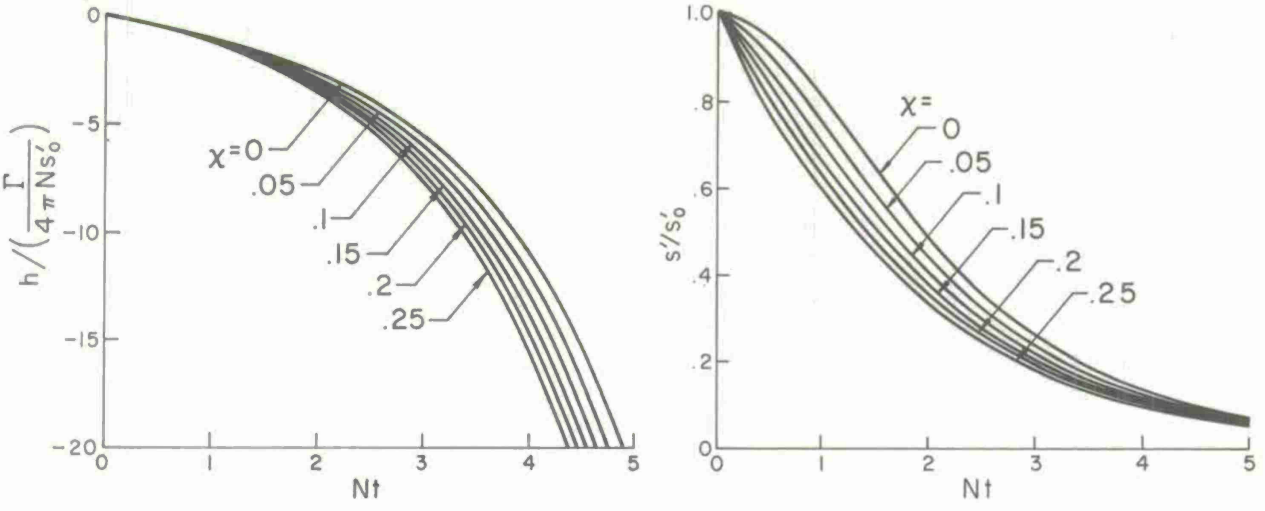

Figure 5.8 Trajectories of vortex tubes in an inviscid stably stratified medium given by Crow [90]

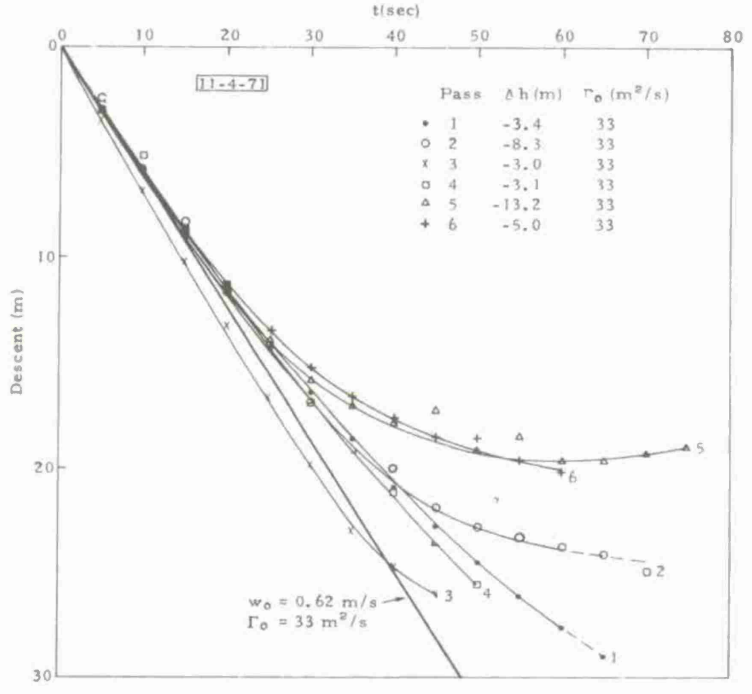

Figure 5.9 Trajectories of wake descent out of ground effect in a stably stratified atmosphere ($\chi \approx 0.2$, an inversion) with negligible turbulence ($\varepsilon^{1/3} \sim 0.3$ cm$^{2/3}$s^{-1}). Δh is the maximum observed vertical vortex separation (measure of tilt). The theoretical initial descent rate is shown (broken lines indicate less reliable data) [54].

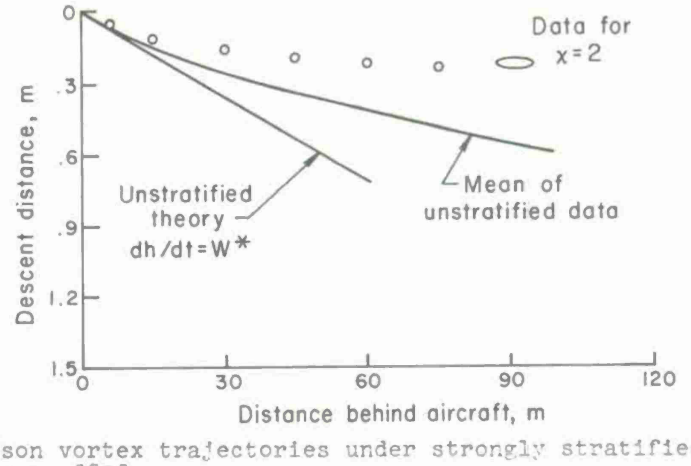

Figure 5.10 Comparison vortex trajectories under strongly stratified and unstratified atmospheric conditions [87]

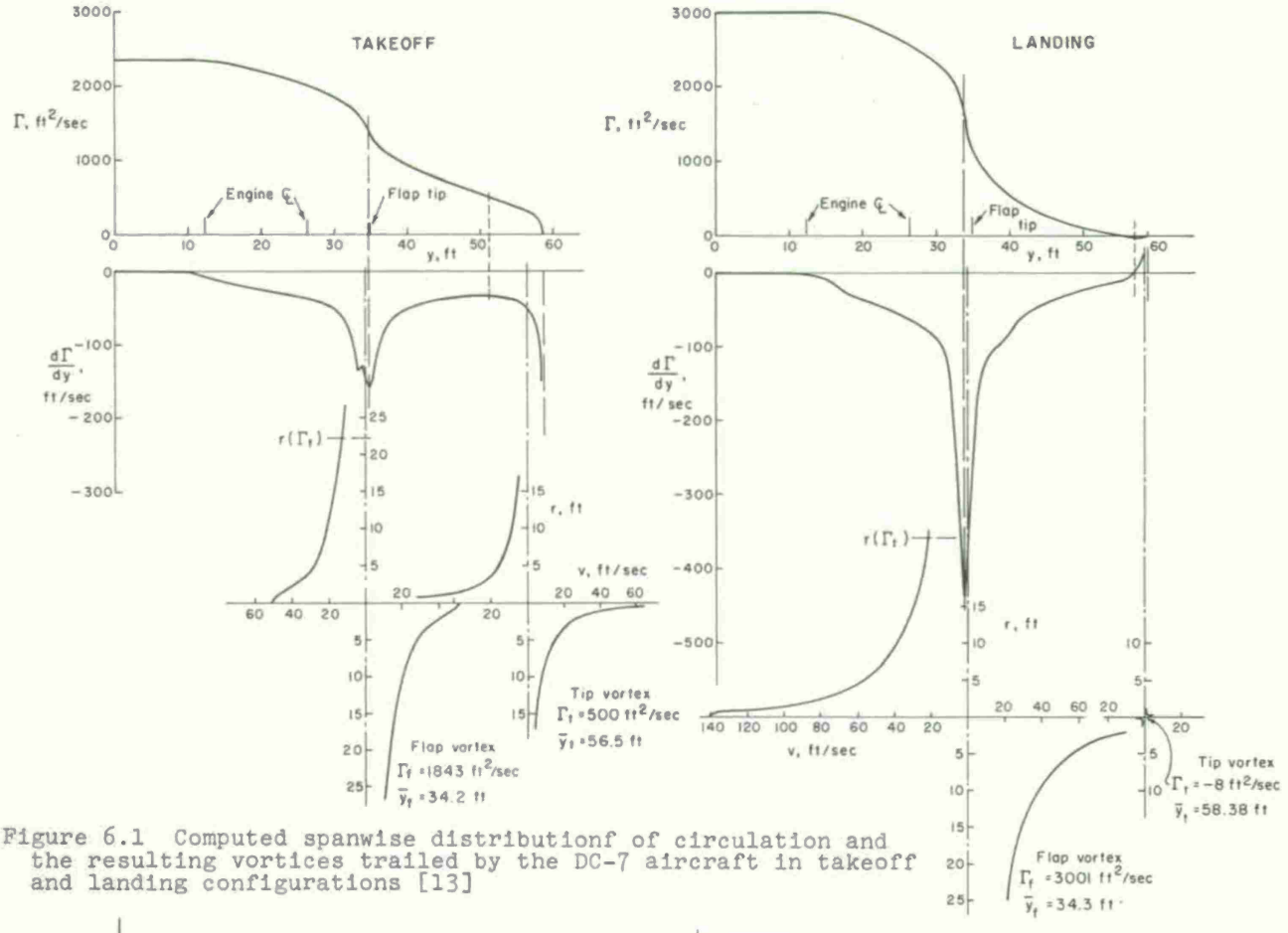

Figure 6.1 Computed spanwise distributionf of circulation and the resulting vortices trailed by the DC-7 aircraft in takeoff and landing configurations [13]

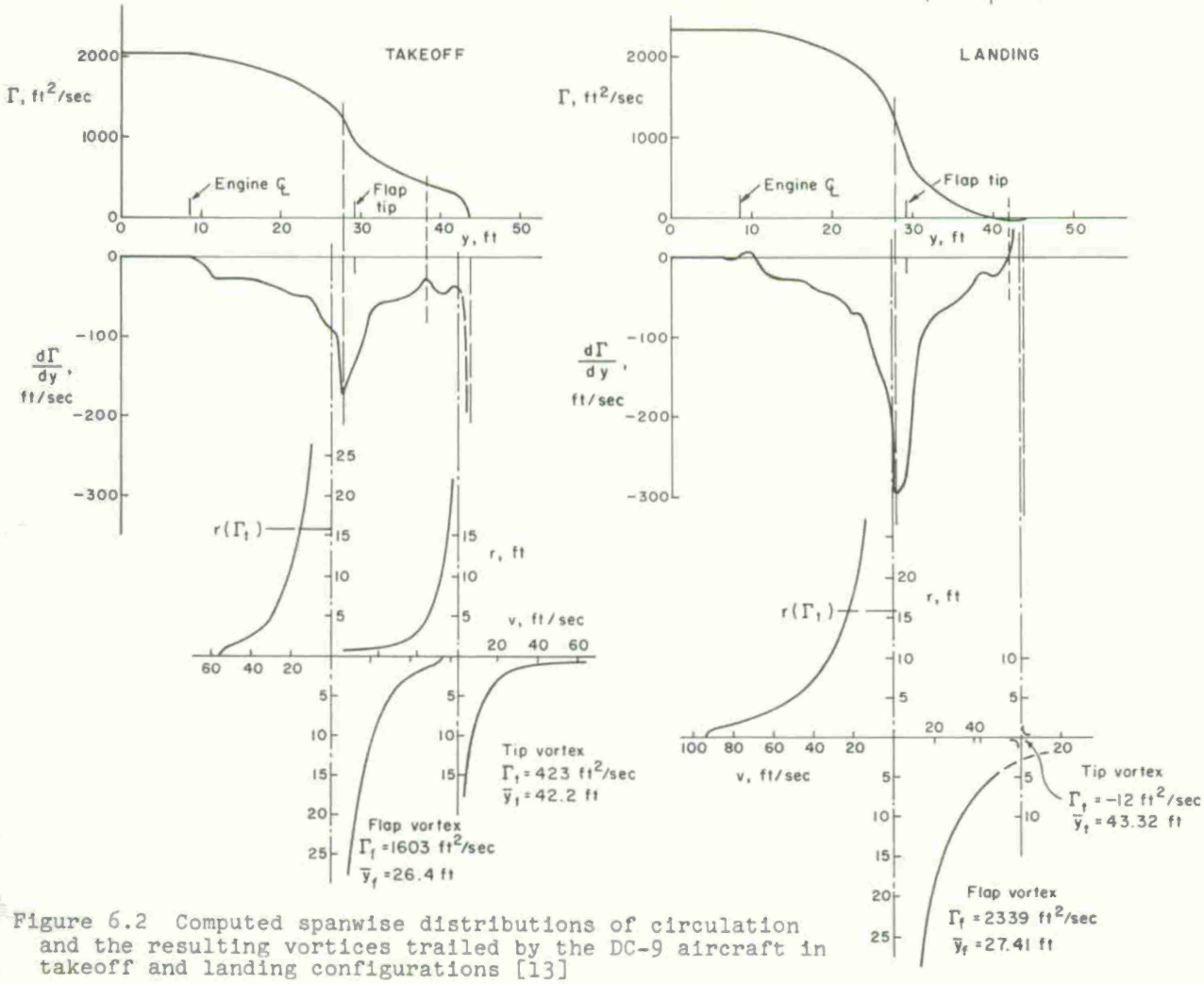

Figure 6.2 Computed spanwise distributions of circulation and the resulting vortices trailed by the DC-9 aircraft in takeoff and landing configurations [13]

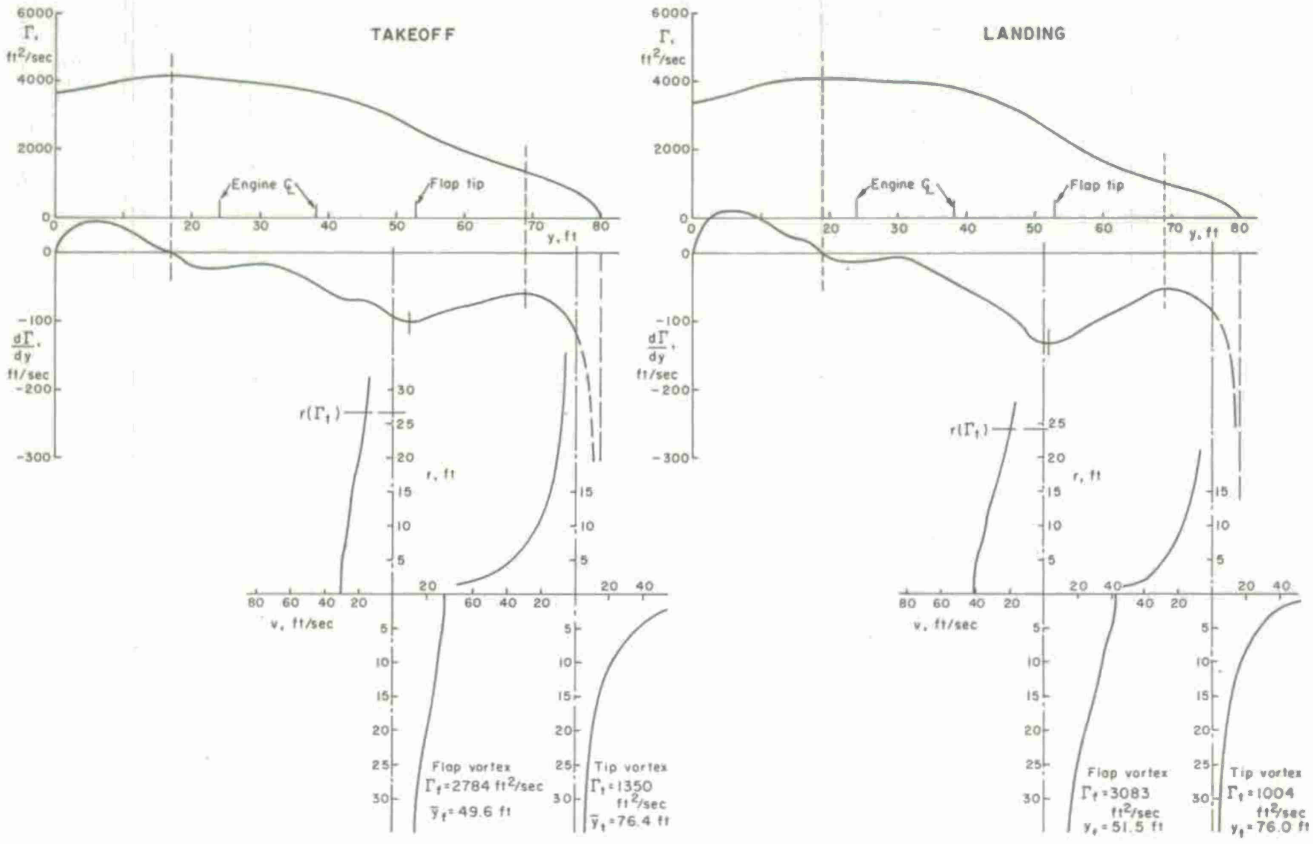

Figure 6.3 Computed spanwise distributions of circulation and the resulting vortices trailed by the C-141 aircraft in takeoff and landing configurations [13]

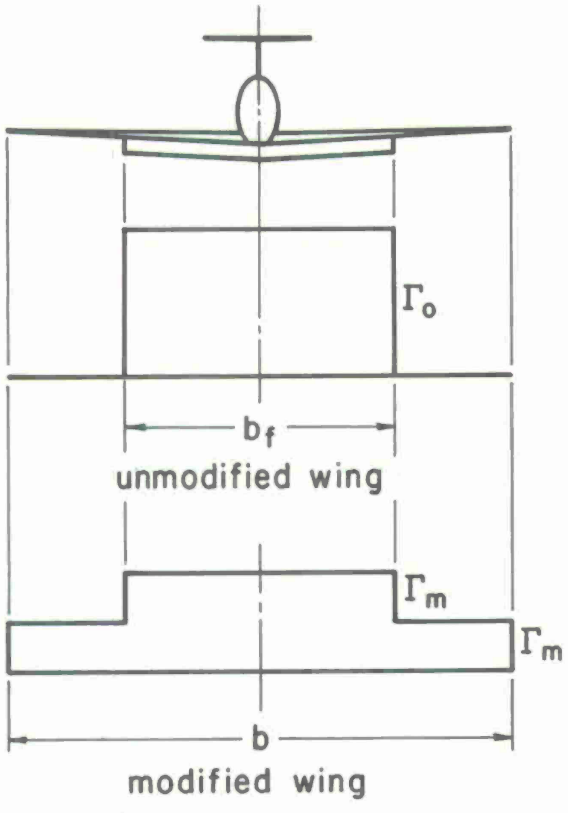

Figure 6.4 Two alternative idealized wing loadings which produce the same lift

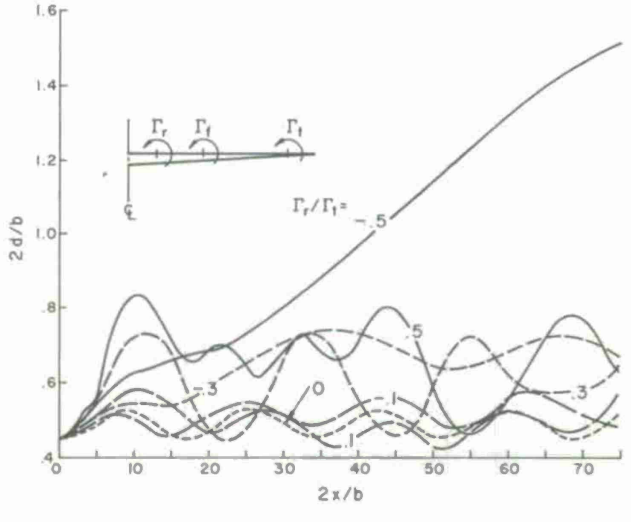

Figure 6.5 Effect of root vortices on the separation of tip and flap vortices for the case when $\Gamma_t = \Gamma_f$

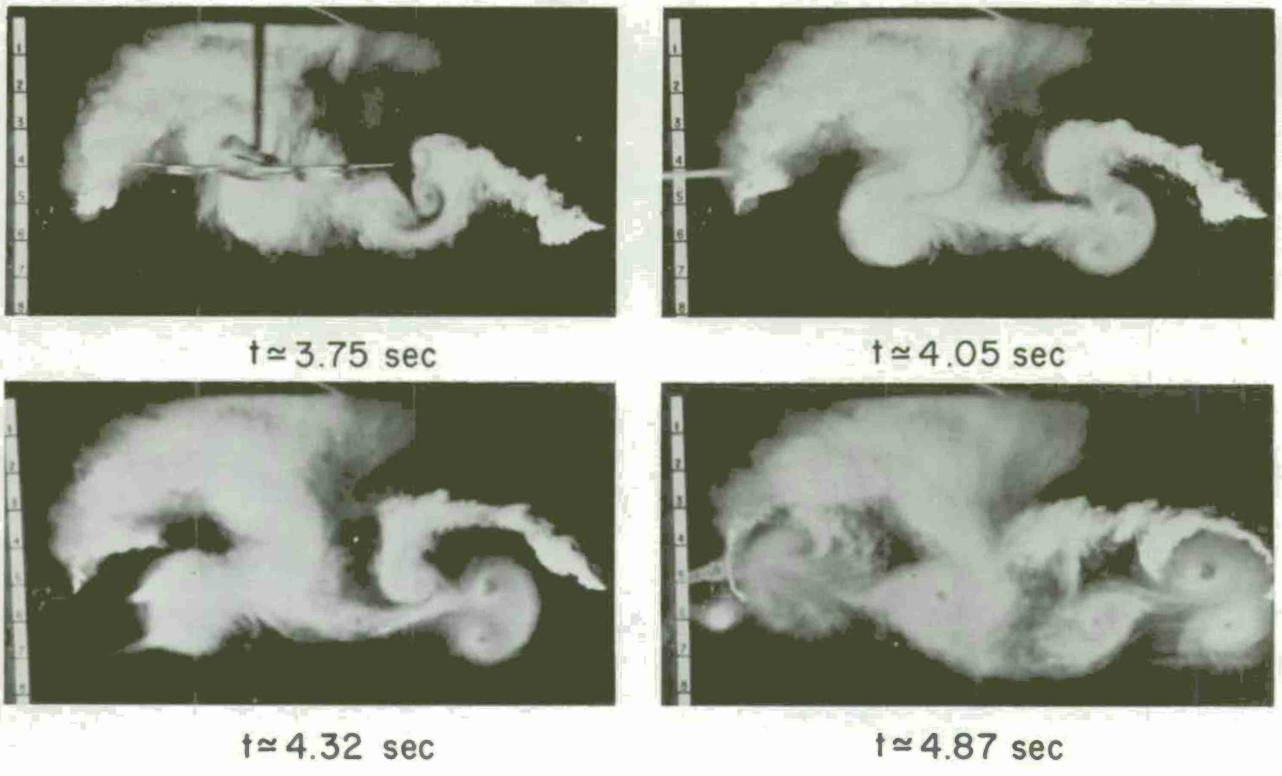

Figure 6.6 This figure illustrates the separation of tip and flap vortex caused by the shedding of a strong negative root vortex. (pictures kindly furnished by J.C.Patterson, Jr., of NASA/Langley Research Center)

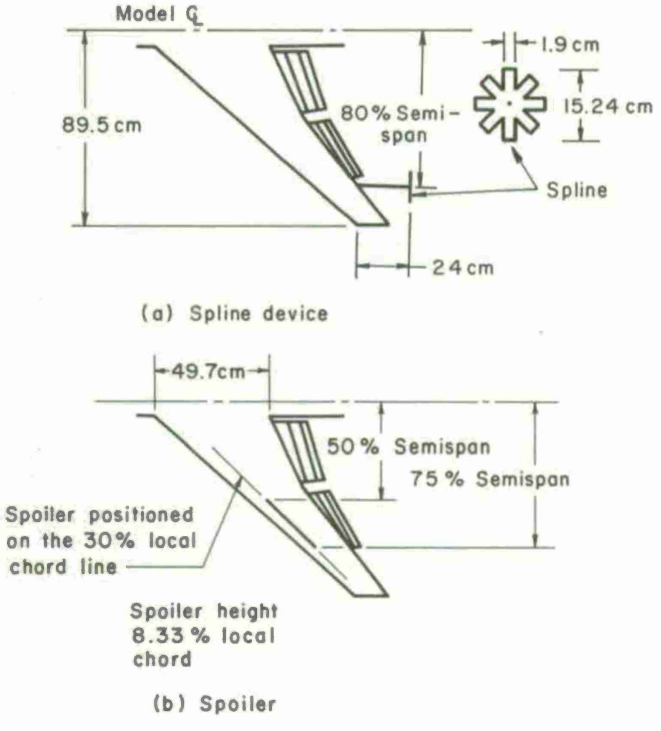

Figure 6.7 Devices tested by NASA for wake alleviation behind a model characteristic of the 747 [75]

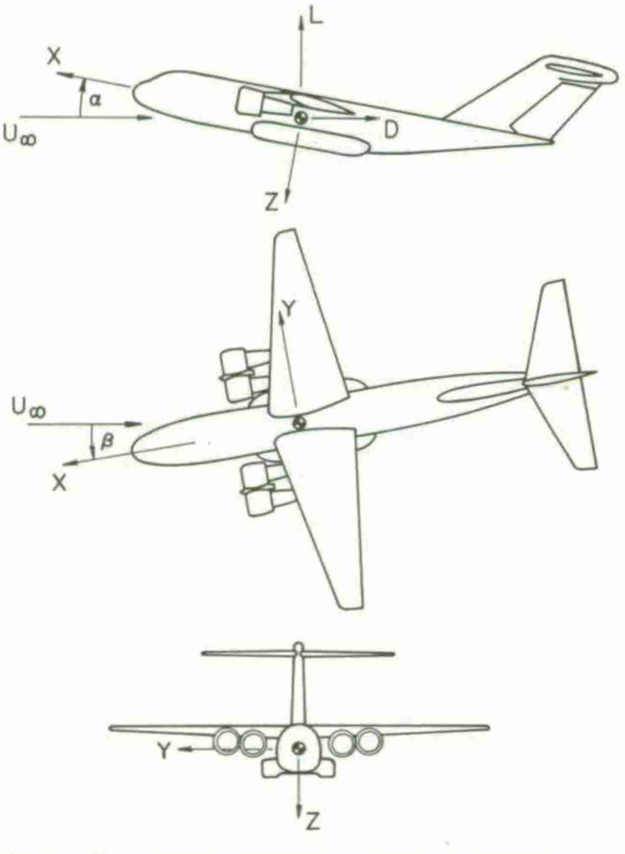

Figure 6.8 STOL aircraft configuration [105]

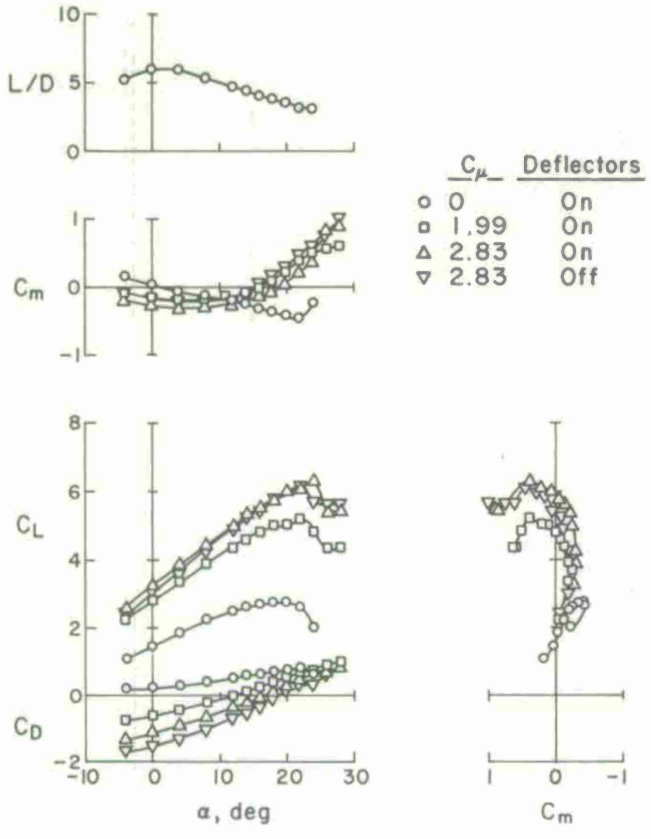

Figure 6.9 Aerodynamic characteristics of STOL configuration shown in Figure 6.8 [105]

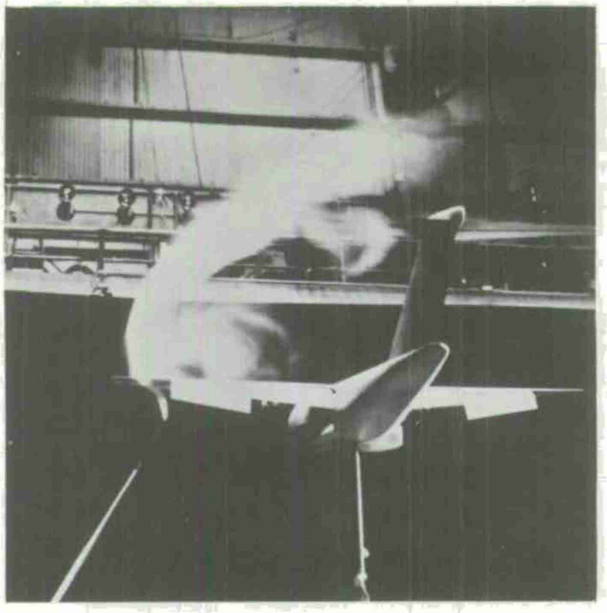

Figure 6.10 Smoke visualization of wing vortices for the STOL configuration shown in Figure 6.8 for high C_L and high C_μ [105]

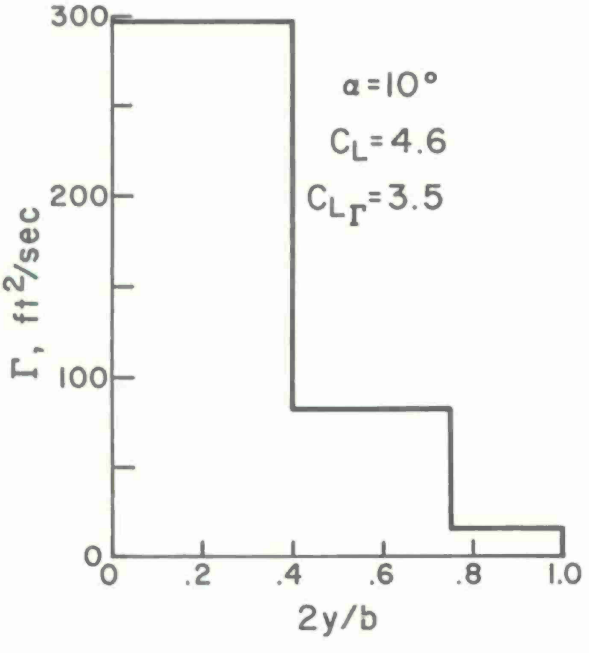

Figure 6.11 Idealized vortex lift distribution for STOL aircraft shown in Figure 6.10

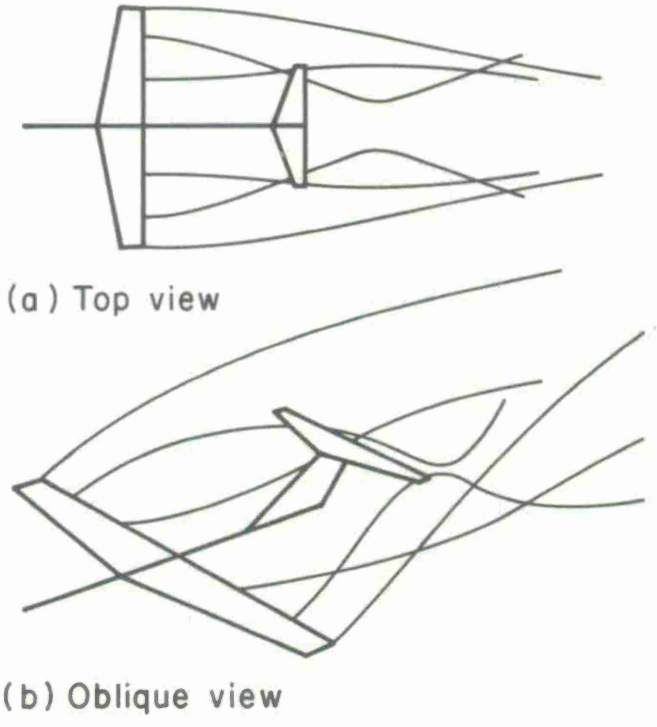

Figure 6.12 Computed wake geometry behind the idealized lift distribution shown in Figure 6.11

REPORT DOCUMENTATION PAGE

1. Recipient's Reference	2. Originator's Reference	3. Further Reference	4. Security Classification of Document
	AGARD-AG-204		UNCLASSIFIED

5. Originator Advisory Group for Aerospace Research and Development
North Atlantic Treaty Organization
7 rue Ancelle, 92200 Neuilly sur Seine, France

6. Title
Vortex Wakes of Conventional Aircraft

7. Presented at

8. Author(s)
Coleman duP.Donaldson
Alan J.Bilanin

9. Date
May 1975

10. Author's Address
Aeronautical Research Associates of
Princeton, Inc., 50 Washington Road, Princeton, New Jersey 08540, USA

11. Pages
80

12. Distribution Statement This document is distributed in accordance with AGARD policies and regulations, which are outlined on the Outside Back Covers of all AGARD publications.

13. Keywords/Descriptors

Vortices
Wakes
Aircraft
Turbulence
Atmospheric disturbances
Reviews

14. UDC
533.6.048.3:629.735.3

15. Abstract

A review is made of the present state of our knowledge of the vortex wakes of conventional aircraft. Included are discussions of wake rollup, geometry, instability, and turbulent aging. In the light of these discussions, a brief review is made of the persistence of vortices in the atmosphere, and design techniques which might be used to minimize wake hazard are considered.

This work was prepared at the request of the Fluid Dynamics Panel of AGARD.

AGARDograph No.204 Advisory Group for Aerospace Research and Development, NATO VORTEX WAKES OF CONVENTIONAL AIRCRAFT Coleman duP.Donaldson and Alan J.Bilanin (Edited by R.J.Korkegi) Published May 1975 80 pages A review is made of the present state of our knowledge of the vortex wakes of conventional aircraft. Included are discussions of wake rollup, geometry, instability, and turbulent aging. In the light of these discussions, a brief review is made of the persistence of vortices in the atmosphere, and design techniques which might be used to minimize wake hazard are considered. This work was prepared at the request of the Fluid Dynamics Panel of AGARD.	AGARD-AG-204 533.6.048.3:629.735.3 Vortices Wakes Aircraft Turbulence Atmospheric distrurbances Reviews	AGARDograph No.204 Advisory Group for Aerospace Research and Development, NATO VORTEX WAKES OF CONVENTIONAL AIRCRAFT Coleman duP.Donaldson and Alan J.Bilanin (Edited by R.J.Korkegi) Published May 1975 80 pages A review is made of the present state of our knowledge of the vortex wakes of conventional aircraft. Included are discussions of wake rollup, geometry, instability, and turbulent aging. In the light of these discussions, a brief review is made of the persistence of vortices in the atmosphere, and design techniques which might be used to minimize wake hazard are considered. This work was prepared at the request of the Fluid Dynamics Panel of AGARD.	AGARD-AG-204 533.6.048.3:629.735.3 Vortices Wakes Aircraft Turbulence Atmospheric disturbances Reviews
AGARDograph No.204 Advisory Group for Aerospace Research and Development, NATO VORTEX WAKES OF CONVENTIONAL AIRCRAFT Coleman duP.Donaldson and Alan J.Bilanin (Edited by R.J.Korkegi) Published May 1975 80 pages A review is made of the present state of our knowledge of the vortex wakes of conventional aircraft. Included are discussions of wake rollup, geometry, instability, and turbulent aging. In the light of these discussions, a brief review is made of the persistence of vortices in the atmosphere, and design techniques which might be used to minimize wake hazard are considered. This work was prepared at the request of the Fluid Dynamics Panel of AGARD.	AGARD-AG-204 533.6.048.3:629.735.3 Vortices Wakes Aircraft Turbulence Atmospheric disturbances Reviews	AGARDograph No.204 Advisory Group for Aerospace Research and Development, NATO VORTEX WAKES OF CONVENTIONAL AIRCRAFT Coleman duP.Donaldson and Alan J.Bilanin (Edited by R.J.Korkegi) Published May 1975 80 pages A review is made of the present state of our knowledge of the vortex wakes of conventional aircraft. Included are discussions of wake rollup, geometry, instability, and turbulent aging. In the light of these discussions, a brief review is made of the persistence of vortices in the atmosphere, and design techniques which might be used to minimize wake hazard are considered. This work was prepared at the request of the Fluid Dynamics Panel of AGARD.	AGARD-AG-204 533.6.048.3:629.735.3 Vortices Wakes Aircraft Turbulence Atmospheric disturbances Reviews

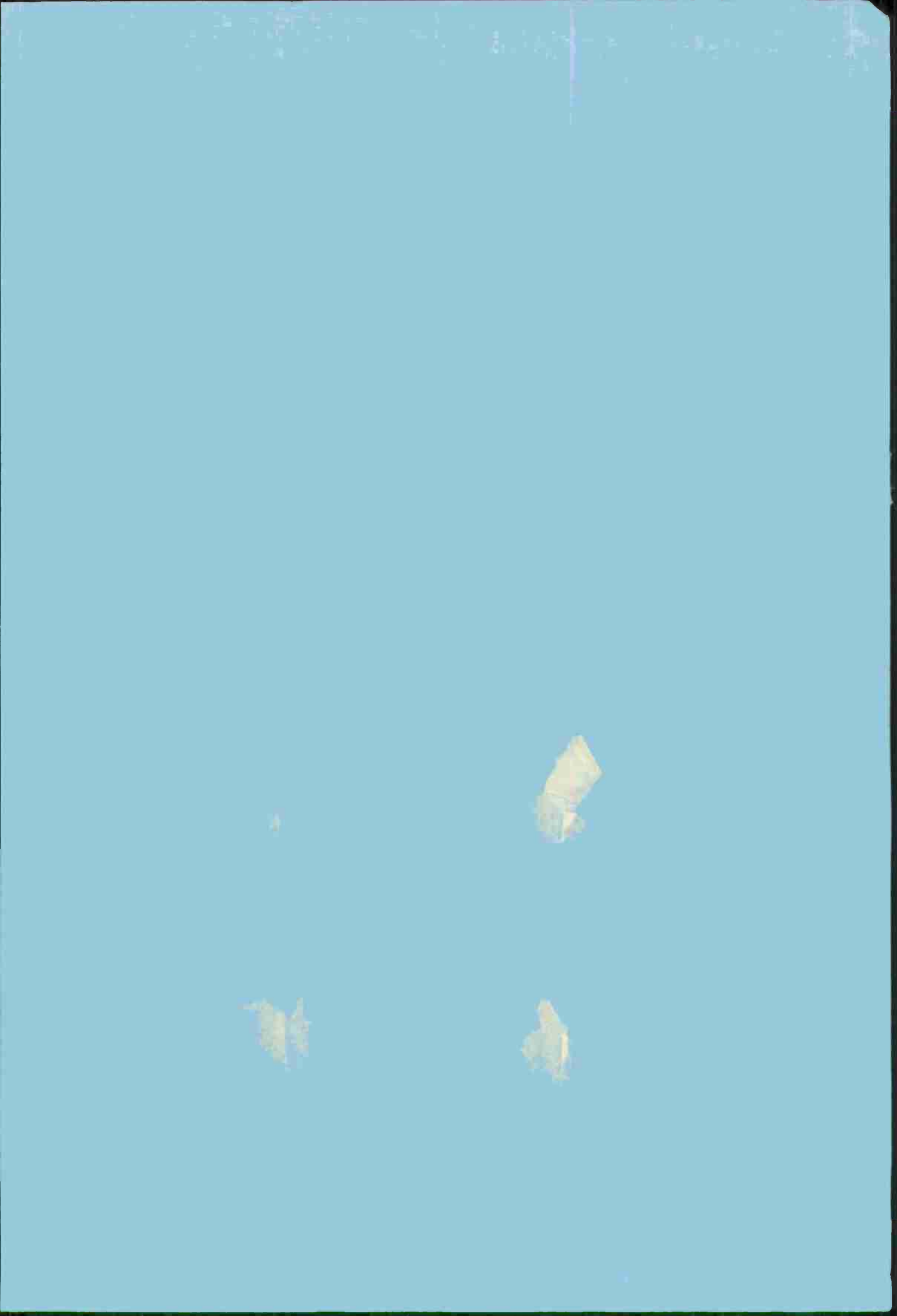

AGARD
NATO OTAN
7 RUE ANCELLE · 92200 NEUILLY-SUR-SEINE
FRANCE
Telephone 722.28.00 · Telex 61176

DISTRIBUTION OF UNCLASSIFIED AGARD PUBLICATIONS

AGARD does NOT hold stocks of AGARD publications at the above address for general distribution. Initial distribution of AGARD publications is made to AGARD Member Nations through the following National Distribution Centres. Further copies are sometimes available from these Centres, but if not may be purchased in Microfiche or Photocopy form from the Purchase Agencies listed below.

NATIONAL DISTRIBUTION CENTRES

BEL ...SL

GREECE
Hellenic ...
D Branch, ...

ICELAND
Director of Aviation ...
c/o Flugrad
Reykjavik

ITALY
Aeronautica Militare
Ufficio del Delegato Nazionale all'AGARD
3, Piazzale Adenauer
Roma/EUR

LUXEMBOURG
See Belgium

NETHERLANDS
Netherlands Delegation to AGARD
National Aerospace Laboratory, NLR
P.O. Box 126
Delft

NORWAY
Norwegian Defence Research Establishment
Main Library
...O. Box 25
...07 Kjeller

... Servico de Material

...olitecnica 42

...D National Delegate

...ent of Research and Development (ARGE)
...y of National Defence, Ankara

...KINGDOM
...fence Research Information Centre
...tation Square House
St. Mary Cray
Orpington, Kent BR5 3RE

...ce Administration (NASA),
...35
Att... and Storage Unit

THE UNITED STATES NAT... ...RIBUTION CENTRE (NASA) DOES NOT HOLD
STOCKS OF AGARD PUBLICATI... ...D APPLICATIONS FOR COPIES SHOULD BE MADE
DIRECT TO THE NATIONAL TECHNICAL ...FORMATION SERVICE (NTIS) AT THE ADDRESS BELOW.

PURCHASE AGENCIES

Microfiche or Photocopy
National Technical
Information Service (NTIS)
5285 Port Royal Road
Springfield
Virginia 22151, USA

Microfiche
ESRO/ELDO Space
Documentation Service
European Space
Research Organization
114, Avenue Charles de Gaulle
92200 Neuilly sur Seine, France

Microfiche
Technology Reports
Centre (DTI)
Station Square House
St. Mary Cray
Orpington, Kent BR5 3RF
England

Requests for microfiche or photocopies of AGARD documents should include the AGARD serial number, title, author or editor, and publication date. Requests to NTIS should include the NASA accession report number. Full bibliographical references and abstracts of AGARD publications are given in the following journals:

Scientific and Technical Aerospace Reports (STAR),
published by NASA Scientific and Technical
Information Facility
Post Office Box 8757
Baltimore/Washington International Airport
Maryland 21240, USA

Government Reports Announcements (GRA),
published by the National Technical
Information Services, Springfield
Virginia 22151, USA

Printed by Technical Editing and Reproduction Ltd
Harford House, 7-9 Charlotte St, London W1P 1HD